SANDIA REPORT

SAND2004-0073
Unlimited Release
Printed June 2004

Blade System Design Studies Volume II: Preliminary Blade Designs and Recommended Test Matrix

Dayton A. Griffin

Prepared by
Sandia National Laboratories
Albuquerque, New Mexico 87185 and Livermore, California 94550

Sandia is a multiprogram laboratory operated by Sandia Corporation,
a Lockheed Martin Company, for the United States Department of Energy's
National Nuclear Security Administration under Contract DE-AC04-94AL85000.

Issued by Sandia National Laboratories, operated for the United States Department of Energy by Sandia Corporation.

Available to DOE and DOE contractors from
U.S. Department of Energy
Office of Scientific and Technical Information
P.O. Box 62
Oak Ridge, TN 37831

Telephone: (865)576-8401
Facsimile: (865)576-5728
E-Mail: reports@adonis.osti.gov
Online ordering: http://www.osti.gov/bridge

Available to the public from
U.S. Department of Commerce
National Technical Information Service
5285 Port Royal Rd
Springfield, VA 22161

Telephone: (800)553-6847
Facsimile: (703)605-6900
E-Mail: orders@ntis.fedworld.gov
Online order: http://www.ntis.gov/help/ordermethods.asp?loc=7-4-0#online

SAND2004-0073
Unlimited Release
Printed June 2004

Blade System Design Studies Volume II: Preliminary Blade Designs and Recommended Test Matrix

Dayton A. Griffin
Global Energy Concepts, LLC
5729 Lakeview Drive NE, #100
Kirkland, Washington 98109

Abstract

As part of the U.S. Department of Energy's Wind Partnerships for Advanced Component Technologies (WindPACT) program, Global Energy Concepts, LLC is performing a Blade System Design Study (BSDS) concerning innovations in materials, processes and structural configurations for application to wind turbine blades in the multi-megawatt range. The BSDS Volume I project report addresses issues and constraints identified to scaling conventional blade designs to the megawatt size range, and evaluated candidate materials, manufacturing and design innovations for overcoming and improving large blade economics. The current report (Volume II), presents additional discussion of materials and manufacturing issues for large blades, including a summary of current trends in commercial blade manufacturing. Specifications are then developed to guide the preliminary design of MW-scale blades. Using preliminary design calculations for a 3.0 MW blade, parametric analyses are performed to quantify the potential benefits in stiffness and decreased gravity loading by replacement of a baseline fiberglass spar with carbon-fiberglass hybrid material. Complete preliminary designs are then presented for 3.0 MW and 5.0 MW blades that incorporate fiberglass-to-carbon transitions at mid-span. Based on analysis of these designs, technical issues are identified and discussed. Finally, recommendations are made for composites testing under Part II of the BSDS, and the initial planned test matrix for that program is presented.

Acknowledgements

This work was completed for Sandia National Laboratories as part of the U.S. Department of Energy's WindPACT. The author wishes to acknowledge the contributions of Sandia Technical Monitor Tom Ashwill, Paul Veers, and other Sandia personnel to this project. The NuMAD interface to ANSYS, developed by Daniel Laird of Sandia, was used extensively to facilitate the blade designs and analyses performed in this work.

This project has also benefited from extensive collaboration with manufacturers of composite materials, wind turbine blades, and other composite structures. Moto Ashizawa, Jeff Engbrecht (Toray Carbon Fibers America), and Mark Elliott consulted throughout the project on material properties, processing and costs. Other manufacturers and experts that contributed to this work include GE Wind Energy and TPI Composites (blade manufacturing and design issues), Fortafil and Zoltek (carbon fibers), SAERTEX and Hexcel Schwebel (hybrid fabrics), Composite Engineering Incorporated (braided structure fabrication), Techniweave (3-D weaving), the National Composite Center (oriented sprayed-fiber preforms), and Hexcel and SP Systems (epoxy resin systems). Mike Zuteck consulted on all phases of this project, and John Mandell of Montana State University made significant technical contributions in material selection, development of laminate properties, and design and planning for composites testing.

Table of Contents

1. Introduction 10

1.1 Background 10

1.2 Project Overview 10

1.3 Technical Approach 11

1.4 Report Scope and Organization 11

2. General Issues for MW-Scale Blades 12

2.1 Historic Blade Structure and Manufacturing Methods 12

2.2 Issues and Constraints to Scaling Conventional Blade Designs 13

2.3 Current Trends in Commercial Blade Manufacturing 13

2.4 Manufacturing and Materials Alternatives 16

2.4.1 Manufacturing Alternatives 16
2.4.2 Structural Configuration Alternatives 17
2.4.3 Alternative Materials 17

2.5 Optimal use of Carbon Fibers 17

2.5.1 Selective Reinforcement/Stiffening 17
2.5.2 Bulk replacement of Spar Material 18
2.5.3 Selective Replacement of Load-Bearing Spar 18
2.5.4 Load Mitigating Blade Designs 18
2.5.5 Carbon Fiber Pricing 20

3. Design Specifications for MW-Scale Blades 21

3.1 General 21

3.2 Turbine Design and Operation 21

3.3 General Blade Specifications 22

3.4 Blade Architecture 22

3.5 Structural Configuration 24

3.6 Materials 25

3.6.1 Baseline Blade Model 25
3.6.2 Candidate Alternative Materials 26

3.7 Criteria for Structural Design 28

3.7.1 Characteristic Material Strength 28
3.7.2 Partial Safety Factors for Loads 28
3.7.3 Static Strength Verification 29
3.7.4 Fatigue Strength Verification 29
3.7.5 Allowable Tip Deflection 29

3.8 Design Loads 31

3.8.1 Coordinate Systems 31
3.8.2 Data Processing 31
3.8.3 Peak Loads 33

3.8.4 Fatigue Loads 33
4. Preliminary Blade Designs 35
4.1 General Design Approach 35
4.2 3.0 MW Blade 35
4.2.1 Spanwise Extent of Spar Modifications 35
4.2.2 3.0 MW Blade with Fiberglass-to-Carbon Spar Transition 38
4.2.3 Effect of ε-N Curve Parameters 39
4.3 5.0 MW Blade 40
4.4 Design/Manufacturing Issues for Spar Transition 41
5. Recommendations for Testing Under Part II BSDS 43
5.1 Summary of Candidate Test Laboratories 43
5.1.1 Montana State University 43
5.1.2 National Wind Technology Center 44
5.1.3 Integrated Technologies Inc. 45
5.2 Planned Test Matrix 46
5.3 Discussion of Candidate Tests/Technical Issues 49
5.3.1 Material Types 49
5.3.2 Thin Coupon Testing 50
5.3.3 Thick Laminate 51
5.3.4 Ply Drops and Transitions 52
5.3.5 4-Point Beam Bending 55
5.3.6 Biased Material Cylinder 58
5.3.7 Margins/Safety Factors 59
5.3.8 Lap Shear Testing of Bonding Materials 59
6. Conclusions 60
6.1 Summary 60
6.2 Current/Future Work under Part II BSDS 60
7. References 61

List of Figures

Figure 1. WindPACT studies concerning composite blade design and manufacture 10
Figure 2. Common structural architecture for wind turbine blade 12
Figure 3. Mass growth for commercial MW-scale blade designs (primarily fiberglass) 15
Figure 4. Biased carbon-fiberglass skins in a twist-coupled blade design 20
Figure 5. Baseline blade chord distribution 23
Figure 6. Airfoils used for baseline blade model 24
Figure 7. Schematic of initial blade tip clearance 30
Figure 8. Coordinate systems for the blade sections 31
Figure 9. Edgewise gravity-induced loads at blade root and maximum chord locations 34
Figure 10. Gravity bending moments and carbon usage 36
Figure 11. Effect of carbon spar spanwise extent on root gravity bending moments 37
Figure 12. Effect of carbon spar spanwise extent on blade tip deflections 37
Figure 13. ANSYS stress contours for 3.0 MW blade with fiberglass /carbon transition at mid-span 39
Figure 14. Effect of ε-N slope parameter on calculated fatigue strength 40
Figure 15. Example candidate fiberglass-to-carbon spar transition 42
Figure 16. Instron 8501 servo-hydraulic testing machine at MSU 44
Figure 17. NWTC blade testing facility 45
Figure 18. Boeing 737 winglet structural testing at Intec 46
Figure 19. Typical test coupon geometries 51
Figure 20. Internal carbon ply drop (single ply, nominal ply thickness) 53
Figure 21. External carbon ply drop (nominal ply thickness) 53
Figure 22. External carbon ply drop with 0.5 mm thick plies 54
Figure 23. Internal carbon ply drop (multiple plies) 54
Figure 24. Multiple internal ply drops with 0.5 mm thick plies 54
Figure 25. Single-ply fiberglass-carbon transition 55
Figure 26. Multiple-ply fiberglass-carbon transition 55
Figure 27. Beam geometry assumed for estimating 4-point beam bending test requirements and cost 57
Figure 28. Schematic of test for biased tube in combined axial/torsional loading 58

List of Tables

Table 1. Baseline Turbine Specifications 22
Table 2. Design Site Wind Definition 22
Table 3. Airfoil Shape Modifications and Baseline Planform (TSR_{Design} = 7, c_{Max} = 8% R) 23
Table 4. Dimensions for Baseline Blade Planforms 24
Table 5. Baseline Structural-Shell Definition 25
Table 6. Summary of Baseline Blade Material Properties 25
Table 7. Static Properties for Candidate Spar Cap Materials 27
Table 8. Fatigue Properties for Candidate Spar Cap Materials 27
Table 9. Dimensions for Allowable Tip Deflections 30
Table 10. Definition of Local Blade Coordinate System 31
Table 11. Design Site Weighting for FAST_AD Runs for IEC Load Case 1.1 32
Table 12. Summary of Characteristic Peak Blade Loads 33
Table 13. Design Strength Margins for 3.0 MW Fiberglass/Carbon Hybrid Blade 38
Table 14. Spar Cap Geometry for 3.0 MW Fiberglass/Carbon Hybrid Blade 40
Table 15. Spar Cap Geometry for 5.0 MW Fiberglass/Carbon Hybrid Blade 41
Table 16. Complete Candidate Test Matrix (as developed at BSDS Part 1 Design Review Meeting) 48
Table 17. Initial Matrix for Planned Part II BSDS Testing 49
Table 18. Sizing Chart for Laminate with Ex = 74.3 GPa (coupon aspect ratio = 3) 52

Nomenclature

Note: This nomenclature list has been copied from the Volume I report, and was updated to reflect the information contained in present document.

c	chord length (m)
C_{ia}	partial safety factors for laminate materials
cm	centimeters
c_{max}	maximum blade chord (% R)
EI_{Edge}	edgewise bending stiffness ($N \cdot m^2$)
EI_{Flap}	flapwise bending stiffness ($N \cdot m^2$)
E_x	elastic modulus of laminate in longitudinal direction
E_y	elastic modulus of laminate in transverse direction
ft	feet
G_{xy}	in-plane shear modulus of laminate
kip	kilo-pounds
KN	kilo-Newtons
kW	kilowatt
lb	pounds force
m	meters
mm	millimeters
N	Newtons force
N	number of loading cycles for fatigue analysis
MW	megawatt
P_{rated}	Rated power output of turbine (kW)
R	rotor radius (m)
R_f	fatigue bending load ratio (minimum/maximum bending moment)
r/R	spanwise blade station (%)
S	blade surface area
t	physical thickness of a blade section (m)
t/c	airfoil thickness-to-chord (%)
TSR	tip-speed ratio
TSR_{Design}	design tip-speed ratio
v_f	volume fraction of fiber in composite laminate
w_f	weight fraction of fiber in composite laminate
x/c	distance along airfoil chord
y/c	distance perpendicular to airfoil chord

ε-N	strain-cycle curve for fatigue analysis
ν_{xy}	major poison's ratio for laminate
ρ	material density (g/cm^3)

1. Introduction

1.1 Background

In recent years both the size of wind turbine blades and the volume of commercial production has been steadily increasing. Rotors of up to 80-m diameter are in current production, and several turbine developers have prototypes in the 100- to 120-m diameter range [1]. It is estimated that over 60 million kilograms of finished fiberglass laminate were used for the production of wind turbine blades in the year 2002, and that worldwide production volume will increase for the next several years (calculations based on the global wind energy market growth trends reported in Reference 2). As a result of these growth trends, research programs in both the United States and Europe have been investigating alternative blade design and materials technologies.

In Europe, jointed blade designs have been evaluated for their potential benefits in transportation and erection costs, and carbon fiber composites were investigated for potential improvements in blade weight and cost [3-6]. In the United States, the U.S. Department of Energy is conducting the Wind Partnerships for Advanced Component Technologies (WindPACT) program. The purpose of the WindPACT program is to explore the most advanced technologies available for improving wind turbine reliability and decreasing the cost of energy (COE).

1.2 Project Overview

Figure 1 illustrates the relationship among the WindPACT studies that concern the design and manufacture of wind turbine blades. In the initial phase of the program, scaling studies were performed in the areas of turbine blades [7], transportation and erection logistics [8], and self-erecting tower concepts [9]. The purpose of the scaling studies is to determine optimum sizes for future turbines, identify size limits for critical components and technologies, and to investigate the potential benefits from advanced concepts. Under the NREL-sponsored Turbine Rotor Design Study, extensive aeroelastic simulations were performed for a wide range of rotor sizes and configurations, and the resulting loads used to quantify the impact on turbine cost and COE [10,11].

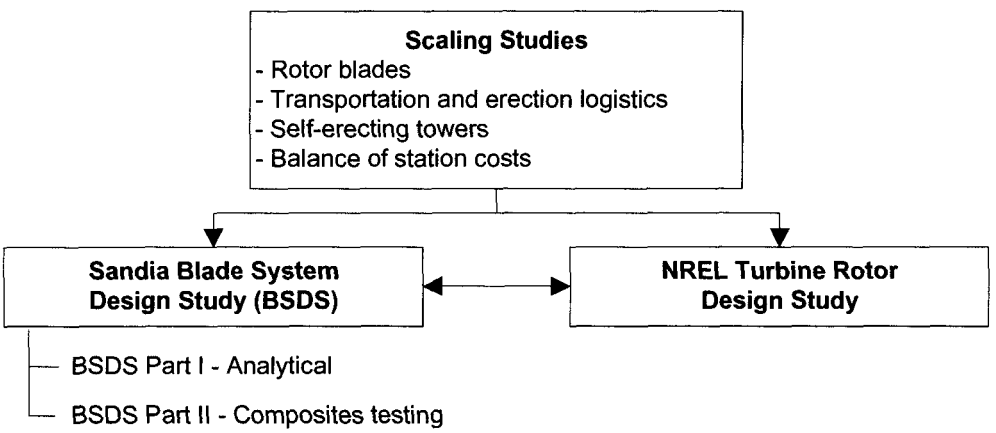

Figure 1. WindPACT studies concerning composite blade design and manufacture

Under the Sandia-sponsored Blade System Design Studies (BSDS), alternative composite materials, manufacturing processes and structural designs are being evaluated for potential benefits for MW-scale

blades [12-14]. As indicted by Figure 1, the BSDS has two parts. Part I is analytical and involves trade-off studies, selection of the most promising technologies, development of design specifications and preliminary design for MW-scale blades, identification of technical issues for alternative materials and manufacturing approaches, and development of recommendations for materials testing. The Part II BSDS involves testing of coupons and blade substructure with the objectives of evaluating composite materials and resolving technical issues identified in the Part I study. The specific objectives of the Part I BSDS are to:

1. Identify issues and constraints for the design, manufacture and use of large wind turbine blades
2. Identify and evaluate alternative materials, manufacturing processes, and structural configurations that may overcome those constraints
3. Develop design specifications for large blades (1.5 MW to 5.0 MW size range)
4. Perform preliminary designs for a megawatt-scale blade, and identify areas of risk that merit testing before proceeding to detailed design
5. Develop recommendations for testing of materials, sub-component and/or sub-scale blades to resolve knowledge gaps
6. Document the project's progress and results in a manner that makes the information readily available to the U.S. wind industry, composite manufacturers, and other interested parties.

Objectives #1 and #2 listed above were addressed in the Volume I BSDS Project Report [12]. The current report addresses objectives #3 through #6.

1.3 Technical Approach

The material in this report was developed from a large number of sources. Throughout this project GEC consulted with manufacturers of composites materials, wind turbine blades and turbine systems. The BSDS has also benefited from extensive synergy with other DOE-funded wind energy research efforts. The Montana State University (MSU) Composites Research Group collaborated substantially in the areas of material properties and test development. Results from the WindPACT Rotor Study were used to develop the baseline blade structural configurations and loads for the BSDS blade designs. GEC performed the majority of the design calculations using the ANSYS finite element analysis code with the Sandia-developed NuMAD interface [15]. The results, conclusions and recommendations in this report reflect an integration of all these diverse technical elements.

1.4 Report Scope and Organization

This report addresses objectives #3 through #6 listed in Section 1.2. The overall structure of this report is as follows:

- Summary of general issues, constraints, and materials/manufacturing options for large wind turbine blades
  - Overview of historic blade materials and manufacturing methods
  - Issues and constraints for scaling-up of historic methods
  - Current trends in commercial blade manufacturing
  - Manufacturing and materials alternatives, including optimal use of carbon fibers
  - Performance of blade laminate at ply drops and fiberglass/carbon transition regions
- Design specifications for blades at 1.5, 3.0 and 5.0 MW
- Development of preliminary blade designs at 3.0 and 5.0 MW
- Matrix of testing planned for the Part II BSDS

2. General Issues for MW-Scale Blades

This section reviews some of the major conclusions from earlier work under the BSDS, and discusses general issues concerning large blades. Current trends in commercial blade manufacturing and some alternative material and manufacturing approaches are reviewed. Options for the use of carbon fiber materials in large blades are discussed, along with some general issues that may influence the cost-effectiveness of carbon fibers in this application. Specific technical issues concerning blade composite materials will be discussed following the development of the preliminary 3.0 MW and 5.0 MW blade designs.

2.1 Historic Blade Structure and Manufacturing Methods

Figure 2 is a section-view illustrating a typical structural architecture for wind turbine blades. The terms "flapwise" and "edgewise" are used to denote bending loads that are perpendicular and parallel, respectively, to the airfoil chord line. The spar cap is a relatively thick laminate with primarily unidirectional content, and provides the primary strength to carry the flapwise bending loads. Blade skins are typically double-bias or triaxial fiberglass, with balsa or foam core used as needed for buckling resistance. Historically, wind turbine blades have been constructed using either all-fiberglass laminate or primarily fiberglass construction with selective use of carbon for local reinforcement. For blade sizes up to 30 m, the most common manufacturing approach has been open-mold, wet lay-up. The most notable exception to that approach is Vestas Wind Systems, which has a long history of using pregpreg fiberglass in their blade manufacturing.

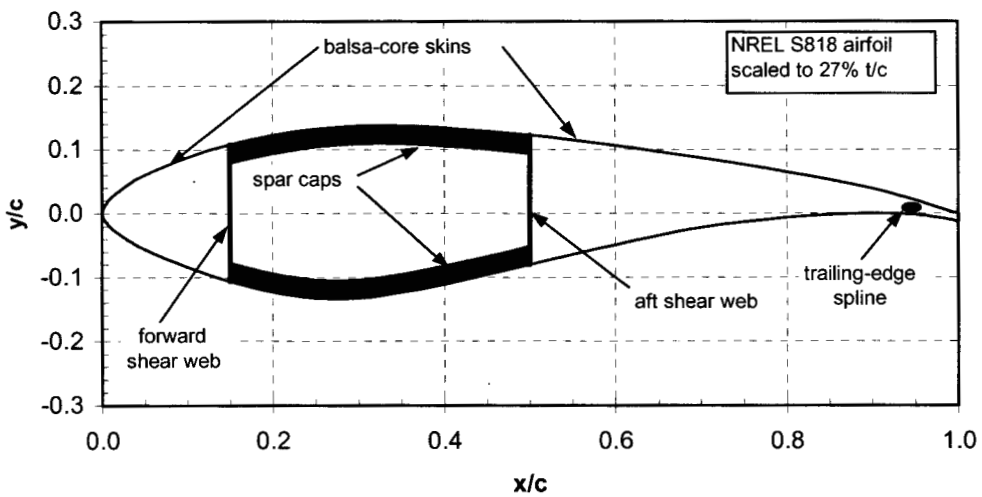

Figure 2. Common structural architecture for wind turbine blade

The wind turbine application for composite materials is very cost sensitive. For conventional fiberglass construction, manufacturing costs are in the range of $9 to $11/kg ($4 to $5/lb) for finished blade structure [12]. Total system cost of energy (COE) is the primary figure of merit for evaluating any change in the turbine design and manufacturing. For reference, the blade costs typically represent 10% to 15% of the installed capital cost for the turbine system [11]. If alternate materials and processes are considered for turbine blades, cost increases must be offset by improvements in other system attributes such as power performance and/or loads.

2.2 Issues and Constraints to Scaling Conventional Blade Designs

Very few fundamental barriers have been identified for the cost-effective scaling of the current commercial blade designs and manufacturing methods over the size range of 80 to 120 m diameter. The most substantial constraint is transportation costs which rise sharply for lengths above 46 m (150 ft) and may become prohibitive for long-haul of blades in excess of 61 m (200 ft).

In terms of manufacturing, it is expected that environmental considerations will prohibit the continued use of processes with high emissions of volatile gasses, such as the open-mold wet layup that has been the wind industry norm. Another manufacturing concern for large blades is bonding compounds. As blade sizes increase, it is natural for the gaps between fitted and bonded parts to grow as well. However, the bonding materials used for smaller blades do not scale well to increasing gap sizes. Blade tooling and production costs for large blades increase rapidly as dimensional tolerances are decreased. There is, therefore, a continual need for improved bonding compounds that have the appropriate viscosity for manufacturing and the desired combination of strength and elasticity so that both static and fatigue strength requirements are met.

Gravity loading is a design consideration but not an absolute constraint to scaling-up of the current conventional materials and blade designs over the size range considered. However, materials and designs that reduce blade weight may be of benefit for megawatt-scale blades, as this would reduce the need for reinforcements in the regions of the trailing edge and blade root transition to accommodate the gravity-induced edgewise fatigue loads.

Another issue for turbine design is the use of larger rotors at a given turbine system rating. The term "specific rating" refers to the rated power output normalized by the swept area of the rotor, typically given in units of kilowatts per square meter. The long-term industry average for utility-scale wind turbines is a specific rating of 0.44 kW/m^2. A trend toward decreased specific rating has been observed in turbines designed for low-to-moderate annual average wind speeds. A Class II GE Wind 1.5 has a rotor diameter of 70 m and a specific rating of 0.39 kW/m^2. Micon has a 1.5 MW with an 82-m rotor (specific rating of 0.28 kW/m^2). It is expected that turbine designs with a low specific rating will be of continued interest for deployment in the low wind speed sites of the Midwest United States. As specific rating is decreased, blade stiffness and the associated tip deflections become increasingly critical for cost-effective blade design.

2.3 Current Trends in Commercial Blade Manufacturing

To the extent practical, this section presents some current trends in the manufacture of commercial wind turbine blades. Developing and reporting such information in a meaningful and reliable way is challenging for several reasons. The research and development efforts of each manufacturer are usually kept proprietary until a new product or innovation is ready to be marketed. Also, both the size and manufacturing technologies of MW-scale blades are rapidly evolving. As a result, any attempt at reporting the "current" status of the industry is bound to be at least slightly outdated by the time it is published. The current data should then be considered as a snapshot of this rapidly changing technology, summarizing the best non-proprietary data available at the time of the writing.

A large number of turbine system manufacturers are currently moving toward in-house production of their own blades, and in doing so are using diverse materials and manufacturing methods. Nordex and GE Wind Energy have both built blades in the 35- to 50-m length range using hand lay-up of primarily

fiberglass structure in open-mold, wet processes. However, GE Wind is using a vacuum-assisted resin transfer molding (VARTM) process for their new blade production, and Nordex is now using prepreg materials in their largest blades. NEG Micon is building 40-m blades with carbon augmented wood-epoxy. TPI Composites is manufacturing 30-m blades using their patented SCRIMP™ (VARTM) process. Bonus has one of the more novel approaches in current use for large blades, where blades in lengths of 30 to 40 m are being produced from a dry preform with a single-shot infusion, eliminating the need for secondary bonding of the blade halves.

Some recent commercial blades now incorporate carbon fiber in the load-bearing spar structure. Vestas (which has a long history of manufacturing with prepreg fiberglass) has announced that the new V90 blades will use carbon fiber spars. Nordex has also incorporated prepreg carbon in the spars of their new 45-m prototype. DeWind is using an innovative approach to produce 40-m carbon/fiberglass hybrid blades. In that process, the spar cap is produced using prepreg carbon. After curing, the spar caps are then placed into a preform and infused into the fiberglass blade skins.

The largest currently installed prototype turbine (as of this writing) is the 4.5 MW Enercon E-112. Marketing data list the E-112 blades as fiberglass-epoxy, but provide no further details on the materials and manufacturing technologies employed.

Figure 3 shows a plot of blade mass versus rotor radius for turbines sizes ranging from 750 kW to 4.5 MW. In the wind industry, scaling relationships are frequently used to estimate changes in power performance, loads, and component weight or cost. A simple self-similar scaling of blades would imply the mass would grow as a cubic power of radius. However, the trend line in Figure 3 indicates that the growth in blade mass with size has maintained a significantly lower exponent ($R^{2.30}$ for the data set shown).

Reference 7 provides a detailed discussion of the mass growth trends for commercial blades and the underlying evolution of the aerodynamic/structural designs, materials, and manufacturing processes. A major contributor to the restrained mass growth in the data shown is the use of airfoils with higher thickness-to-chord (t/c) ratios in the larger blades. Over the 25- to 50-m size range, increases in Reynolds number have allowed the use of higher t/c foils with minimal adverse effects on aerodynamic performance. However, for the largest current blades, the potential to further exploit these effects is diminishing. Structural efficiency may be further improved by the use of thicker airfoils, but the trade-offs in aerodynamic performance must also be considered.

The set presented in Figure 3 is limited to blades that are primarily fiberglass (either all-glass or selective use of carbon). Blades with carbon spars such as the Vestas V90 and DeWind 40 m are not included in the trend line. Material-related contributions to the restrained mass growth may therefore be attributed to such aspects as improved laminate consistency, better fiber alignment, increased fiber volume fractions, and reductions in non-structural material within the blade.

Inspection of Figure 3 shows a relatively large degree of scatter in the blade mass data. This is attributed primarily to two causes: the materials/manufacturing approach and the design criteria for the blades. Commercial blade manufacturers apply different strategies concerning the trade-offs between material quality and labor costs. Low-performing materials may be less expensive but will result in a heavier product. Because touch labor is strongly correlated with material volumes, this approach may take more labor hours, but the level of skill required and quality-control requirements may be reduced. Higher-performing materials allow a lighter product, but will likely be more expensive. Touch labor can be reduced, but the skill level and quality control requirements may be increased to maintain the higher level of laminate quality and structural performance.

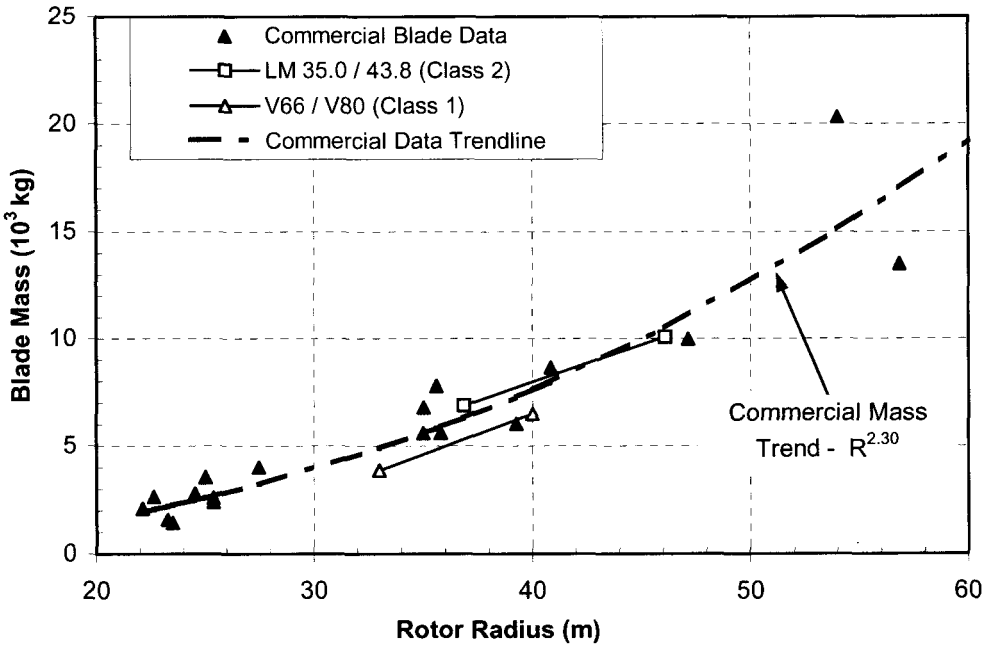

Figure 3. Mass growth for commercial MW-scale blade designs (primarily fiberglass)

Wind loading is a major design criterion that can substantially influence blade weight. The most widely recognized design standard for wind turbines is the International Electrotechnical Commission (IEC) 61400-1 [16]. The IEC standard specifies wind loading according to "design class." Class I is the most severe loading, assuming an annual average wind speed of 10 m/s and a 50-year extreme wind of 70 m/s. Class II design presumes an 8.5 m/s annual average and a 60-m/s 50-year extreme. Because aerodynamic forces generally scale as the square of the speed, the peak aerodynamic loading may be 36% higher for a Class I design than for Class II.

For selected data points, Figure 3 identifies the blade manufacturer and design wind speed class for which the blade mass applies. It is counter-intuitive that the lowest points identified (Vestas V66 and V80) are both designed to Class I loads whereas the higher set of points (LM 35.0 and 43.8) represent masses for Class II designs. However, these mass trends are in fact consistent with the manufacturing approach taken by the respective companies. Vestas has a long history of manufacturing with prepreg fiberglass materials and has traditionally produced some of the lightest and most flexible blades among commercial designs. LM Glasfiber has historically used lower-cost materials resulting in heavier blades.

Additional insight may be gleaned by investigating mass growth trends for a particular manufacturer at a fixed design class. For the Vestas blades, the mass difference between the V66 and V80 blade scales as $R^{2.7}$. This value is much closer to the cubic self-similar scaling relationship. Because the V66 is already a lightweight design using relatively high-performing prepreg material, limited opportunity for additional weight savings from material performance remained for the larger blade (assuming no change in fiber type). The fact that the growth rate was held to a lower-than-cubic value is likely attributable to the use of thicker airfoil sections and other design refinements.

In contrast, the mass difference between the LM 35.0 and LM 43.8, at IEC Class II, scales as $R^{1.7}$ which is substantially lower than the overall industry trend line. The implication is that LM has taken advantage

of significant improvement in material performance between these designs, in conjunction with the use of thicker airfoil sections.

Note, however, that comparing IEC design class does not tell the entire story concerning the governing loads for any given blade design. The control systems used, composite materials, airfoil thickness, and specific rating can all influence the governing load cases and structural requirements (i.e., whether the design is governed by peak loading, fatigue loading, buckling, deflection, or some combination). Therefore, while the discussion above may provide some useful insight, it should not be taken as a definitive explanation for the mass growth trends observed.

2.4 Manufacturing and Materials Alternatives

Several innovations have been identified over the course of this project as showing potential for reductions in weight, increased stiffness and improved manufacturing and transportation costs. Some are listed below with summary discussions of anticipated benefits and design considerations. As noted in the previous section, many of these alternatives are currently employed in commercial blade manufacturing.

2.4.1 Manufacturing Alternatives

Although some manufacturers are still using open-mold, wet lay-up processes, increasingly stringent environmental restrictions will likely result in a move toward processes with lower emissions. In current production, two methods are emerging as the most common replacement for traditional methods. These are the use of preimpregnated materials and resin infusion, with VARTM being the most common infusion method. Both VARTM and prepreg materials have particular design challenges for manufacturing the relatively thick laminate typical of large wind turbine blades. For VARTM processes, the permeability of the dry preform determines the rate of resin penetration through the material thickness. For prepreg material, sufficient bleeding is required to avoid resin-rich areas and eliminate voids from trapped gasses.

Another promising alternative is partially pre-impregnated fabric. The generic term for this technology is "semi-preg," and versions are presently marketed by SP Systems under the name SPRINT, and by Hexcel Composites as HexFIT. When layed-up, the dry fabric regions provide paths for air to flow, and vacuum can be used to evacuate the part prior to heating. Under heat and pressure, the resin flows into the dry fabric regions to complete the impregnation.

An elevated temperature post-cure is desirable for both prepreg and VARTM processes. Current commercial prepreg materials generally require higher cure temperatures (90° to 110°C) than epoxies used in VARTM processes (60° to 65°C). Heating and temperature control/monitoring becomes increasingly difficult as laminate thickness is increased. Mold and tooling costs are also strongly affected by the heat requirements of the cure cycle. In all cases, achieving the desired laminate quality requires a trade-off between the extent of fiber compaction, fabric/preform architecture, resin viscosity, and the time/temperature profile of the infusion and cure cycles.

The use of automated preforming or automated lay-up technologies is also a potential alternative to hand lay-up in the blade molds. Benefits could include improved quality control in fiber/fabric placement and a decrease in both hand labor and production cycle times.

2.4.2 Structural Configuration Alternatives

Although several structural configuration alternatives were evaluated in the project work to date, none has emerged as showing strong promise for improvements over the baseline blade configuration. The most fundamental constraint to scaling-up the baseline blade design is transportation cost, which rises sharply for blade lengths over 45 m and becomes prohibitive for long-haul transportation of blades in excess of 61 m. Two alternatives have emerged as promising for overcoming this constraint to cost-effective shipping, either a jointed blade structure or on-site fabrication of the entire blade. On-site manufacturing has been demonstrated by TPI Composites under Sandia contract [17]. Several manufacturers are evaluating major spanwise joints and it appears that some commercial designs may incorporate this feature within the next few years.

2.4.3 Alternative Materials

In several recent studies, the use of carbon fiber in the load-bearing spar structure of the blade has been identified as showing substantial promise for cost-effective weight reductions and increased stiffness. In particular, new low-cost, large-tow carbon fibers could result in improved blade structural properties at a reduced cost relative to an all-fiberglass blade.

Further economies may be realized if the carbon fibers can be processed into a form that favors both structural performance and manufacturing efficiency. Stitched hybrid fabrics and other automated preforming technologies have potential benefit in this area. Maintaining fiber straightness is crucial to achieving desirable compressive strength properties from composite materials. While carbon fibers tend to have excellent stiffness and tensile strength properties, realizing the full benefits from carbon fibers will require fabric/preform architectures that also result in good compressive strength.

2.5 Optimal use of Carbon Fibers

Optimal use of carbon fibers in turbine blades is related both to the cost performance of the fibers and the overall strength and stiffness properties of the material. A greater premium can be paid for carbon materials if used selectively to enhance the performance of other materials or in a way that yields other structural or aeroelastic benefits. Although carbon materials have decreased in price in recent years, they are more expensive and have higher performance than the fiberglass materials that have been the industry norm. It appears unlikely that all-carbon blades will be the most cost-effective approach for MW-scale wind turbine blades. The following sections present some considerations for optimal hybridization of carbon fibers with other composite materials.

2.5.1 Selective Reinforcement/Stiffening

Carbon fiber is used in many applications for selective reinforcement and stiffening. For utility-scale wind turbine blades selective stiffening with carbon has been more prevalent in wood-epoxy than for fiberglass blade designs. This is because the strain-to-failure of wood and carbon fibers is better matched than fiberglass and carbon. As a result carbon can be used to selectively reinforce and stiffen wood-epoxy laminate with a high degree of structural efficiency. Examples of wood-epoxy turbine blades that employ selective carbon reinforcement are the AWT-26/27 blades (developed in the mid-1990s) and the recent Micon 1.5 MW with an 82-m diameter rotor.

2.5.2 Bulk replacement of Spar Material

Because of the mismatch in strain-to-failure between fiberglass and carbon fibers, a combination of these fibers in a primary load-bearing direction is inefficient. The stiffer carbon fibers will tend to take the majority of the load and will fail at a strain level that is too low for the fiberglass to realize its potential load-carrying capability. A more efficient use of carbon in a fiberglass/carbon hybrid blade is a bulk replacement of the load-carrying unidirectional fibers in the spar material. Unidirectional carbon spar material is well suited to provide the primary flapwise bending strength of the blade and can be efficiently combined with off-axis fiberglass materials (i.e., biaxial fabrics) that provide torsional rigidity and retard crack propagation.

Analyses performed under both U.S. and European research efforts indicate that bulk replacement of load-bearing fiberglass laminate with commercial carbon fibers is a cost-effective option for MW-scale blades. For a 120-m diameter rotor, the E.C.-funded work of Reference 5 estimates that carbon fiber spars could result in a 38% reduction in total blade mass and a 14% decease in cost relative to the baseline all-fiberglass design. Similar analyses performed earlier in the BSDS predicted mass reductions of up to 32% and a cost decrease up to 16% compared with the baseline fiberglass blade [12]. Substantial reductions in blade tip deflection under load (18% to 29%) were also predicted. However, in both of those studies it was assumed that the fiberglass/carbon hybrid material extended the entire length of the blade spar. Not addressed in the previous work is the extent to which the structural benefit per unit amount of carbon used may vary along the blade span.

2.5.3 Selective Replacement of Load-Bearing Spar

Absolute blade mass is not typically a design driver for wind turbine blades. For transportation, the costs tend to be dominated by length, and for erection, crane sizes are driven by height requirements or by the heavier mechanical components located in the nacelle. Of greater importance to the blade design are the gravity-induced, self-bending loads in the root region of the blade. These loads are highest at the leading and trailing edges of the blade airfoil section and go through one fully reversed cycle for each rotation of the rotor. Although reinforcement and improvements in load path can accommodate these loads, there is a significant advantage in mitigating the loading itself.

Because it is the gravity-induced bending moment rather than the absolute weight that drives this load case, mass reductions in the outer blade span yield the greatest benefit. Section 4.2.1 of this report presents a parametric study on selective replacement of fiberglass spar material with carbon. For the case investigated, the greatest reduction in gravity-induced bending loads per unit kilogram of carbon fiber used is realized for a carbon spar extending from the tip to mid-span. If the carbon spar was carried farther inboard, the reductions in total blade mass would be large, but because the distance to the root section is also decreasing, the mass reductions would have a diminishing effect on the gravity-induced moments. The parametric analysis results also showed the largest reduction in tip deflection (per unit of carbon fiber used) for a design with a carbon spar in the outer half of the blade span.

2.5.4 Load Mitigating Blade Designs

The options presented above generally focus on replacement of load-bearing fiberglass with carbon in an otherwise conventional blade design. However, carbon fibers may also be used to enable more innovative blade designs. In considering such innovation, the primary goals are increased energy capture and/or mitigated loads. These two objectives may generally be considered equivalent. For a given baseline turbine system, a load-reducing blade design can enable the use of a larger rotor, thus increasing the energy capture at the original load level.

2.5.4.1 Slender Planforms

For a blade designed with a given set of airfoils, operating loads can generally be reduced by a reduction in the chord dimensions along the blade. To maintain aerodynamic efficiency, this implies that the design rotation speed for the turbine is correspondingly increased. Aeroelastic simulations have demonstrated that such designs can reduce both static and fatigue loading on the blades and other major turbine system components [11]. However, as blade chord dimensions are reduced, the thickness of the airfoil sections decreases proportionally. As a result, the blade sections become less structurally efficient and the tip deflections (at fixed material strain values) increase. Relative to fiberglass, the increased stiffness and strength of carbon fiber may improve the structural efficiency and deflection characteristics of slender planform designs.

2.5.4.2 Twist-Coupled Designs

Twist-coupling is a form of aeroelastic tailoring in which a flapwise bending load results in a twist of the blade section, changing the local airfoil angle of attack and the corresponding aerodynamic forces. In recent years, a substantial research effort has investigated the potential for load mitigation through such designs. In the WindPACT rotor study, a 8.2% reduction in cost of energy (COE) was predicted for a rotor that had the combined features of a slender planform with twist-coupling, with about 2% of the COE benefits attributed to the twist-coupling and the remainder of the improvements due to other the design features.

Carbon fibers, in combination with fiberglass, can be used to achieve a high degree of structural coupling in blade laminate [18-22]. Figure 4 depicts such a design, where the carbon fibers are biased at -20° from the longitudinal blade axis, and the glass fibers are perpendicular at +70°. Work is ongoing under several concurrent programs to further investigate the feasibility of such blade designs from the standpoint of manufacturability, structural integrity, and cost-effectiveness.

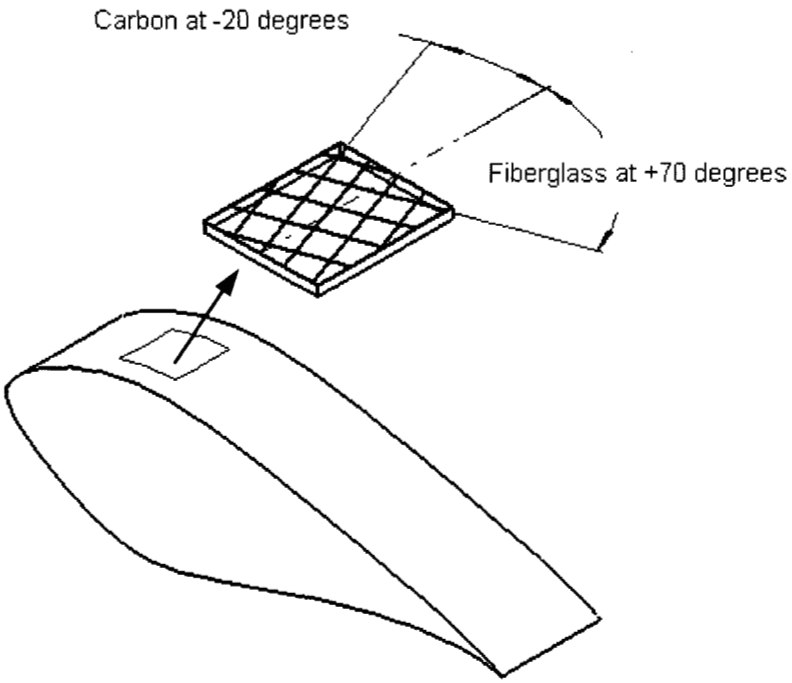

Figure 4. Biased carbon-fiberglass skins in a twist-coupled blade design

2.5.5 Carbon Fiber Pricing

The general trend in the past decades has been one of increasing usage and decreasing cost for carbon fiber materials. In the trade-off studies conducted earlier in the BSDS, carbon fiber prices of $19.80/kg and $12.10/kg were assumed, respectively, for "currently available" and "next-generation" large-tow carbon fibers. Although these price estimates were based on consultation with several carbon fiber manufacturers, the long-term price and price stability of carbon fibers remains questionable.

At a 2001 international carbon industry meeting, several speakers and panel discussions focused on the question of whether carbon producers could profitably sustain current carbon fiber prices. A detailed analysis was presented showing the current manufacturing cost (before profit) of 12k tow carbon to be approximately $19/kg and 50k tow production cost to be about $14/kg [23]. It has been speculated that increased demand for commercial carbon fiber (i.e., through applications such as wind turbine blades, fuel cell, infrastructure, automotive and other transportation) could result in economies of scale to further reduce carbon fiber production costs. However, to date the carbon fiber industry remains dominated by aerospace applications that can pay a high premium for materials with low weight and desirable structural and thermal properties.

3. Design Specifications for MW-Scale Blades

Specifications were written to guide the development of preliminary designs for megawatt-scale blades. The following sections provide a summary of these specifications, including turbine design and operation, blade architecture, design loads and criteria for determining structural integrity.

3.1 General

The blade specification material was developed from several sources. The aerodynamic designs and loads are based on work performed in the WindPACT Blade Scaling and Rotor System Design Studies. Design criteria are based on standards and regulations from the IEC, Germanischer Lloyd [24], Det Norske Veritas and Risø National Laboratory [25]. Specifications concerning composite materials and manufacturing are based on earlier work performed under the BSDS, and on extensive research carried out at Montana State University [26-28].

Specifications are given for three rotor sizes with system ratings of 1.5, 3.0 and 5.0 MW, respectively. For these three configurations the blade dimensions and loads are representative of turbines with a specific rating of 0.39 kW/m^2 of rotor swept area. An additional set of blade dimensions and loads is given for a 1.5 MW rotor with a specific rating of 0.31 kW/m^2.

The specified design criteria are based on recognized international standards and are generally applicable to turbine blades spanning a wide range of design parameters. However, the design loads were derived from aeroelastic simulations that were carried out for specific aerodynamic and structural designs. While the loads herein may not be generalized to other turbine and rotor configurations, these specifications do contain approximate methods for scaling the edgewise fatigue bending loads for blades with mass distributions differing from the baseline designs.

The preliminary blade designs are being developed to investigate alternative structural designs, materials and manufacturing processes for application to megawatt-scale wind turbine blades and to guide composites testing to further evaluate the most promising alternatives. Of particular interest are designs, materials and manufacturing options that may address any issues or constraints to scaling of current conventional blade designs over the size range of 1 to 10 MW. As such, the blade designs will contain varying levels of innovation. These specifications are not intended to restrict innovation in the blade designs, but are intended to establish the baseline design parameters and criteria for evaluation.

3.2 Turbine Design and Operation

The following turbine architecture and system design parameters are assumed:

- Three blade, upwind rotor with independent full-span blade pitch-to-feather control
- Variable speed below rated power
- Cone angle fixed at zero degrees
- Nacelle tilt angle fixed at 5 degrees (hub up)

Table 1 gives specifications for the baseline turbine rotors. The dimensions and speeds given correspond to a system specific rating of 0.39 kW/m^2. Dimensions for a 1.5 mw rotor at 0.31 kW/m^2 specific rating are given in Section 4.4.

Table 1. Baseline Turbine Specifications

	Turbine System Rating (kW)		
Design Parameter	**1500**	**3000**	**5000**
Rotor Diameter (m)	70	99	128
Rated Wind Speed (m/s)	11	11	11
Maximum Operating Tip Speed (m/s)	75	75	75
Minimum Rotor Speed, n_1 (rpm)	5.7	4.1	3.1
Rated Rotor Speed (rpm)	20.5	14.5	11.2
Hub Height (m)	84	119	154
Cut-In Wind Speed (m/s)	3.0	3.0	3.0
Cut-Out Wind Speed (m/s)	27.6	29.0	30.1

3.3 General Blade Specifications

The blades shall be designed to withstand the specified operational and non-operational loads and environment for a period of 20 years. All designs shall meet the IEC 61400-1 design code for wind turbine generator systems. The IEC 61400-1 requires a 'limit states' design approach which is based on ISO 2394 General Principles on Reliability for Structures [29]. To ensure an acceptably low probability of failure, the limit state design requires that uncertainties and variability in loads and materials are accounted for by partial safety factors.

The IEC 61400-1 requires different safety factors to be applied according to the type of analysis (ultimate versus fatigue), the type of component (fail-safe versus non fail-safe), and the type of load (aerodynamic, gravity, etc.). The IEC-specified safety factors shall be used for all designs where no other explicit design standard is in place. More detail can be found in Section 3.7.

Blades shall be designed for an IEC Class II design site. The Class II site is defined by the parameters given in Table 2, where all values are for hub height. All design wind conditions were derived using the parameters of Table 2, according to the definitions and equations contained in IEC 61400-1.

Table 2. Design Site Wind Definition

Hub-height reference wind speed, V_{ref}		42.5 m/s
Hub-height average wind speed, V_{ave}		8.5 m/s
Turbulence parameters, A	I_{15}	0.18
	a	2
Weibull shape factor, k		2 (Rayleigh)
Design air density at sea level standard atmospheric conditions, ρ_{air}		1.225 kg/m^3

3.4 Blade Architecture

The blade planform for the current study, shown in Figure 5, is the same as is being used for the WindPACT Rotor Design Study baseline. The maximum chord dimension is 8% R (located at 25% r/R), and the chord dimensions decrease linearly to a value of 2.6% R at the blade tip. A circular blade root is located at 5% r/R. The blade shape is assumed to remain circular to 7% r/R before transitioning to a pure

airfoil shape located at 25% r/R. The dimensions given for the root transition region are nominal and may be modified as needed during the development of blade designs.

The blade designs incorporate NREL S-series airfoils [30]. The S818/S825/S826 family was initially identified as having desirable aerodynamic properties. However, in the work of Reference 7 the airfoils were deemed to be too thin for efficient application to megawatt-scale blades. A more structurally suitable set of airfoil shapes was derived by scaling the S818/S825/S826 foils and by the addition of a finite-thickness trailing edge. The shape modifications and locations of airfoils along the blade are summarized in Table 3; the resulting airfoil shapes are shown in Figure 6.

During the work of References 7 and 31, the PROPID code was used to develop near-optimal blade aerodynamic shapes for a wide range of operational parameters. Reference 7 details the effects of design tip speed ratio and maximum chord dimension on blade aerodynamic and structural performance. However, the trade-offs involved were similar throughout the size range considered and the non-dimensional aerodynamic performance (i.e., C_P-TSR curve) was found to be largely invariant for a fixed, non-dimensional chord and twist distribution over the 750 kW to 5.0 MW size range. As such, Table 3 specifies a single non-dimensional chord and twist distribution for all blade sizes and configurations.

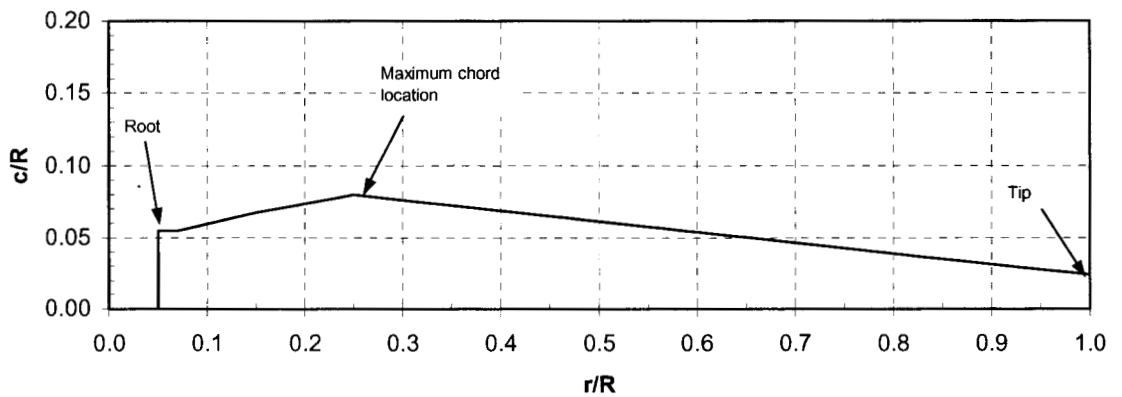

Figure 5. Baseline blade chord distribution

Table 3. Airfoil Shape Modifications and Baseline Planform (TSR_{Design} = 7, c_{Max} = 8% R)

Station R (%)	Airfoil	Original t/c (%)	Scaled t/c (%)	Trailing-edge thickness (% c)	Chord c/R (%)	Twist (degrees)
5 - 7	Cylinder	100	-	-	5.40	10.5
25	S818	24	30/33*	1.3	8.00	10.5
50	S825	17	21	1.0	6.13	2.5
75	S826	14	16	0.75	4.27	0.0
100	S826	"	"	"	2.59	-0.6

* 30% t/c for 1.5 MW rotor, 33% t/c for 3.0 and 5.0 MW

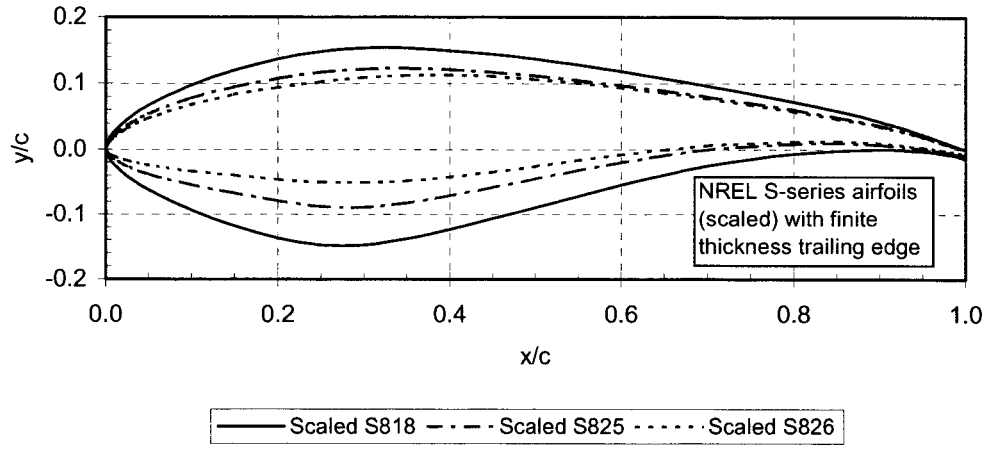

Figure 6. Airfoils used for baseline blade model

The blade dimensions between the blade root and 25% span section are nominal. The dimensions and shape of this root transition region may be changed (if required) in the blade design development without significantly affecting the aerodynamic forces and associated design loads in this specification. However, the external blade shape outboard of the 25% span station should not be modified.

The blade geometry of Table 3 was developed for a design tip speed ratio of $TSR_{Design} = 7$ and a maximum chord of 8% R. The corresponding pitch angle (at 75% span) for optimal variable-speed power performance is 2.6°. The planform dimensions are given in physical units in Table 4.

Table 4. Dimensions for Baseline Blade Planforms

	Turbine System Rating (kW)			
Dimensions	**1500***	**1500**	**3000**	**5000**
Rotor Diameter (m)	78	70	99	128
Rotor Radius (m)	39	35	49.5	64
Blade Length (m)	37	33	47	61
Root Chord (m)	2.12	1.89	2.67	3.45
25% Span Chord (m)	3.14	2.80	3.96	5.11
50% Span Chord (m)	2.40	2.15	3.03	3.92
75% Span Chord (m)	1.67	1.49	2.11	2.73
Tip Chord (m)	0.94	0.84	1.19	1.53

* 1.5 MW at specific rating = 0.31 kW/m^2

3.5 Structural Configuration

The following sections describe the structural configuration and materials for the baseline blade, which was selected as being representative of current commercial blade designs. It is expected that the new blade designs developed under this work will closely resemble the baseline configuration, but this should not be taken as a constraint against innovative alternatives.

The primary structural member for the baseline structural configuration is a box-spar, with two shear webs and a substantial build-up of spar cap material between the webs. The exterior skins and internal shear webs are both sandwich construction with triaxial fiberglass laminate separated by balsa core. This

general arrangement was depicted earlier in Figure 2, where the S818 airfoil section (25% span station) is shown. However, to improve the buckling stability in the spar cap region, the MW-scale carbon spar designs were developed with the aft shear web at 45% chord rather than the 50% chord location used in the baseline fiberglass blade and depicted by Figure 2.

3.6 Materials

3.6.1 Baseline Blade Model

Table 5 lists the layers in the shell of the baseline blade structural model, and describes the material contained in each. The balsa shear web cores are assumed to be 1% of airfoil chord (c) thick, with triaxial skins of 1.27 mm. The skins and spar cap are E-glass/epoxy laminate. The triaxial fabric is designated CDB340, and has a 25%, 25%, and 50% distribution of +45°, -45°, and 0° fibers, respectively. The spar cap is composed of alternating layers of triaxial and uniaxial (A260) fabric. This stacking sequence results in spar cap laminate with 70% uniaxial and 30% off-axis fibers by weight.

Table 5. Baseline Structural-Shell Definition

Layer #	Material	Thickness
1	gel coat	0.51 mm
2	random mat	0.38 mm
3	triaxial fabric	1.27 mm
4 0%-15% c 15%-50% c 50%-85% c	 balsa spar cap mixture balsa	 0.5% c specified % t/c 1.0% c
5	triaxial fabric	1.27 mm

Characteristic material properties for the baseline blade lamina were determined at Montana State University (MSU) based on a combination of test data and laminate theory calculations. Table 6 summarizes the mass and stiffness properties for each material. Strength properties are given in the following section.

Table 6. Summary of Baseline Blade Material Properties

Property	A260	CDB340	Spar Cap Mixture	Random Mat	Balsa	Gel Coat	Fill Epoxy
E_x (GPa)	31.0	24.2	25.0	9.65	2.07	3.44	2.76
E_y (GPa)	7.59	8.97	9.23	9.65	2.07	3.44	2.76
G_{xy} (GPa)	3.52	4.97	5.00	3.86	0.14	1.38	1.10
ν_{xy}	0.31	0.39	0.35	0.30	0.22	0.3	0.3
v_f	0.40	0.40	0.40	-	N/A	N/A	N/A
w_f	0.61	0.61	0.61	-	N/A	N/A	N/A
ρ (g/cm^3)	1.75	1.75	1.75	1.67	0.144	1.23	1.15

3.6.2 Candidate Alternative Materials

Tables 7 and 8 list the mechanical properties (stiffness, density, static and fatigue strength) for several candidate materials to be used in developing preliminary blade designs. The list shown is a subset of the alternative materials evaluated in the BSDS Task #2 trade-off study. Additional details are available in Reference 12.

Material strengths are give in terms of strain rather than stress. Fatigue strength is presented by ε-N curves the form:

$$\frac{\varepsilon}{\varepsilon_o} = A \cdot N^{-1/m} \tag{1}$$

where

ε_o ≡ single-cycle design fatigue strain
A ≡ coefficient of the ε-N curve
N ≡ number of loading cycles
m ≡ inverse slope of the ε-N curve

Values of A and m are listed in Table 8 for each of three different fatigue loading conditions, $R_f = 0.1$ (tension-tension), $R_f = 10$ (compression-compression), and $R_f = -1$ (fully reversed), where the loading ratio, R_f, is equal to the minimum load divided by the maximum load occurring in each loading cycle. In the present work, ε-N curves were normalized to the tensile static strength for $R_f = 0.1$, and to the compressive static strength for $R_f = 10$ and -1.

Table 7. Static Properties for Candidate Spar Cap Materials

Material #	Description	v_f	Moduli (GPa)			ν_{xy}	Density (kg/m^3)	$\varepsilon_{char.}$ (%)		Total Factor	ε_{design} (%)	
			E_x	E_y	G_{xy}			Tens.	Comp.		Tens.	Comp.
1	Woven glass uni + stitched glass triax, 70% 0°	0.4	25.0	9.2	5.0	0.35	1750	2.70	1.20	2.67	1.01	0.45
2	Woven glass uni + stitched glass triax, 70% 0°	0.5	29.0	10.2	6.0	0.31	1880	2.70	1.05	2.67	1.01	0.39
3	Prepreg glass uni + triax, 70% 0°	0.5	29.0	10.2	6.0	0.31	1880	2.70	1.55	2.45	1.01	0.63
4	Stitched hybrid carbon/fiberglass triax, 70% 0°	0.5	74.3	10.0	4.8	0.35	1621	1.35	0.90	2.67	0.50	0.34
5	Prepreg hybrid carbon/fiberglass triax, 70% 0°	0.5	74.3	10.0	4.8	0.35	1621	1.35	0.90	2.45	0.55	0.37
6	"P4A" oriented discontinuous carbon preform	0.55	94.3	20.0	6.1	0.55	1540	1.35	1.10	2.67	0.50	0.41

Table 8. Fatigue Properties for Candidate Spar Cap Materials

Material #	Description	v_f	$\varepsilon_{char.}$ (%)		Total Factor	Single-Cycle ε (%)		ε-N Curve Coefficients					
								R = 0.1		R = 10		R = -1	
			Tens.	Comp.		Tens.	Comp.	A	m	A	m	A	m
1	Woven glass uni + stitched glass triax, 70% 0°	0.4	2.70	1.20	1.63	1.65	0.74	1.24	9.5	1.10	15.0	1.06	13.5
2	Woven glass uni + stitched glass triax, 70% 0°	0.5	2.70	1.55	1.63	1.65	0.95	1.30	7.4	1.10	15.0	1.06	13.5
3	Prepreg glass uni + triax, 70% 0°	0.5	2.70	1.55	1.63	1.65	0.95	1.15	12	1.07	18.4	1.02	16.9
4	Stitched hybrid carbon/fiberglass triax, 70% 0°	0.5	1.35	0.9	1.63	0.83	0.55	1.01	48	1.03	28	1.02	17
5	Prepreg hybrid carbon/fiberglass triax, 70% 0°	0.5	1.35	0.9	1.63	0.83	0.55	1.01	48	1.03	28	1.02	17
6	"P4A" oriented discontinuous carbon preform	0.55	1.35	1.1	1.78	0.76	0.62	1.01	48	1.03	28	1.02	17

3.7 Criteria for Structural Design

The structural design verifications will be performed using the limit states approach as prescribed by the IEC 61300-1 Standard and the Germanischer Lloyd (GL) Regulations. The calculations begin with "characteristic" values of blade load and material strength. "Design" values for loads and material strength are determined by dividing the characteristic values by specified partial safety factors. Verification of the design adequacy requires that the stresses resulting from the design load do not exceed the design strength of the material:

$$S \geq {R_K}/{\gamma_{Mx}} = R_d \tag{2}$$

where

S ≡ stresses from the design loads
R_k ≡ characteristic material strength
R_d ≡ design material strength
γ_{Mx} ≡ combined partial safety factor for the material

3.7.1 Characteristic Material Strength

The GL Regulations specify that characteristic stresses/strains are to be derived for α = 5% fractile (95% exceedance) for a probability P = 95% (confidence interval) assuming a normal distribution. The GL default value for the coefficient of variation is v = 15%. Applying the default GL values results in:

$$R_K = \bar{x}\left[1 - 0.15\left(1.645 + \frac{1.645}{\sqrt{n}}\right)\right] \tag{3}$$

where

n ≡ the number of material tests
$\bar{x}$ ≡ the mean of material test values

3.7.2 Partial Safety Factors for Loads

Based on IEC 61400-1, the partial factor for loads is as follows:

γ_f = 1.35 ultimate loads
γ_f = 1.00 fatigue loads

IEC 61400-1 also specifies a "consequences of failure" factor of γ_n = 1.15 for fatigue analyses of "non fail-safe components." However, a comparison of the GL and IEC safety factors implies that combining the IEC consequences of failure factor with GL fatigue material safety factors would be conservative. As the GL factors are used for materials in these specifications, the IEC consequences of failure factors are not applied.

3.7.3 Static Strength Verification

The GL regulations provide an explicit list of partial safety factors for composite materials. For a static-strength evaluation of fiberglass and carbon reinforced plastics, the GL factors are:

γ_{M0} = 1.35 general material factor
C_{2a} = 1.50 influence of aging
C_{3a} = 1.10 temperature effect
C_{4a} = 1.10 laminates made from prepreg or semi-automated manufacturing
1.20 hand lay-up laminate
C_{5a} = 1.00 post-cured laminate
1.10 non post-cured laminate

The GL regulations state that γ_{M0} is to be used in all cases, but that the C_{ia} may be adjusted if demonstrated by experimental verification.

3.7.4 Fatigue Strength Verification

For fatigue verification, the GL regulations state that γ_{M0} is to be used as described above. Default values for S-N curves are also given, but alternate forms are acceptable with experimental verification. In addition to γ_{M0}, the default partial material factors for fatigue analysis are:

C_{3b} = 1.10 temperature effect
C_{4b} = 1.00 for unidirectional reinforcement (UD) products
1.10 for non-woven fabrics and UD woven rovings
1.20 for all other reinforcement products
C_{5b} = 1.00 post-cured laminate
1.10 non post-cured laminate

3.7.5 Allowable Tip Deflection

Figure 7 shows a schematic of the initial blade tip clearance, which is the distance between the tower outer diameter and the blade surface at the tip with one blade vertically down and no loading. For the baseline rotor design, the nacelle is tilted 5°, hub up, and the coning angle is 0°. According to the GL regulations, the allowable tip deflections under normal turbine operation are 50% of the initial tip clearance if deflections are determined by a quasi-static analysis, and 70% of the initial tip clearance if the deflections are calculated from aeroelastic simulations. Table 9 lists the initial tip clearance and allowable tip deflections for blades at 1.5, 3.0 and 5.0 MW. As the design loads are based on simulation results from the WindPACT rotor study, the 70% criterion was used.

Table 9. Dimensions for Allowable Tip Deflections

Specific Rating (kW/m^2)	Rotor Radius (m)	Initial Tip Clearance (m)	Allowable Tip Deflection (m)
0.31	39.25	4.46	3.12
0.39	35.0	4.27	3.00
0.39	49.5	6.14	4.30
0.39	64.0	8.06	5.64

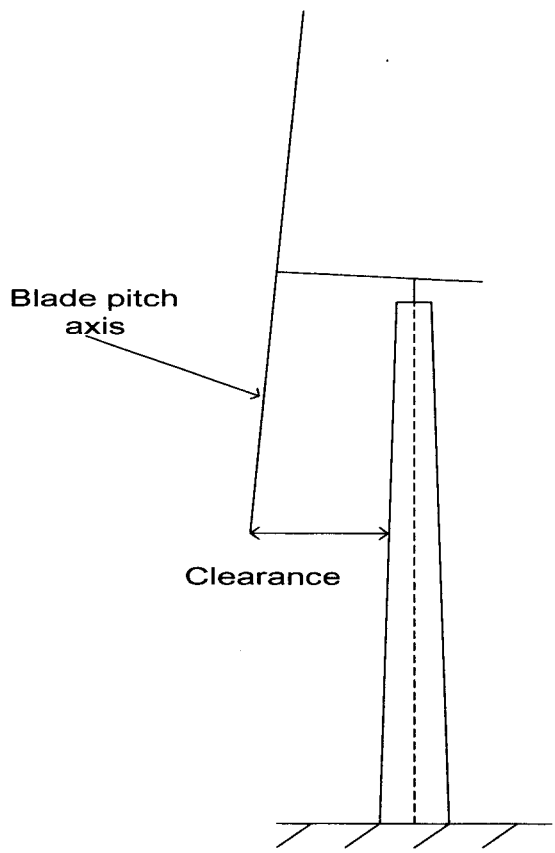

Figure 7. Schematic of initial blade tip clearance

3.8 Design Loads

3.8.1 Coordinate Systems

The coordinate system for the blade load information is described in Table 10 and depicted in Figure 8. The origin is the intersection of the blade pitch axis with the rotor plane of rotation. Subscripts "B" denote the blade frame of reference.

Table 10. Definition of Local Blade Coordinate System

	Orientation	Positive
X	Perpendicular to local chord line	High to low pressure surface
Y	Parallel to local chord line	Leading to trailing edge
Z	Along blade pitch axis	Root to tip

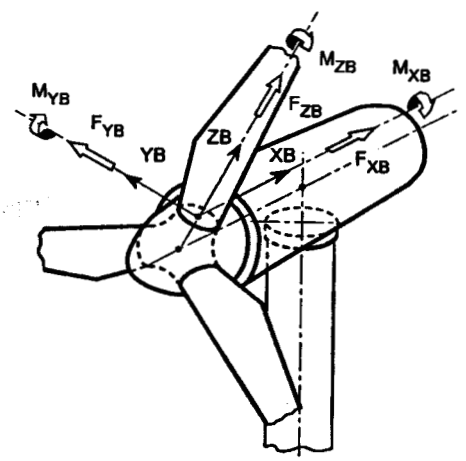

Figure 8. Coordinate systems for the blade sections

3.8.2 Data Processing

The ultimate design loads presented in this document were developed from the FAST_AD time series outputs using the following approach:

1. Scan the time series for the peak value of each signal, including some composite signals such as the net force vector (F_{XY}) and net moment vector (M_{XY}) magnitudes at each load application point.
2. While scanning, multiply by the appropriate partial safety factor for load to allow evaluation of the peak design load rather than the peak characteristic load.
3. For the peak of each signal, store the values of the other load components associated with the corresponding load application point.
4. Output design load combinations at each load application point corresponding to the peak of each of the load signals at that application point.

Fatigue loads are generated by rainflow counting each load signal from each run of the FAST_AD time series output that is specified for fatigue in the IEC standard. Table 11 shows the amount of simulation

time (30 minutes = three 10-minute simulations) for the normal operating runs. The multipliers in Table 11 are determined from the design site wind distribution as the number of hours in the wind speed range shown in the table. This multiplier is the ratio of the number of hours in 20 years to the simulation time in the given wind speed interval.

Table 11. Design Site Weighting for FAST_AD Runs for IEC Load Case 1.1

Simulation Wind Speed, m/s	Wind Distribution Range, m/s	Simulation time in minute	Multiplier
8	4 to 8	30	119710
12	8 to 12	30	101513
16	12 to 16	30	51562
20	16 to 20	30	17146
24	20 to 24	30	3862

The full spectrum of rainflow counts for each load is used to calculate the number cycles at each load range over the turbine lifetime. Equation 1 is used in a Miner's Rule summation to calculate the fatigue life as a fraction of the 20 year design life by:

$$Life = \sum_i n_i \cdot \left(\frac{\varepsilon_i}{\varepsilon_0 \cdot A} \right)^m \tag{4}$$

where n_i is the number of cycles at the i^{th} load range over a 20-year design life and ε_i is the range of the cyclic strain at the i^{th} load range. As an alternative the fatigue equivalent loads may be calculated as follows:

$$R_{eq} = \left[\frac{\sum (n_i R_i^m)}{N_{eq}} \right]^{(1/m)} \tag{5}$$

where R_{eq} is the equivalent fatigue load range, N_{eq} = 20*3600*8760 = 630,720,000 cycles/lifetime is based on 1 Hz cycles, and n_i is the number of lifetime cycles at load range R_i. Note that this formulation is correct only if the fatigue curve is of the form given in Equation 1 and has no endurance limit or other changes in slope. To determine life as a fraction of 20 years, apply the equation:

$$Life = \frac{1}{N_{eq}} \left(\frac{u}{A} R_{eq} \right)^{-m} \tag{6}$$

where u is the normalized (by ε_0) strain per unit load for the given part.

3.8.3 Peak Loads

Table 12 lists the characteristic peak blade bending loads at selected spanwise locations. A partial safety factor of 1.35 must be applied to the loads of Table 12 to determine the design peak bending loads.

Table 12. Summary of Characteristic Peak Blade Loads

Station/Load	Sense	1.5MW*	1.5MW	3.0MW	5.0MW
Root Flap (M_Y)	Max	4,343	3,048	8,412	18,050
	Min	-2,407	-1,658	-4,246	-9,699
Root Edge (M_X)	Max	1,367	860.4	2,977	7,624
	Min	-1,405	-1,023	-3,167	-7,701
25% R Flap (M_Y)	Max	2,569	1,791	5,022	10,680
	Min	-1,517	-1,050	-2,140	-6,214
25% R Edge (M_X)	Max	733.3	459.6	1,594	3,899
	Min	-718.3	-520.7	-1,611	-3,731
50% R Flap (M_Y)	Max	1,084	749.1	2,085	4,507
	Min	-793.4	-555.7	-1,205	-3,327
50% R Edge (M_X)	Max	262.8	170.2	636.9	1,483
	Min	-257.8	-182.7	-524.2	-1,277
75% R Flap (M_Y)	Max	243.4	175.6	466.6	1,020
	Min	-216.3	-152.2	-341.1	-926.8
75% R Edge (M_X)	Max	47.1	32.5	118.2	250.6
	Min	-44.4	-26.8	-81.3	-189.5

* 1.5 MW at specific rating = 0.31 kW/m^2

The peak bending loads of Table 12 were extracted from aeroelastic simulations including the full set of IEC load cases. In this process it was noted that the peak flapwise bending loads (M_Y) resulted from the 50-year peak gust of 59.5 m/s. For this load case the rotor is assumed to be parked in an unfaulted condition with the blades pitched to full feather. The lift generated by the vertical blade results in the peak flapwise bending loads. However, for this condition the blade tips are nominally deflecting in the rotor plane of rotation rather than toward the tower. As such, the loads of Table 12 are not appropriate for evaluating the allowable blade tip deflections.

The data from the full set of aeroelastic simulations were reviewed further. The bending loads that resulted in maximum out-of-plane tip deflections were identified and correlated with the peak bending loads of Table 12. The correlations were found to be relatively constant with blade size and spanwise location along the blade. On average, the flapwise bending loads that resulted in maximum out-of-plane deflections were about 70% of the peak bending loads. For evaluating the allowable tip deflections in the present study, the flapwise bending loads of Table 12 will therefore be multiplied by (0.7).

3.8.4 Fatigue Loads

The baseline fatigue load tables are tabulated in Appendix A. As the partial load factor for fatigue is unity, no additional factor need be applied to determine the design loads. However, in the fatigue analyses an additional 50% margin on design life is applied to account for extrapolation of fatigue cycles in the low-cycle, high-load end of the spectrum.

The edgewise fatigue loading (M_X) spectra contain contributions from torque, gravity loading, and other aeroelastic/inertial forces. Although these spectra are correct for the baseline structural design, they would be significantly in error for blade designs that have reduced gravity-induced bending loads (i.e., blades employing lighter-weight carbon materials in the blade spar). However, an approximate adjustment to the edgewise fatigue spectra can be made by subtracting the incremental change in gravity loading at each blade station.

Edgewise gravity-induced bending loads are indicated graphically in Figure 9 for both the blade root and maximum chord blade sections. At the blade root, the gravity-induced bending load is the product of the blade mass times the distance from the root to the blade center of mass (L_1). At any other blade station, the gravity-induced bending load is the product of the blade mass outboard of the selected station times the distance between the station and center of mass for the outboard blade (L_2 in Figure 9).

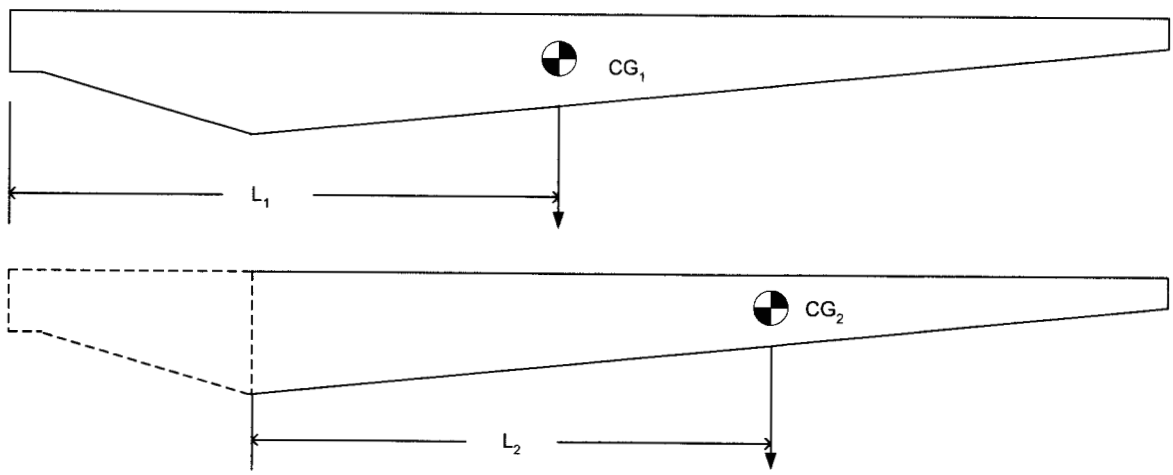

Figure 9. Edgewise gravity-induced loads at blade root and maximum chord locations

For blade designs that have mass distributions differing from the baseline blade an adjustment will be made to the edgewise fatigue loading spectra. The incremental change in gravity bending loads is approximated as:

$$\Delta M_{X,Gravity} = L_0 \cdot Mass_0 - L \cdot Mass \tag{8}$$

where

L_0 ≡ Distance between blade section and appropriate center of mass for baseline blade
$Mass_0$ ≡ Mass of baseline blade outboard of blade section under evaluation
L ≡ Distance between blade section and appropriate center of mass for the modified blade
$Mass$ ≡ Mass of modified blade outboard of blade section under evaluation

For each new design it will be assumed that the incremental change in gravity-induced loading can be subtracted directly from the appropriate edgewise fatigue spectra tabulated in Appendix A. This will be done by shifting the cycle counts to a lower load range by the amount of $2 \cdot \Delta M_{X,\,Gravity}$, rounded to the nearest multiple of the load range increment. To avoid making a non-physical adjustment, this approximation will only be applied for load ranges above the baseline gravity loads ($2 \cdot L_0 \cdot Mass_0$).

4. Preliminary Blade Designs

Preliminary blade designs were developed at two sizes, 3.0 MW and 5.0 MW. In both cases, an all-fiberglass baseline version of the blade was established, then selected portions of the spar cap were replaced by hybrid carbon fiber/fiberglass laminate.

For the 3.0 MW blade, a parametric analysis was performed to investigate varying spanwise extent of the carbon spar cap replacement. A design with a fiberglass-to-carbon spar transition at 50% span is then used to illustrate the effects of the carbon spar on the blade design criteria (static and fatigue strength, allowable tip deflections), and the effect of the carbon fatigue ε-N curve properties are investigated.

A second design was developed at 5.0 MW, again assuming a fiberglass-to-carbon spar transition at 50% span. The length of the 5.0 MW blade is 61 m, which would likely be cost-prohibitive for long-haul ground transportation. Future commercial blade designs may incorporate major spanwise joints to facilitate the manufacture and transportation of such large blades. Options for such joints were considered earlier in this project, but the preliminary design effort on the 5.0 MW blade stopped short of any substantial effort on joint designs. Nonetheless, the dimensions and loading specifications reported herein may provide some guidance into the size and loading requirements for such joints.

4.1 General Design Approach

The preliminary blade designs were developed iteratively, beginning with an initial design of the blade structure at selected spanwise stations. Each station was evaluated to determine the governing flapwise strength requirement (static or fatigue) and the blade spar was sized using the ANSYS/NuMAD codes so that the flapwise strength criteria were met. Once all blade sections were sized for flapwise strength, the resulting blade was evaluated for allowable tip deflections. If the tip deflection criterion was met, then the mass distribution was calculated and compared with the mass distribution in the baseline blade design. These data were used to adjust the baseline edgewise bending fatigue spectra (as described in Section 3.8.4) to develop bending loads that are appropriate for the new blade design. The adjusted spectra were then used to evaluate the edgewise bending strength of the blade sections. If necessary, additional reinforcement was added to blade sections to ensure the edge bending strength requirements were met. Once the design of the blade sections was converged, an ANSYS model was developed in which the blade sections are connected in a complete 3-dimensional blade.

4.2 3.0 MW Blade

4.2.1 Spanwise Extent of Spar Modifications

The 3.0 MW blade design was developed in two stages. First, an all-fiberglass version of the blade was developed and analyzed using the spar material #2 of Table 7. The design calculations were carried out at spanwise stations of 5%, 7%, 25%, 50%, 75% and the blade tip. Next, the 25%, 50% and 75% span sections were redesigned substituting a carbon hybrid spar cap (material #4 of Table 7) for the original fiberglass spar.

The resulting blade section designs were used to perform a parametric analysis to evaluate the sensitivity of design parameters to the spanwise extent of the carbon spar. Figures 10 through 12 illustrate the results. The x-axis of each plot indicates the extent of the "spar modification" modeled. Zero percent modification represents the baseline blade with an all-fiberglass spar cap. The spar modifications were

assumed to occur from the blade tip inward, so a 25% spar modification implies that the outer quarter of the blade spar is carbon/fiberglass hybrid, 50% modification implies the outer half of the blade is carbon hybrid, and so on.

Figure 10 shows the mass of carbon fiber used and the value of the gravity-induced root bending moment, both as functions of the carbon spar extent. Note that the gravity-induced component of root bending is primarily oriented in the edgewise direction of the blade structure. As would be expected, the mass of carbon fiber mass used increases, and the gravity-induced bending loads decrease as the carbon spar is extended inward along the blade span.

Figure 11 shows the percentage change in gravity-induced root bending moment (Δ root moment), and also the "normalized" Δ root moment, where the normalization represents the percentage change per 100 kg of carbon fiber used. The figure shows that the greatest reduction in gravity-induced bending loads per unit carbon is realized for a carbon spar extending from the tip to mid-span. If the spar were carried farther inboard, the reductions in total blade mass would be large, but because the distance to the root section is also decreasing, the mass reductions have a diminishing effect on the gravity-induced moments.

Figure 12 shows a similar trend for changes in tip deflection as a function of carbon spar extent. Again, the greatest reductions in deflection per unit carbon are shown for a carbon spar cap that spans the outer half of the blade.

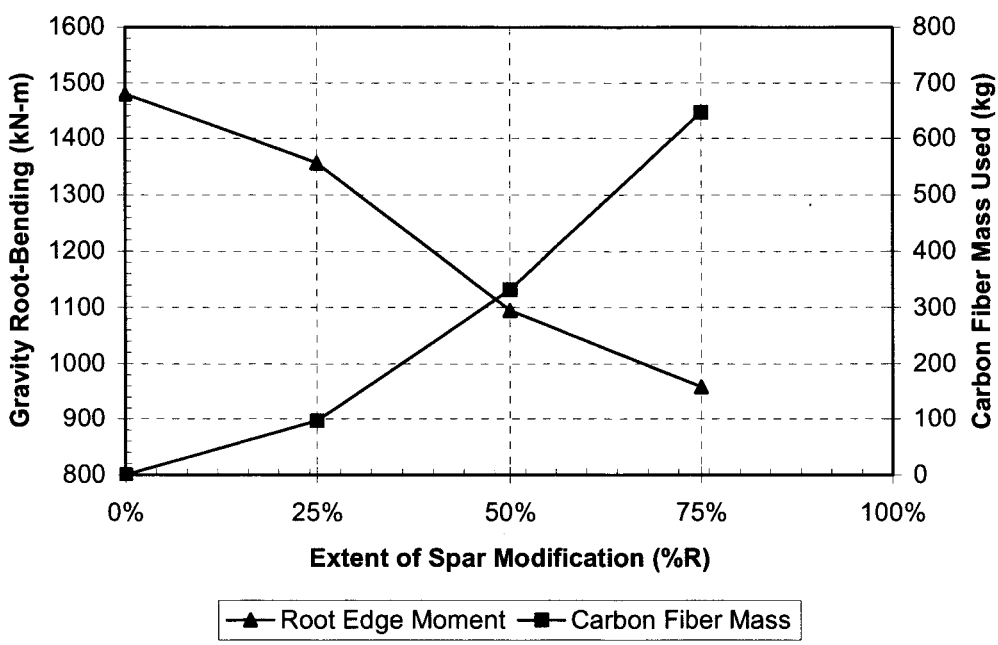

Figure 10. Gravity bending moments and carbon usage

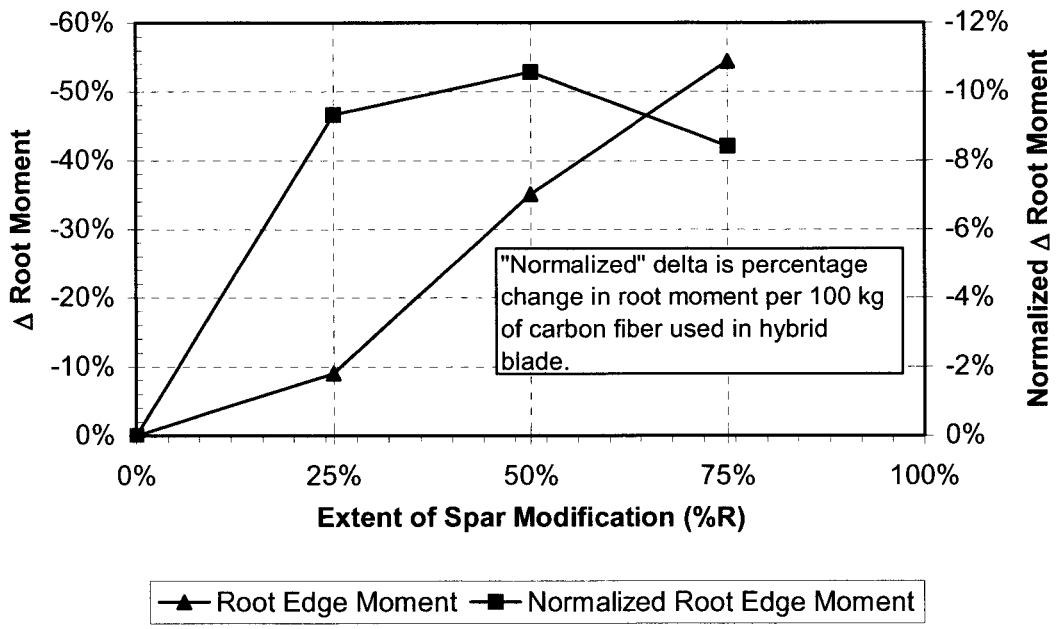

Figure 11. Effect of carbon spar spanwise extent on root gravity bending moments

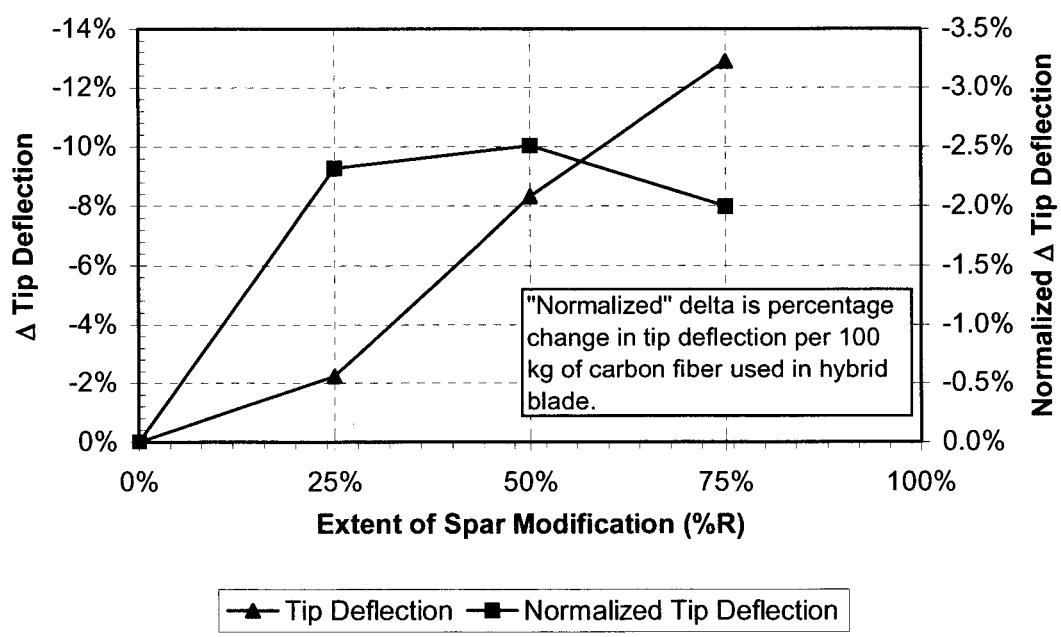

Figure 12. Effect of carbon spar spanwise extent on blade tip deflections

The results shown in the above figures are dependent on the selected initial blade geometry, structural design and mass distribution, and the optimal use of carbon fiber in hybrid blade spars will vary with the details of the blade and rotor system design. Although the trends described are valid, there are significant challenges to designing a carbon-to-fiberglass spar transition that is structurally efficient and cost-effective to manufacture. One issue in a spar transition is the mismatch between the carbon and fiberglass ply stiffness and strain-to-failure. Another concern is maintaining straightness in the carbon plies for preserving static compressive strength. The following sections present 3.0 MW and 5.0 MW blade designs that assume a mid-span transition from fiberglass to carbon hybrid spar caps. Further discussion on the challenges of designing such a transition is presented in Section 4.4.

4.2.2 3.0 MW Blade with Fiberglass-to-Carbon Spar Transition

Table 13 lists the design margins for static and fatigue strength at each spanwise section for both the fiberglass and fiberglass/carbon hybrid blade designs. Shaded entries indicate that a margin is at or near governing. Compressive, tensile, and "reversed" margins correlate, respectively, to the upper, lower, and trailing edge regions of the blade sections.

In terms of strength, static compression governs the inboard region of the all-fiberglass blade. At mid-span the design is critical in both compressive static and fatigue strength, and at 75% span the fiberglass section is governed by compressive fatigue strength. The all-fiberglass blade design also has a negative 5.5% margin on allowable tip deflection (not shown in the table). Although the negative margins on edgewise bending and tip deflection could be remedied by selective use of additional fiberglass materials, the substitution of a carbon hybrid spar in the outer blade can also be used to increase blade stiffness and decrease gravity-induced bending loads.

Table 13. Design Strength Margins for 3.0 MW Fiberglass/Carbon Hybrid Blade

Blade	Station	Static Margins (%)		Fatigue Margins (% Strength)		
	(% R)	Comp.	Tens.	Comp.	Tens.	Reversed
Fiberglass	Root	0.4	158	13.0	25.6	35.1
"	25% R	0.2	149	16.2	25.7	-5.3
"	50% R	-0.4	145	0.8	14.5	34.7
"	75% R	10.5	168	0.1	10.0	262.3
Fiberglass/Carbon Hybrid	Root	0.4	158	13.0	25.6	50.4
"	25% R	0.2	149	16.2	25.7	7.3
"	50% R	0.6	44	43.5	139.8	51.3
"	75% R	-0.2	41	24.7	106.3	266.0

The lower half of Table 13 shows the strength margins for the 3.0 MW blade with a fiberglass-to-carbon transition at mid span. The root and 25% span sections are structurally unchanged from the all-fiberglass design as reflected by the flapwise margins (compression and tension). However, due to the reduced mass in the outboard part of the blade the edgewise bending margins are improved over the entire blade span and the margin at the 25% station is increased from -5.3% to +7.3%. The margin on tip deflection is also increased from -5.5% to +2.5% (not shown in the table). In the outer blade span the governing criterion has shifted from compressive fatigue to compressive static strength.

Figure 13 shows an example stress-contour plot from the ANSYS model of the complete 3.0 MW blade with a fiberglass-to-carbon hybrid transition at 50% span. The hybrid blade design resulted in a 16% mass reduction (9790 to 8235 kg) and a 26% reduction in gravity-induced root bending moment (1480 to 1095 kN-m) relative to the fiberglass blade.

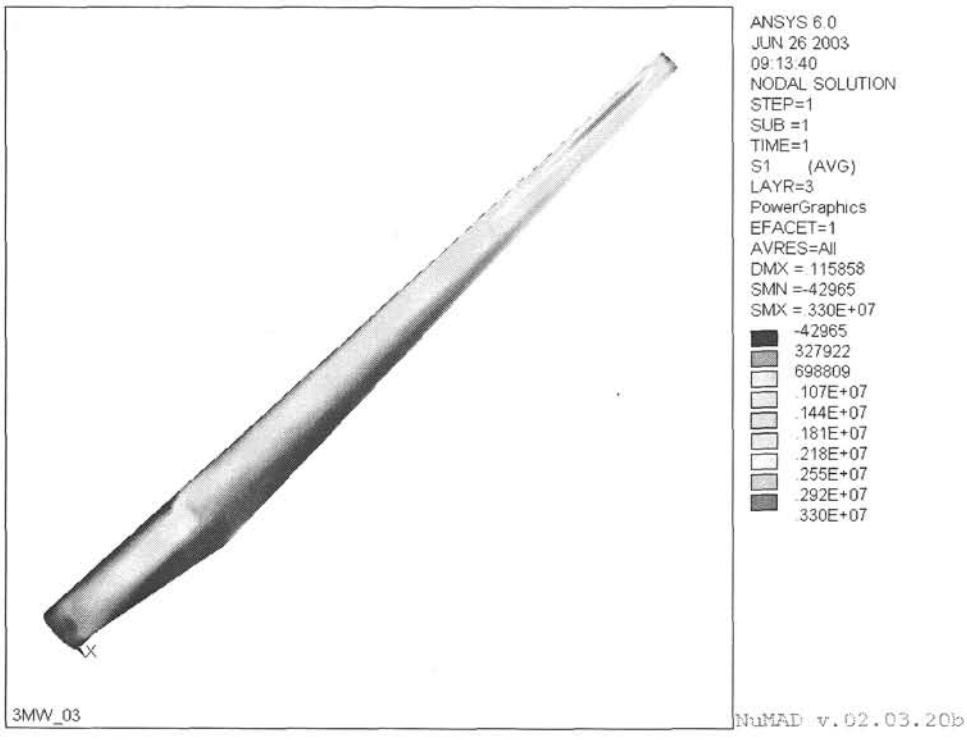

Figure 13. ANSYS stress contours for 3.0 MW blade with fiberglass /carbon transition at mid-span

At 50% and 75% span the carbon hybrid blade sections show large positive margins in both tensile and compressive fatigue. This result might be predicted by reviewing the large ε-N curve slope parameter values attributed to the carbon hybrid material. Table 8 shows these values as $m = 48$ for tension-tension and $m = 28$ for compression-compression loading. Flat ε-N curves are a well-recognized characteristic of carbon fiber composites; however, this attribute also makes experimental verification of the fatigue properties difficult.

4.2.3 Effect of ε-N Curve Parameters

A parametric analysis was performed to investigate the sensitivity of the fatigue life calculation to the value of ε-N slope parameter used. The results are shown in Figure 14. For the 50% span blade section the ε-N slope values were systematically adjusted until the fatigue life margins approached zero. The figure shows that the design margins remained positive for m values of 12 and 16, respectively, for tensile and compressive fatigue. Note that in this analysis the coefficient A in Equation 1 was held constant, so the results shown are conservative (assuming a fixed ε-N data set, curve-fitting with a lower value of slope parameter would result in a higher value of the coefficient A).

This analysis indicates that fatigue of the basic carbon laminate is unlikely to govern the design of fiberglass/carbon blade spars, even if significantly lower slope values that those of Table 8 are used. It appears more likely that details such as ply drops, bonds, and fiberglass-to-carbon transitions will be the fatigue-critical elements of a hybrid blade.

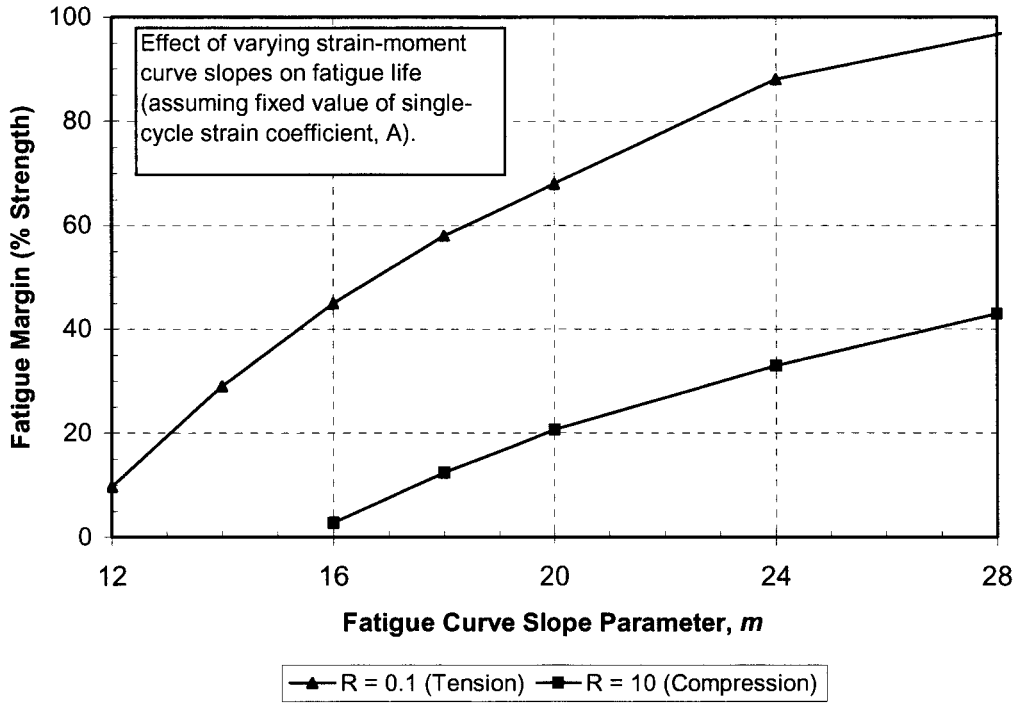

Figure 14. Effect of ε-N slope parameter on calculated fatigue strength

Table 14 summarizes the spar cap geometry for the 3.0 MW blade design. The ply number was approximated assuming an average ply thickness of one millimeter. For the 50% span station, dimensions are given for both an all-fiberglass and a carbon hybrid spar. A mid-span transition from a fiberglass to carbon spar would therefore represent an approximate halving of the spar cap thickness.

Table 14. Spar Cap Geometry for 3.0 MW Fiberglass/Carbon Hybrid Blade

Blade Section	Spanwise Location (m)	Spar Cap Dimensions		Approximate # of Plys
		Width (mm)	Thickness (mm)	
25% R, Fiberglass	12.4	1385	39.7	40
50% R, Fiberglass	24.8	1060	40.8	41
50% R, Carbon Hybrid	24.8	910	18.3	18
75% R, Carbon Hybrid	37.2	630	7.0	7

4.3 5.0 MW Blade

A second design was developed at 5.0 MW, again assuming a fiberglass-to-carbon spar transition at 50% span. The overall design approach used was the same as for the 3.0 MW blade. All of the trends illustrated and discussed in Figures 10 through 12 and Table 13 were found to be qualitatively the same for the 5.0 MW blade, and are therefore are not repeated in this section. Table 15 summarizes the spar cap geometry for the 5.0 MW blade design, again showing spar cap dimensions for both fiberglass or a carbon hybrid spar cap replacement at mid-span.

The length of the 5.0 MW blade is 61 m, which would likely be cost-prohibitive for long-haul ground transportation. Future commercial blade designs may incorporate major spanwise joints to facilitate the manufacture and transportation of such large blades. Options for such joints were considered earlier in this project, but the preliminary design effort on the 5.0 MW blade stopped short of any substantial effort on joint designs. Nonetheless, the dimensions in Table 15 and the loading specifications given in Section 3.0 may provide some guidance into the size and loading requirements for such joints.

Table 15. Spar Cap Geometry for 5.0 MW Fiberglass/Carbon Hybrid Blade

Blade Section	Spanwise Location (m)	Spar Cap Dimensions		Approximate # of Plys
		Width (mm)	Thickness (mm)	
25% R, Fiberglass	16.0	1790	51.5	52
50% R, Fiberglass	32.0	1370	55.9	56
50% R, Carbon Hybrid	32.0	1175	24.0	24
75% R, Carbon Hybrid	48.0	820	12.1	12

The preliminary designs presented in the previous sections were developed to illustrate and quantify some major trends concerning MW-scale blades in general and the potential inclusion of carbon fiber materials in particular. State-of-the-art methods (international design standards, ADAMS simulations, ANSYS structural analyses) were used, and several design criteria were considered. However, these designs are preliminary in several respects and several simplifying assumptions have been made in this process. As a result, the designs presented should not be taken as accurately representing the details of a blade that is designed for optimal structural performance or manufacturing.

4.4 Design/Manufacturing Issues for Spar Transition

As shown in the previous section, carbon fiber spars appear to be of greatest advantage for reducing gravity-induced bending loads and tip deflections when located in the outer blade span. The option exists for extending the load-carrying carbon laminate all the way to the root plane, but that brings its own challenges. For instance, the thermal expansion coefficients for fiberglass and carbon are substantially different. If large regions of both materials exist at the root plane, then temperature variations would cause warping stresses at the root-hub interface. An all-carbon root region would solve this problem, but would likely be expensive relative to the fiberglass alternative. These considerations provide the motivation for transitioning the load-bearing carbon laminate into an all-fiberglass structure at some point along the spar. However, there are significant challenges to designing a fiberglass-to-carbon spar transition that is structurally efficient and cost-effective to manufacture.

One issue in a spar transition is the mismatch between the carbon and fiberglass ply stiffness and strain-to-failure. The most simple ply transition coupon would be one with a single butt-joint between the dissimilar plies. However, this is not likely to be a favorable option from either a manufacturing or structural performance standpoint, and so that arrangement is not depicted herein. In any approach, maintaining straightness in the carbon plies will be desirable for preserving static compressive strength.

For reference, Figure 15 depicts a candidate spar cap design with a fiberglass-to-carbon transition. The thickness scale of these figures correctly reflects the assumption that carbon layers are 1.0 mm thick whereas the fiberglass layers are 1.25 mm thick. The horizontal scale has been compressed to show the complete transition. The transition dimensions were developed assuming materials #2 (fiberglass) and #4 (carbon hybrid) as described by Table 7. As a result of the stiffness and compressive design strain, a 2.5-to-1.0 ratio of fiberglass-to-carbon laminate thickness is required in regions where both materials are

present. Because the fiberglass materials have larger design strains than the carbon, one of the fiberglass layers is shown as being dropped following the transition region. The ratios shown are only valid for specific combinations of material and design strains, and could be higher or lower for alternate materials.

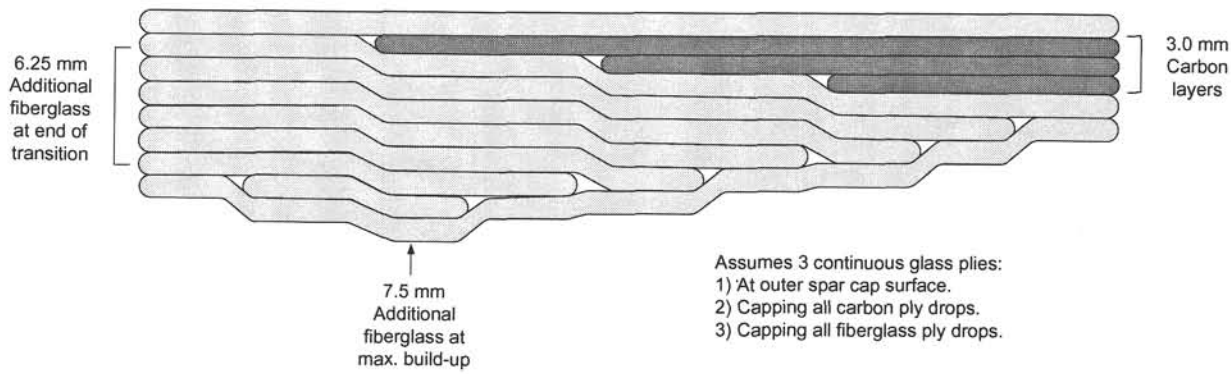

Figure 15. Example candidate fiberglass-to-carbon spar transition

5. Recommendations for Testing Under Part II BSDS

5.1 Summary of Candidate Test Laboratories

Both the MSU Composite Technologies Research Group and the National Wind Technology Center (NWTC) have long-established experience and capability in testing composite materials and turbine structure. It is expected that material coupons and small sub-structures can be economically tested at the MSU Laboratories, and large structural members and sub-scale blades could be tested at the NWTC Blade Test facility. In addition to these laboratories, GEC has identified and evaluated a number of additional organizations that can help support the testing of coupons and substructures. These organizations are capable of providing additional test capacity and possibly to assist on related design, fabrication and analytical activities as needed.

GEC investigated more than 20 composite testing organizations in addition to MSU and the NWTC. Each organization was evaluated for their capability to perform composite testing in support of the Part II BSDS project. Cost estimates for standard ASTM D3039 static coupon tension tests, including mounting supplied strain gauges, were requested from several labs. Straight as well as tapered and tabbed coupon preparation costs were also requested when available. In addition to testing capabilities, several other criteria were used to evaluate each lab, including:

- interest and availability to work on the program,
- experience and capability in test design and results interpretation,
- ability to offer additional services such as design assistance and fabrication,
- ease of travel for GEC and Sandia personnel,
- lead times, and
- cost.

Full-service organizations that can offer panel and specimen fabrication, design services and results interpretation assistance are favored over labs specializing in only one type of test. Especially for blade component and sub-scaled blade tests, assistance from the test lab in developing the test plan and methodology will be of great value. Of the labs investigated, those that offer a full range of services were not consistently more expensive. Therefore, no economic gain was identified by using the more narrowly focused organizations.

Laboratories that were found to offer services that are compatible and complementary to those of MSU and the NWTC include Integrated Technologies Inc. (Intec), the National Institute for Aviation Research (NIAR) at the Wichita State University, and the Center for Composites Materials (CCM) at the University of Delaware. Of these, Intec was found to have the best combination of price, capability and experience. Other advantages of Intec include proximity to GEC's offices and the ability to support test design, fabrication of test articles, and analysis. Initial testing under this program is planned for Intec. However, other university and private laboratories will be considered and recommended as needed to meet the project test objectives within the planned budget and schedule. The following sections provide brief summaries of the test capabilities and experience of the MSU, NWTC and Intec laboratories.

5.1.1 Montana State University

Montana State University, located in Bozeman, is a full-service testing and analysis laboratory. Their capabilities include manufacturing, test design/development and post-test analysis. Although primarily

set up to perform static and fatigue tests on standard coupons, their abilities include hot-wet testing, 3- and 4-point bending and larger structure testing under tension, compression, shear and bending.

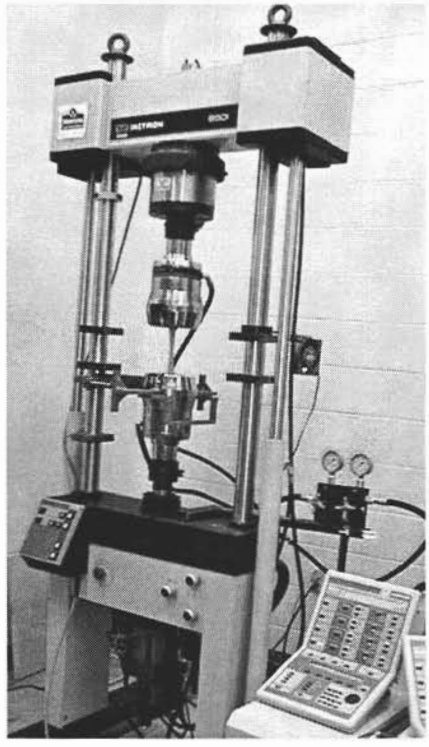

Figure 16. Instron 8501 servo-hydraulic testing machine at MSU

Montana State University's testing capabilities include:

- General
  - 4 universal servo-hydraulic testing machines
  - 2 universal servo-electric testing machines
  - multiple actuators for use on a 6.4 m x 14.6 m (21 ft x 27 ft) structural testing platform

- Static Testing
  - Maximum loads – tension 890 kN (200 kips), compression 1335 kN (300 kips)
  - Maximum displacement – 914 mm (36 inches)
  - Displacement/stiffness/strain measurements

- Fatigue Testing
  - Uniaxial, maximum 245 kN (55 kips),
  - Maximum displacement – 254 mm (10 in)
  - Testing frequencies – static to 100 Hz
  - Hydraulic flow capacity – 87 LPM (23 GPM)

5.1.2 National Wind Technology Center

The National Wind Technology Center is capable of testing MW-scale wind turbine blades in their specially built laboratory shown in Figure 17. Static testing is performed by applying progressive multiple spanwise loads using a whiffle-tree arrangement. Fatigue testing is performed by applying an

alternating load at one specified spanwise location with one or two actuators. The NWTC is also capable of testing blade components, such as root structures, at ambient, hot/wet and other conditions.

Figure 17. NWTC blade testing facility

NWTC testing capability includes:

- General
  - Three test bays
  - Length capacity – 34 meters (IUF Bay)
  - A2LA accredited
  - Testing conforms to IEC or GL
  - Non-destructive evaluation
- Static Testing
  - Maximum load – 5.4×10^3 kN-m (4×10^3 ft-kips)
  - Hoist capacity – 310.8 kN (70 kips)
  - Displacement/stiffness/strain measurements
  - Modal property measurements
- Fatigue Testing
  - Maximum load 168.7 kN (38 kips)
  - Maximum displacement – 1.52 m (60-in)
  - Hydraulic flow capacity – 684 LPM (180 GPM)

5.1.3 Integrated Technologies Inc.

Integrated Technologies Inc. (Intec), located in Bothell, Washington, is a full service composites design and testing laboratory. Intec is located approximately 12 miles from GEC's offices in Kirkland, Washington. Their capabilities include test design/development and assisting in test result interpretation.

Intec routinely fabricates composite panels and prepares coupon and component test articles. In addition to coupon testing, they are capable of testing components or sub-scaled blades up to approximately 12 m (39.4 ft) in length. They have performed aircraft wing and winglet structural tests for the aerospace industry (Figure 18). Their standard strong back will accommodate approximately 60 kN-m of maximum bending load. They have built larger structures to accommodate higher loads when necessary in the past. They are one of the few labs identified to have existing cantilever testing capabilities.

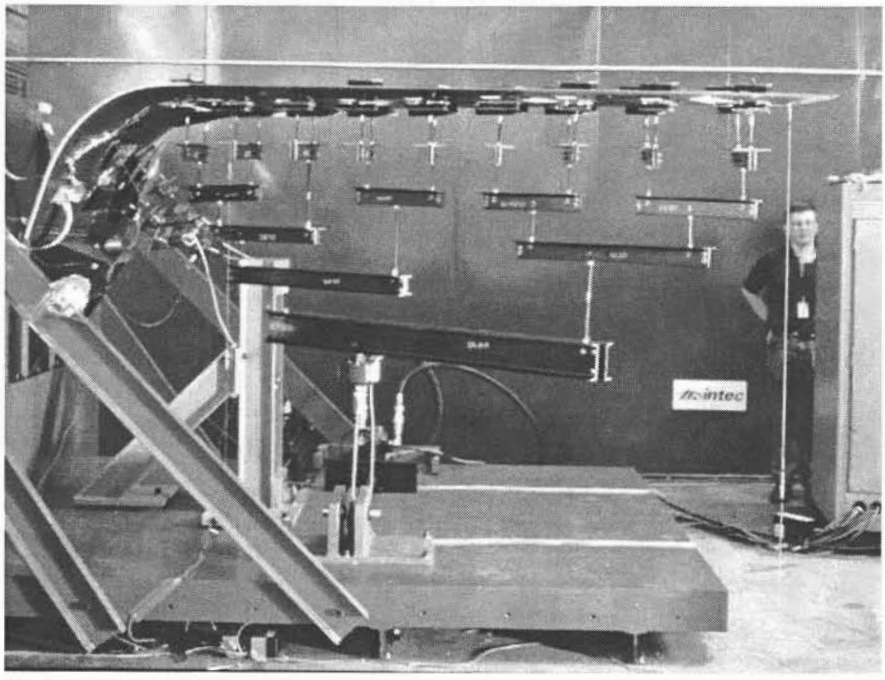

Figure 18. Boeing 737 winglet structural testing at Intec

With the exception of near full-scale blade testing, Intec appears capable of providing most test services that will be required for this program. Intec also expressed willingness to fabricate test panels, coupons or fixtures to be tested elsewhere. Intec's relevant test capabilities include:

- General
  - Multiple strong backs and load floors
  - Damage growth detection (acoustic, crack growth)
  - Over 500 channels of data acquisition
- Static Testing
  - Multiaxial, 0.5 N to 1.11×10^4 kN (0.11 Lb to 2500 kips)
  - Bending, 60 kN-m up to 12 m test article length
  - Multi-tier whiffle tree loading
- Fatigue Testing
  - Multiaxial, 0.5 N to 1023 kN (0.11 Lb to 230 kips)

5.2 Planned Test Matrix

This section discusses the development and prioritization for testing planned under the Part II BSDS. Further discussion of the technical issues to be investigated in the test program is provided in Section 5.3.

Table 16 shows the full matrix of candidate tests for the Part II BSDS, organized according to technical issues and type of tests proposed to investigate and resolve each issue. A numeric scale indicates the relative priority assigned to each test, with a rank of 1 corresponding to the highest priority and 5 indicating the lowest. The priority rankings were developed during the discussions held at the BSDS Part 1 Project Design Review Meeting, held at Sandia on June 11-12, 2002. Table 16 also provides an alphabetic identifier (I.D.) for each candidate test, which correlates to the test matrix breakout in the following table.

Table 17 shows a summary of the initial testing planned under this program, with the number of tests and other assumptions for each type. The tests selected for this matrix, and the number of each test type, were developed to be consistent with the priority assignment shown in Table 16, the planned budget, and with the range of materials and design details of interest.

Table 16. Complete Candidate Test Matrix (as developed at BSDS Part 1 Design Review Meeting)

Issues	Thin Coupon		Thick Laminate		4-Point Beam Bending		Biased Material Cylinder		Margins/ Safety Factors	Lap Shear
	Static	Fatigue	Static	Fatigue	Static	Fatigue	Static	Fatigue		
Materials:										
1) Large tow carbon, VARTM & prepreg	2 / A	5 / B							4 / R	
2) Moderate tow carbon, VARTM & prepreg	2 / A	5 / B							4 / R	
3) Carbon/glass hybrid fabric (MMWK), VARTM, large tow	1 / A	1 / B	1 / G		3 / J	4 / K			4 / R	
4) Carbon/glass hybrid fabric (MMWK), VARTM, mod. tow	1 / A	1 / B	1 / G		3 / J	4 / K				
5) Dry carbon uni + glass biax, VARTM, large tow	1 / A	1 / B	1 / G		3 / J	4 / K				
6) Dry carbon uni + glass biax, VARTM, mod. tow	1 / A	1 / B	1 / G		3 / J	4 / K				
7) Prepreg carbon uni + prepreg glass biax, large tow	2 / A	1 / B	1 / G		3 / J	4 / K				
8) Prepreg carbon uni + prepreg glass biax, mod. tow	2 / A	1 / B	1 / G		3 / J	4 / K				
9) P4A oriented discontinuous carbon	5 / C	5 / D								
10) "Anti-fatigue" resin, toughened VE	5 / A	5 / B								
Transitions:										
11) Carbon-to-glass (single ply)	2 / E	2 / F								
12) Carbon-to-glass (multiple plies)			2 / H	2 / I	4 / L	4 / M			4 / R	
13) Spar cap design concepts					3 / L	4 / M			4 / R	
14) Ply drops in carbon / glass hybrid	2 / E	2 / F	2 / H	2 / I	4 / L	4 / M			4 / R	
Other:										
15) Bend-twist (biased hybrid) materials							3 / N	3 / O		
16) Bonding compounds										5 / S
17) As-manufactured laminate properties			3 / P	4 / Q						

Key: Letters A - S denote cost category ID (see following table)
Numbers denote priority;
1 = Essential
2 = Very important
3 = Important
4 = As funding allows
5 = Not worth spending program resources on

Table 17. Initial Matrix for Planned Part II BSDS Testing

ID	Test	Assumptions	# of Tests
A	Thin coupon, static	5 tensile, 5 compressive	10
B	Thin coupon, S-N curve to 10^6 cycles (single R value)	4 ea. at 3-4 stress levels	4
B*	Add S-N data to 10^7 cycles (single R value)	4 ea. at 10^7 stress level	0
C	Thin P4A coupon, static	5 tensile, 5 compressive	0
D	Thin P4A S-N curve to 10^6 cycles (single R value)	5 ea. at 3-4 stress levels	0
E	Thin coupon with single ply drop / transition, static	5 tensile, 5 compressive	4
F	Thin coupon with single ply drop / transition, S-N to 10^6	4 ea. at 3-4 stress levels	4
G	Thick laminate, static compression	5 specimens	4
H	Thick laminate with transition or ply drops, static	5 specimens	4
I	Thick laminate with transition or ply drops, S-N to 10^6	4 ea. at 3 stress levels	4
J	4-point beam with uniform cap laminate, static	Single article to failure	1
K	4-point beam with uniform cap laminate, fatigue	Single article to 10^6	0
L	4-point beam with cap laminate details, static	Single article to failure	1
M	4-point beam with cap laminate details, fatigue	Single article to 10^6	0
N	Biased material tube in axial / torsion loading, static	5 specimens	2
O	Biased material tube in axial / torsion loading, fatigue	4 ea. at 3 stress levels	1
P	Thick laminate + defects in static compression	5 specimens	3
Q	Thick laminate + defects in fatigue	4 ea. at 3 stress levels	0
R	Determine margins / safety factors	See report text	0
S	Lap shear tests of bonding compounds	Low priority, not costed	0

5.3 Discussion of Candidate Tests/Technical Issues

The following sections provide additional context and background information for the matrix of testing planned under the Part II BSDS.

5.3.1 Material Types

Table 16 lists several items under the general heading of "materials." Items that were assigned high priority include large and moderate tow size carbon fiber, prepreg and vacuum-assisted resin transfer molded (VARTM) infusion, and hybrid carbon-fiberglass multi-layer multi-axial warp knit (MMWK) fabric. In addition to a hybrid MMWK fabric, dry carbon unidirectional fabric with thermoplastic bead adhesion is a material form of high interest. It is assumed that coupons to evaluate Materials #1 and #2 in Table 16 (large and moderate tow carbon in VARTM and prepreg forms) will be primarily unidirectional carbon, with fiberglass facings. Materials #3 to #8 presume coupons that have interspersed layers of unidirectional carbon and off-axis glass as would be expected in a hybrid blade spar build-up.

It is expected that for a given fiber, laminate manufactured with prepreg resin will have the best static and fatigue strength. As a result of induced waviness and other details, dry fabrics that are then infused by VARTM are expected to have lower strength performance. However, prepreg materials have historically been more expensive and require higher cure temperatures than liquid epoxy resin systems. Currently, the majority of turbine blade manufacturers use a "wet" process, either VARTM or an open mold layup and impregnation. Dry layup of preforms and subsequent infusion therefore remains as a process of high interest for the wind industry.

To address this issue, the proposed Part II BSDS testing will seek to answer several questions: What is the best strength performance that can be obtained by combining commercial carbon fibers in a low-cost fabric/preform process with VARTM infusion? How do the strength and estimated production costs

compare with prepreg versions of corresponding fibers? Is the performance/cost ratio better for large or moderate tow fibers? What combinations appear to be the most cost-effective?

To answer these and other questions, the Part II BSDS program will use a building-block approach, beginning with thin coupon testing for a wide range of material types, fabric architectures and processes, then moving to thick coupon and sub-structure testing for a reduced set of material/process options.

5.3.2 Thin Coupon Testing

Figure 19 shows the typical coupon geometries used for thin coupon testing. The maximum coupon thickness, with tabs, is 11.4 mm, which is the maximum grip opening of the hydraulic wedge grips. The standard maximum width of hydraulic grips is 51 mm. Typical coupon thickness without tabs is approximately 2.5 mm.

Fiber content and percent zero degree fibers in the load path determine which coupon geometry will be tried first. If acceptable (gage section) failures occur, the geometry is not altered; if the failures are not as desired, the geometry is changed until the failure mode is acceptable. For tensile static testing a standard rectangular coupon typically works well. For fatigue and compressive static testing, more care needs to be taken to achieve the desired failure modes. This test challenge is expected to increase as the coupons contain larger tows, heavier fabrics and stiffer fibers.

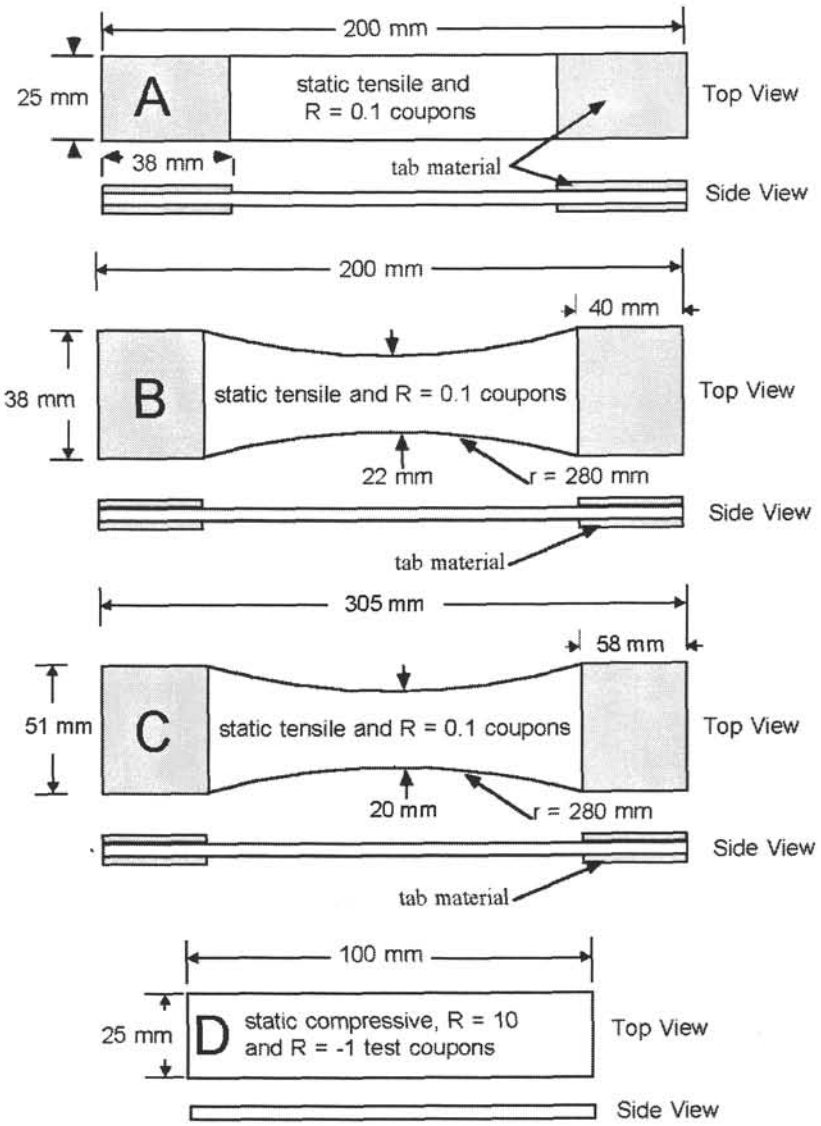

Figure 19. Typical test coupon geometries

5.3.3 Thick Laminate

Thick laminate tests are expected to be of value to evaluate several technical issues. The first is simply thickness scaling of basic carbon/hybrid spar cap laminate. In laminate with perfect fiber alignment, some increase in compressive strength may be expected as the thickness increases. However, the thicker laminate will also include a greater distribution of naturally occurring material defects than the smaller coupons, and also a greater opportunity for fabrication-related irregularities. Given the relatively large strand size of commercial carbon fibers and the heavy-weight fabrics in use for large blades, some investigation of basic thickness effects is planned.

Thick laminates can also be used to investigate details that are not amenable to testing in thin coupons. Examples in the current test matrix are multiple ply drops, multiple ply transitions, and as-manufactured laminate properties (effects of defects).

Table 18 shows a calculation of coupon dimensions for several values of maximum load and target strain levels. The calculations were performed for an axial modulus of Ex = 74.3 GPa, which corresponds to the upper end of the expected range for carbon/fiberglass hybrid laminates of interest. The calculations also assume a coupon aspect ratio (width-to-thickness) of 3.

At the Intec facility, available frame sizes are 20, 50 and 220 kips. For static testing of "thick" specimens, the 220 kip frame is assumed. For fatigue testing of "thick" specimens, the 50-kip frame is assumed. Inspection of the values in Table 18 indicates that these frame sizes should be sufficient to meet the anticipated size range of interest for this test program. The larger technical challenge will be obtaining proper load introduction and gage-section failures for the thick test articles. In all the cost-planning for this project it is assumed that "thin" coupons will be sized for testing on a 20-kip load frame.

Table 18. Sizing Chart for Laminate with Ex = 74.3 GPa (coupon aspect ratio = 3)

P_{max}			t		W	
(kips)	(kN)	ε_{max} (%)	(mm)	(inch)	(mm)	(inch)
20	89.0	1.2	5.77	0.23	17.3	0.68
20	89.0	1.0	6.32	0.25	19.0	0.75
20	89.0	0.8	7.06	0.28	21.2	0.83
20	89.0	0.6	8.16	0.32	24.5	0.96
50	222.4	1.2	9.12	0.36	27.4	1.08
50	222.4	1.0	11.17	0.44	33.5	1.32
50	222.4	0.8	11.71	0.46	35.1	1.38
50	222.4	0.6	12.90	0.51	38.7	1.52
110	489.3	1.2	13.52	0.53	40.6	1.60
110	489.3	1.0	14.82	0.58	44.4	1.75
110	489.3	0.8	16.56	0.65	49.7	1.96
110	489.3	0.6	19.13	0.75	57.4	2.26
220	978.6	1.2	19.13	0.75	57.4	2.26
220	978.6	1.0	20.95	0.82	62.9	2.48
220	978.6	0.8	23.43	0.92	70.3	2.77
220	978.6	0.6	27.05	1.06	81.1	3.19

5.3.4 Ply Drops and Transitions

Analyses performed under the BSDS and recent results from parallel European research efforts indicate that bulk replacement of load-bearing fiberglass laminate with commercial carbon fibers is a cost-effective option for MW-scale blades. Work under the BSDS and other research further indicates that the structural benefit (i.e., reduced gravity loads and tip deflections) per unit mass of carbon used is greatest in the outer portion of the blade span. However, work to date has not addressed the effect of ply drops in carbon spar structure or the implications of carbon-to-fiberglass transitions in a blade spar.

It is expected that ply drops in load-bearing carbon spars will cause a greater decrease in fatigue strength than in an equivalent fiberglass structure. This is due to the fact that the carbon fibers are more highly loaded than the fiberglass and as a consequence will shear a higher load per unit area into the resin-rich region at the ply termination. An additional effect may be due to any waviness or jogs that are introduced in the remaining carbon plies as a result of the ply drop. The latter effect is illustrated in Figures 20 through 24. In all of the following coupon sketches, the carbon and fiberglass layer thicknesses are drawn to scale, but the length scale shown does not necessarily represent dimensions and spacing that would be used in an actual test article. In all cases, the "carbon" layers could be either pure unidirectional fabric/tape or a hybrid construction of unidirectional carbon fibers and off-axis fiberglass.

Note that in all of Figures 20 through 26, the coupon geometries shown are balanced (symmetric about the center plane" to ensure that they are suitable for testing in a standard axial loading fixture. It is expected that coupon testing of such specimens will allow evaluation of the dominant material performance features for ply drops and ply transitions. However, the double-sided taper employed by these specimens to achieve symmetry is not likely to be feasible from a cost and manufacturing viewpoint in an actual blade spar. Feasible spar designs for actual blades will likely have ply drops and/or transitions that result in unbalanced laminate. Such designs are discussed in Section 3.4.

Figure 20 shows a candidate thin coupon with a single internal ply drop. The figure shows that all surrounding carbon plies will have a jog or induced waviness at the ply drop location. It is expected that such a jog in fiber alignment would be detrimental to both the static and fatigue strength of the laminate, and that this effect would be more pronounced for carbon fiber materials than for equivalent fiberglass laminate. Figure 21 shows a coupon where the carbon layers are allowed to remain straight by moving the ply drops to the outer region of the carbon layers.

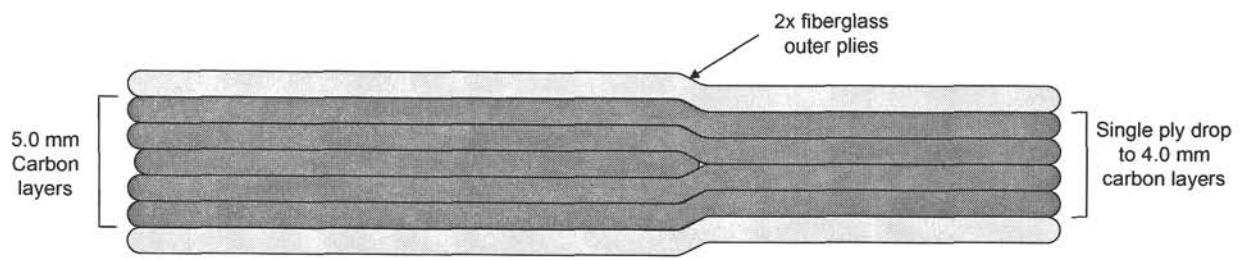

Figure 20. Internal carbon ply drop (single ply, nominal ply thickness)

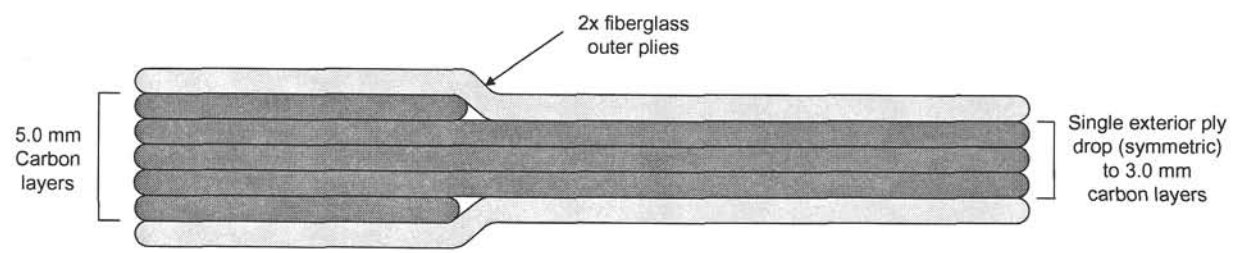

Figure 21. External carbon ply drop (nominal ply thickness)

Both Figures 20 and 21 use a nominal carbon ply thickness of 1.0 mm. This value was selected to represent relatively heavy fabric weights of practical interest for MW-scale blades. Figure 22 shows a coupon with overall geometry corresponding to that of Figure 21, but assumes that the carbon ply thicknesses are one half of the nominal 1.0 mm value. The technical issue at hand is the trade-off

between the increase in processing/handling efficiency of blade construction and the decrease in fatigue performance at ply drops which would be expected for the thicker carbon plies.

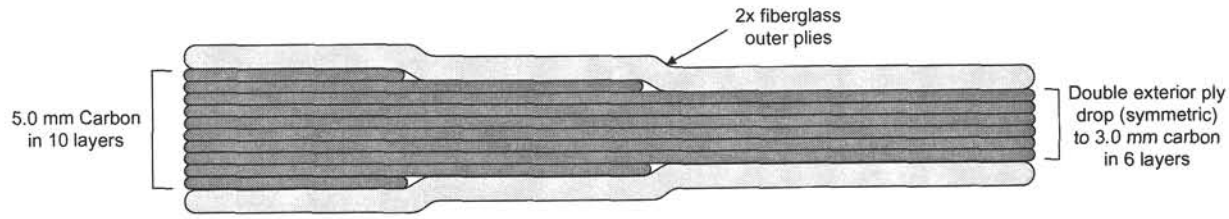

Figure 22. External carbon ply drop with 0.5 mm thick plies

Figures 20 through 22 have overall dimensions that are expected to be practical for a "thin" coupon (note that two plies are the minimum number that can be dropped in an external arrangement while preserving symmetry). Figures 23 and 24 show dimensions representing "thick" specimens, with 1.0 mm and 0.5 mm ply thickness variants. These figures represent multiple internal ply drops. Not shown are candidate test articles for thick coupons with multiple external ply drops.

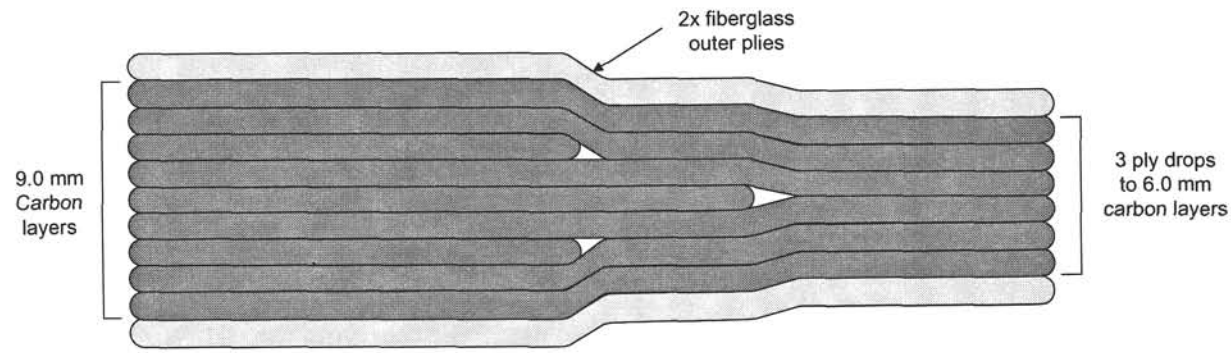

Figure 23. Internal carbon ply drop (multiple plies)

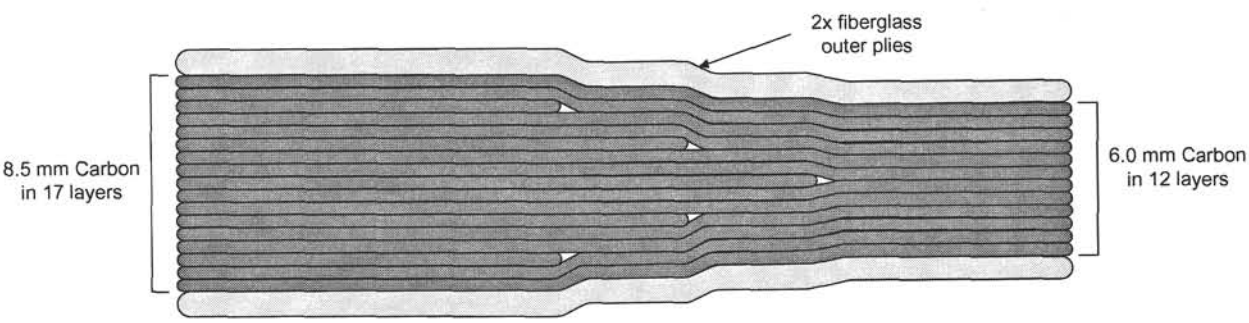

Figure 24. Multiple internal ply drops with 0.5 mm thick plies

In general, carbon-to-fiberglass ply transitions have all of the technical considerations of carbon ply drops (i.e., sensitivity to carbon layer straightness and ply thickness). However, ply transitions also add the consideration of mismatch between the carbon and fiberglass ply stiffness and strain-to-failure. The most simple ply transition coupon would be one with a single butt-joint between the dissimilar plies. However, this is not likely to be a favorable option from either a manufacturing or structural performance standpoint, and so that arrangement is not depicted here.

Figures 25 and 26 show candidate transition coupons. Figure 25 depicts a single ply transition in an overall coupon thickness representative of a "thin" coupon, and Figure 26 shows a multi-ply transition with dimensions appropriate for a "thick" specimen. The thickness scale of these figures correctly reflects the assumptions that carbon layers are 1.0 mm thick whereas the fiberglass layers are 1.25 mm thick. As a result of the differential in stiffness and design strain (strain to failure in static compression), a 2.5-to-1.0 ratio of fiberglass-to-carbon laminate thickness is required in regions where both materials are present. This ratio is only valid for specific combinations of material and design strains and could be higher or lower for alternate materials.

Not shown are variants of spar transition coupons with decreased ply thickness or alternative ply arrangements that induce waviness in the carbon plies. The former variant is expected to improve the structural performance of the spar laminate, whereas the latter would have a deleterious effect.

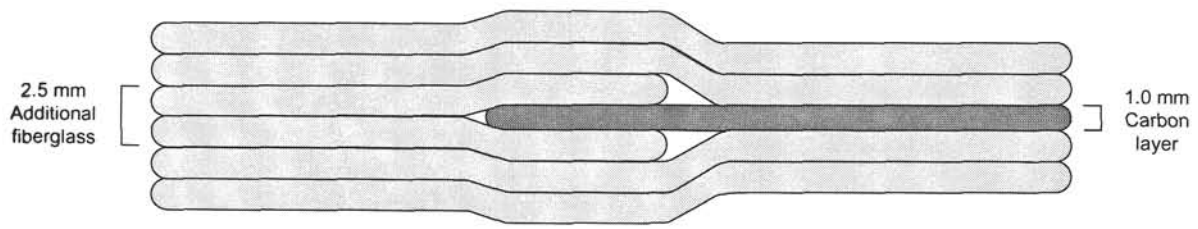

Figure 25. Single-ply fiberglass-carbon transition

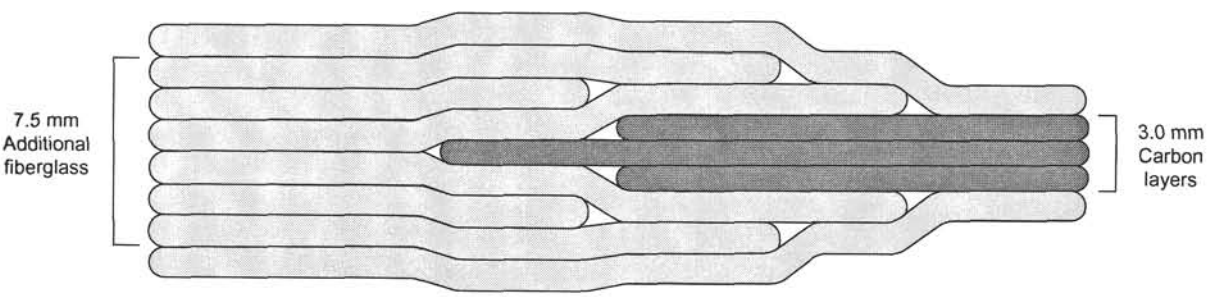

Figure 26. Multiple-ply fiberglass-carbon transition

5.3.5 4-Point Beam Bending

As noted above, the specimen geometries in Figures 20 through 26 were developed to maintain balance under axial loading but do not reflect the material arrangement in a feasible blade spar design. The major advantages of 4-point beam bending tests would be to evaluate spar cap laminate in an arrangement that more closely matches the actual blade structure, and to provide a greater volume of stressed material than would occur in pure axial loading. In general, 4-point beam bending tests would be suitable for evaluating basic spar cap laminate, spar cap laminate with selected details, or actual candidate spar designs.

Figure 27 shows the dimensions that were developed for sizing the test equipment required for 4-point beam bending tests and for estimating the cost of beam fabrication and testing. For the dimensions shown, an applied load of 40 kips would result in maximum spar cap material strains of about 1%, with

an actuator displacement of about 11.4 cm (4.5 inches). For costing purposes, a test arrangement of a 60-kip actuator mounted on a strong back (with necessary fixturing for beam restraint and loading) was assumed. This arrangement has sufficient load capacity for both static and fatigue testing of beam articles similar to that shown in Figure 27. For fatigue testing, the load application rate (and associated test cost) would depend more heavily on the displacement requirements rather than the magnitude of the applied load.

For reference, Figure 15 depicts a candidate spar cap design with a carbon-to-fiberglass transition. The ply thickness dimensions are again representative of a 2.5-to-1.0 ratio between the carbon and fiberglass plies in the region where both materials exist. As a result of the fiberglass materials having larger design strains (in static compression) than the carbon, one of the fiberglass layers is shown as being dropped following the transition region. Again, note that the ply thicknesses are shown to scale, but the horizontal axis has been compressed relative to the actual design of a blade or test article.

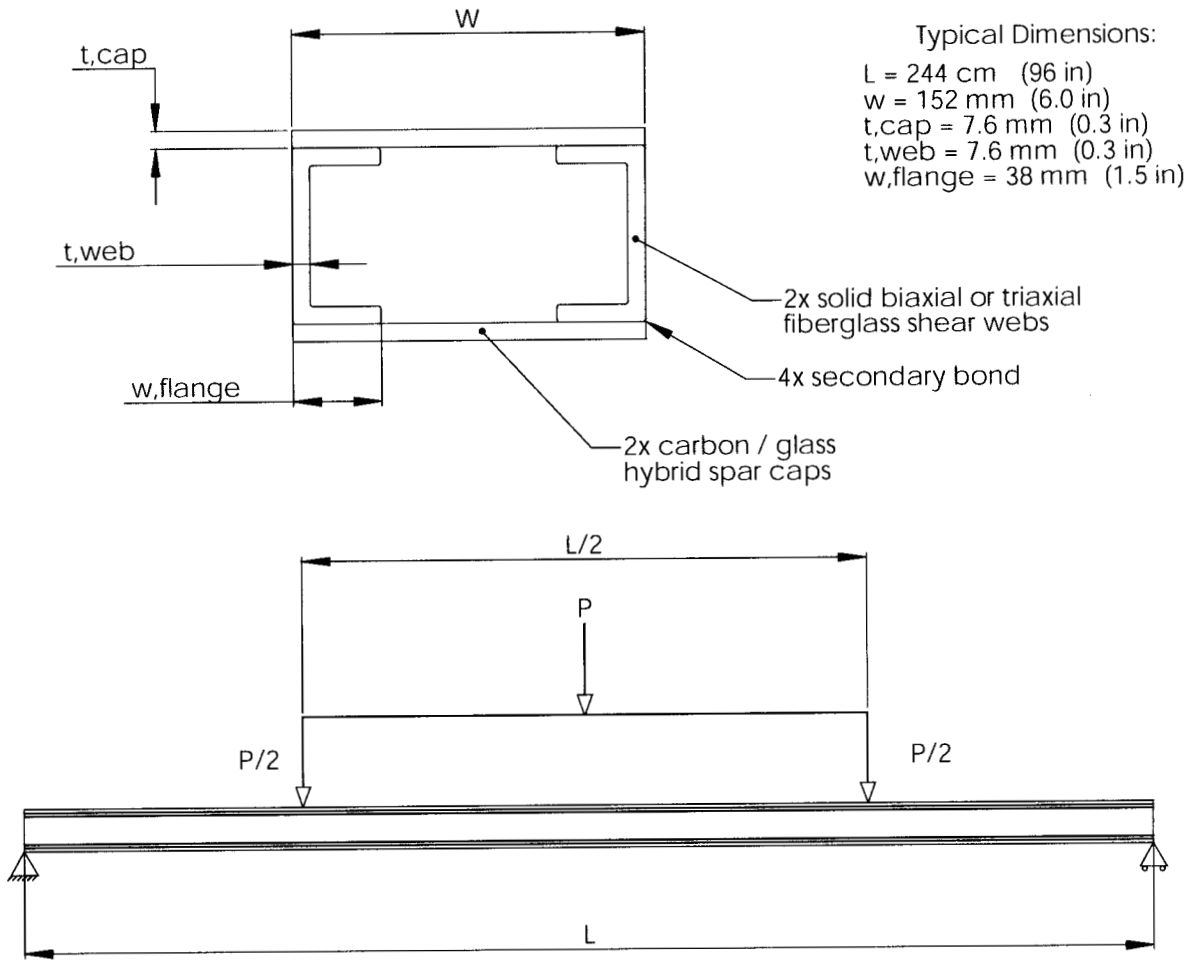

Figure 27. Beam geometry assumed for estimating 4-point beam bending test requirements and cost

5.3.6 Biased Material Cylinder

Figure 28 shows a schematic representation of a test that incorporates biased carbon/fiberglass laminate in a tubular specimen with combined axial and torsional loading. The dimensions and fiber orientation angles shown in Figure 28 are nominal, but were used in specifying the required test equipment and estimating costs for part fabrication and testing. The costs estimated for these tests assume a 50-kip load frame is used.

It is assumed that the parts can be fabricated by wrapping a biased carbon/fiberglass fabric around a foam core, with subsequent infusion or roller-impregnation/bagging. The article would then have an extension-twist bias. When loaded axially, the laminate would respond much as biased material would on either the upper or lower surface of a turbine blade (assuming mirror symmetry of upper and lower surface laminate to achieve bend-twist coupling).

With the proposed design, the axial and torsional degrees of freedom can be loaded independently or either can be left free. With appropriate strain gauging, it is expected that this test arrangement can be used to measure the EA, GJ and coupling coefficient for the test article. From these measurements, the laminate properties E_x, G_{xy}, and $\eta_{x,xy}$ (measure of the amount of shear strain generated in the x-y plane per unit strain in the x-direction) can be inferred. Following an evaluation of the material stiffness properties, the article can be progressively loaded to failure. The measured stiffness and strength properties can then be compared with values predicted by micromechanics.

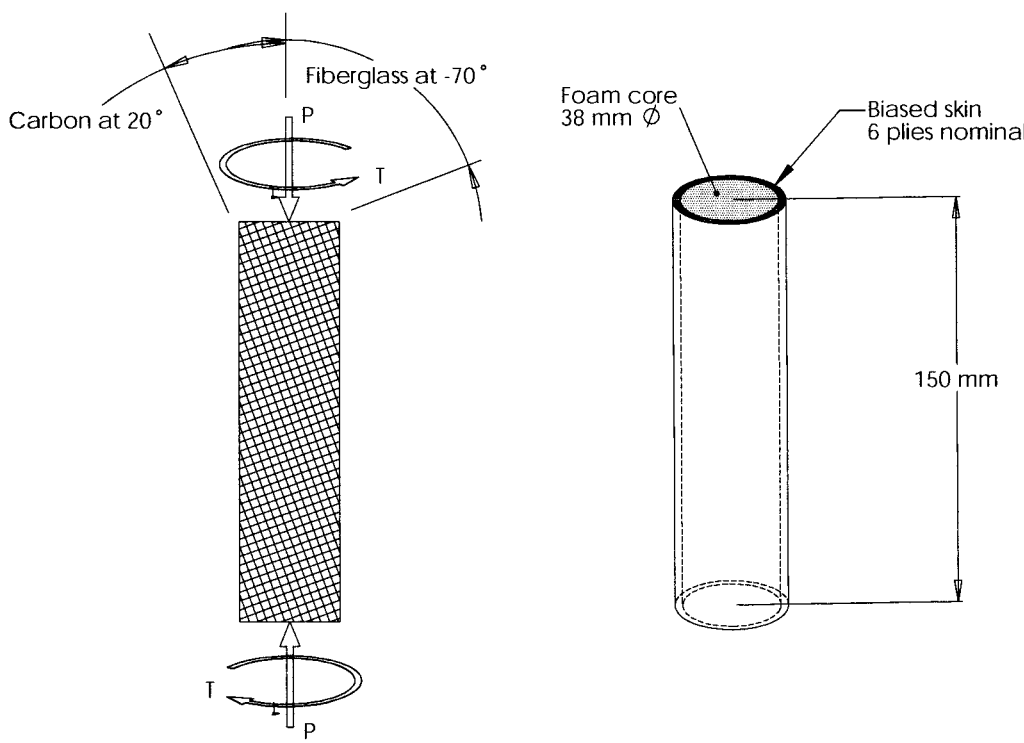

Figure 28. Schematic of test for biased tube in combined axial/torsional loading

The proposed specialty cylinder tests have been developed to avoid the edge effects that would occur in flat panels or spar designs with mirror symmetry of biased laminate. While the cylinder tests cannot be used to evaluate edge effects, they could provide valuable material characterization data to improve confidence in modeling of the biased laminate stiffness and strength properties.

Evaluating edge effects and load path considerations would require a test article that closely matches the structural approach and material layout in question, and it is likely that each result would be specific to the arrangement selected. As summarized in their report on bend-twist design concepts, GEC concluded that a structural arrangement that minimizes deleterious load path and edge effects is one that combines unbiased carbon hybrid spar cap with biased hybrid blade skins. However, the material characterization data that could be generated from the proposed tube test would be of value in supporting the design of twist-coupled blades that incorporate biased laminate in either a load-bearing or non-load-bearing arrangement.

The preliminary test matrix shown in Table 17 includes static testing of two material configurations and fatigue testing of one material configuration for the biased tube. This inclusion resulted from GEC's judgment that these tests will be of high value in supporting parallel work under other Sandia blade development efforts and current SBIR/STTR program contracts. However, GEC's enthusiasm for these tests is tempered by the concern that they provide truly useful results. It is therefore recommended that effort on these tests is incremental, with a greater definition of the test design developed and carefully reviewed prior to dedicating substantial resources for development of hardware and test articles.

5.3.7 Margins/Safety Factors

One aspect of determining margins and safety factors is to develop a sufficient number of data points so that statistically based values can be derived. For a given material/process/load condition, 30 data points is a reasonable number from which to derive characteristic (i.e., 95% exceedance with 95% confidence) properties.

Another aspect of margins and safety factors is the difference between material properties as generated in coupon tests and the performance of similar material in an as-built blade. This encompasses a wide range of effects, some of which are inherent (natural variations of material properties, unavoidable variations in fiber and fabric alignment, volume and thickness effects, inherent process-related effects) and some of which can vary depending on the execution of the manufacturing approach (avoidable misalignment of fabric, irregularities due to varying quality control of fabrication/process).

The tests listed in Table 17 to address this issue (I.D. P and Q) assume thick laminate that is constructed with designed and controlled irregularities in the fiber alignment and/or void content. Such testing is more correctly characterized as evaluating the "effects of defects" and only addresses a subset of the effects that combine in "as-manufactured properties."

5.3.8 Lap Shear Testing of Bonding Materials

Lap shear test of bonding materials was given very low priority at the Part I BSDS Design Review Meeting. No subsequent effort has been spent in specification and cost estimation for these tests.

6. Conclusions

6.1 Summary

This report provides an overview of general issues for large wind turbine blades. Current manufacturing trends are summarized, and several design options for incorporating carbon fiber in blades are presented. Preliminary blade designs were developed at 3.0 and 5.0 MW, and parametric analyses were performed to investigate the potential benefits and options for inclusion of carbon fiber in MW-scale blade spars. Critical performance aspects of the carbon material and blade structure are discussed within the context of coupon and sub-structure testing planned for the next phase of this project. Finally, recommendations are made for composites testing under Part II of the BSDS, and the initial planned test matrix for that program is presented.

6.2 Current/Future Work under Part II BSDS

The BSDS Part II Project Kickoff Meeting was held on May 29, 2003. As of that date, some fibers and fabric styles had been selected for thin-coupon testing and were in the process of procurement/fabrication of test specimens. Testing under this program is planned to occur over an 18-month time period.

GEC will continue to work with several manufacturers to identify promising fibers and material forms for potential coupon testing under the Part II BSDS program. In the process, GEC will continue to collaborate with Sandia, MSU, TPI Composites, GE Wind Energy, and others to ensure the work carried out under this program is of high value to the U.S. wind industry and is complementary with research and development efforts under parallel programs. While the test matrix of Table 17 has been used for planning and cost-estimation purposes, it will be subject to review and possible revision as the project progresses.

7. References

1. Hinsch, C. "The Race for Size." *New Energy.* October 2002 (No. 5), pp. 24-26.
2. BTM Consult ApS. March 2003. *World Market Update.*
3. Dutton, A.G., et. al. (March 1-5, 1999). *Design Concepts for Sectional Wind Turbine Blades.* Proceedings of the 1999 European Wind Energy Conference, Nice, France. p.p. 285-288.
4. Joosse, P.A., et al. (January 10-13, 2000). *Economic Use of Carbon Fibres in Large Wind Turbine Blades*? Proceedings of AIAA/ASME Wind Energy Symposium. Reno, NV.
5. Joosse, P.A., et al. (July 2-6, 2001). *Toward Cost Effective Large Turbine Components with Carbon Fibers.* Presented at the 2001 European Wind Energy Conference and Exhibition, Copenhagen.
6. Joosse, P.A., et al. (July 2-6, 2001). *Fatigue Properties of Low-Cost Carbon Fiber Material.* Presented at the 2001 European Wind Energy Conference and Exhibition, Copenhagen.
7. Griffin, D.A. (March, 2001). *WindPACT Turbine Design Scaling Studies Technical Area 1 – Composite Blades for 80- to 120-Meter Rotor.* NREL/SR-500-29492. Golden, CO: National Renewable Energy Laboratory.
8. Smith, K. (March, 2001). *WindPACT Turbine Design Scaling Studies Technical Area 2 – Turbine, Rotor and Blade Logistics.* NREL/SR-500-29439. Golden, CO: National Renewable Energy Laboratory.
9. Vandenbosche, J. (March, 2001). *WindPACT Turbine Design Scaling Studies Technical Area 3 – Self-Erecting Tower Structures.* NREL/SR-500-29493. Golden, CO: National Renewable Energy Laboratory.
10. Malcolm, D., Hansen C. (June, 2001) *Results from the WindPACT Rotor Design Study.* Proceedings Windpower 2001, American Wind Energy Association, Washington DC.
11. Malcolm, D.J.; Hansen, A.C. *WindPACT Turbine Rotor Design Study: June 2000–June 2002.* 82 pp.; NICH Report No. SR-500-32495. National Renewable Energy Laboratory. August 2002.
12. Griffin, D.A. (July, 2002). *Blade System Design Studies Volume I: Composite Technologies for Large Wind Turbine Blades.* SAND2002-1879. Albuquerque, NM: Sandia National Laboratories.
13. Griffin, D.A., Ashwill T.D. "Alternative Composite Materials for Megawatt-Scale Turbine Blades: Design Considerations and Recommended Testing." *Proceedings of the 2003 AIAA/ASME Wind Energy Symposium.* Reno, NV. January 2003.
14. Griffin, D.A., Ashwill T.D. (May 11-15, 2003). "Alternative Composite Materials for Megawatt-Scale Turbine Blades: Design Considerations and Test Evaluation." *Proceedings of the 48th International SAMPE Symposium and Exhibition.* Long Beach, CA.
15. Laird, D.L. (January 11-14, 2001). *2001: A Numerical Manufacturing and Design Tool Odyssey.* Proceedings of AIAA/ASME Wind Energy Symposium. Reno, NV.
16. International Electrotechnical Commission. (1999). *IEC 61400-1: Wind turbine generator systems – Part 1: Safety Requirements*, 2nd Edition. International Standard 1400-1.
17. TPI Composites Inc. (May 2003). *Blade Manufacturing Improvements: Remote Blade Manufacturing Demonstration.* SAND2003-0719. Albuquerque, NM: Sandia National Laboratories.
18. Lobitz, D.W., et al. *The Use of Twist-Coupled Blades to Enhance the Performance of Horizontal Axis Wind Turbines.* SAND2001-1303. Albuquerque, NM: Sandia National Laboratories. May 2001.
19. Ong, C.H. and Tsai, S.W. *The Use of Carbon Fibers in Wind Turbine Blade Design: a SERI-8 Blade Example.* SAND 2000-0478. Albuquerque, NM: Sandia National Laboratories. March 2000.

20. Zuteck, M. *Adaptive Blade Concept Assessment: Curved Planform Induced Twist Investigation.* SAND2002-2996. Albuquerque, NM: Sandia National Laboratories. October 2002.
21. Locke, J. and Hidalgo, I.C. *The Implementation of Braided Composite Materials in the Design of a Bend-Twist Coupled Blade.* SAND2002-2425. Albuquerque, NM: Sandia National Laboratories. August 2002.
22. Griffin, D.A. *Evaluation of Design Concepts for Adaptive Wind Turbine Blades.* SAND2002-2424. Albuquerque, NM: Sandia National Laboratories. August 2002.
23. Service, D. (October 16-18, 2001). *PAN Carbon Fibre Precursor.* Proceedings of Intertech's Carbon Fiber 2001, Bordeaux, France.
24. Germanischer Lloyd (1999) Rules and Regulations IV – Non-Marine Technology, Part 1 – Wind Energy, *Regulation for the Certification of Wind Energy Conversion Systems.*
25. Det Norske Veritas/Riso National Laboratory (2001). Guidelines for Design of Wind Turbines, 1st Edition.
26. Mandell, J.F., Samborsky, D.D. (1997). "*DOE/MSU Composite Material Fatigue Database: Test Methods, Materials and Analysis.*" SAND97-3002. Sandia National Laboratories. Albuquerque, NM.
27. Mandell, J.F., et al. "Effects of Materials Parameters and Design Details on the Fatigue of Composite Materials for Wind Turbine Blades." *1999 EWEC Proceedings.* Nice, France. March 1999.
28. Mandell, J.F., et al. *Fatigue of Composite Materials and Substructures for Wind Turbine Blades.* SAND2002-0771. Albuquerque, NM: Sandia National Laboratories. March 2002.
29. International Electrotechnical Commission. (1986). *IEC 2394: General Principles on Reliability for Structures.*
30. Tangler, J.L.; Somers, D.M. (March 26-30, 1995). "NREL Airfoil Families for HAWTs". Presented at the American Wind Energy Association Windpower '95 Conference. Washington, DC.
31. Griffin, D.A. (August 2000). *NREL Advanced Research Turbine (ART) Aerodynamic Design of ART-2B Rotor Blades.* NREL/SR-500-28473. Golden, CO: National Renewable Energy Laboratory.

Appendix A

Tabular Blade Bending Fatigue Load Spectra

Table A-1. Blade Fatigue Loads, 1.5 MW Rotor at Specific Rating = 0.31 (Page 1 of 2)

75% Station Mx	
Range (kN-m)	Counts
1.0	434,301,275
3.0	168,802,822
5.0	101,046,262
7.0	68,967,027
9.0	46,747,485
11.0	33,679,244
13.0	23,354,282
15.0	17,099,532
17.0	11,095,387
19.0	6,786,551
21.0	4,709,105
23.0	3,352,495
25.0	1,844,775
27.0	1,444,834
29.0	2,652,790
31.0	11,507,118
33.0	20,364,457
35.0	25,727,375
37.0	25,336,578
39.0	18,800,923
41.0	12,332,532
43.0	9,482,744
45.0	6,361,720
47.0	5,791,013
49.0	2,762,511
51.0	2,056,900
53.0	1,923,846
55.0	641,827
57.0	827,545
59.0	529,837
61.0	303,975
63.0	112,728
65.0	265,219
67.0	27,129
69.0	100,226
71.0	31,341
73.0	8,425
75.0	35,554
77.0	27,129
79.0	4,213
81.0	8,425
83.0	0
85.0	0
87.0	0
89.0	0
91.0	4,213
93.0	0
95.0	0
97.0	0
99.0	0
101.0	0
103.0	0
105.0	0

75% Station My	
Range (kN-m)	Counts
2.5	725,717,446
7.5	142,084,049
12.5	75,591,935
17.5	48,240,988
22.5	36,018,146
27.5	26,632,712
32.5	21,063,336
37.5	13,657,053
42.5	12,409,873
47.5	10,724,435
52.5	8,546,458
57.5	6,026,527
62.5	6,763,706
67.5	4,790,488
72.5	4,069,375
77.5	3,491,494
82.5	2,297,941
87.5	2,075,693
92.5	1,430,707
97.5	1,860,380
102.5	1,439,641
107.5	1,220,249
112.5	932,044
117.5	915,228
122.5	767,957
127.5	918,389
132.5	851,166
137.5	419,195
142.5	465,532
147.5	242,072
152.5	313,040
157.5	392,433
162.5	584,791
167.5	277,485
172.5	146,059
177.5	218,648
182.5	147,911
187.5	119,160
192.5	175,271
197.5	241,931
202.5	127,586
207.5	22,916
212.5	87,588
217.5	56,246
222.5	56,246
227.5	22,916
232.5	4,213
237.5	0
242.5	0
247.5	18,703
252.5	4,213
257.5	0
262.5	56,246

50% Station Mx	
Range (kN-m)	Counts
5.0	276,395,442
15.0	110,691,682
25.0	72,213,168
35.0	48,017,072
45.0	31,507,942
55.0	23,668,024
65.0	15,837,697
75.0	9,607,107
85.0	6,455,308
95.0	4,844,931
105.0	2,720,752
115.0	1,914,828
125.0	1,130,321
135.0	548,406
145.0	510,631
155.0	357,160
165.0	116,941
175.0	161,056
185.0	227,676
195.0	1,393,229
205.0	3,299,286
215.0	15,772,937
225.0	24,804,531
235.0	26,495,001
245.0	22,064,670
255.0	15,440,496
265.0	11,152,166
275.0	8,138,914
285.0	4,968,197
295.0	3,791,935
305.0	2,853,699
315.0	1,627,242
325.0	1,336,929
335.0	1,019,535
345.0	733,994
355.0	458,257
365.0	444,238
375.0	226,937
385.0	79,534
395.0	204,021
405.0	110,504
415.0	12,638
425.0	12,638
435.0	27,129
445.0	45,832
455.0	4,213
465.0	22,916
475.0	4,213
485.0	0
495.0	4,213
505.0	0
515.0	0
525.0	4,213

50% Station My	
Range (kN-m)	Counts
10.0	325,935,323
30.0	100,502,825
50.0	66,811,305
70.0	40,725,063
90.0	31,282,800
110.0	28,053,040
130.0	21,238,827
150.0	13,208,000
170.0	14,023,319
190.0	11,639,311
210.0	10,292,691
230.0	7,175,582
250.0	8,408,030
270.0	6,710,235
290.0	4,582,204
310.0	4,427,688
330.0	3,459,593
350.0	2,730,481
370.0	2,143,093
390.0	1,808,986
410.0	1,584,645
430.0	1,715,757
450.0	1,512,693
470.0	1,282,292
490.0	1,023,136
510.0	935,413
530.0	660,149
550.0	488,310
570.0	780,430
590.0	314,663
610.0	348,825
630.0	273,780
650.0	498,960
670.0	267,071
690.0	267,071
710.0	281,562
730.0	83,375
750.0	127,586
770.0	264,847
790.0	50,045
810.0	114,948
830.0	56,246
850.0	8,425
870.0	139,621
890.0	0
910.0	22,916
930.0	0
950.0	22,916
970.0	56,246
990.0	0
1,010.0	0
1,030.0	0
1,050.0	0

Table A-1. Blade Fatigue Loads, 1.5 MW Rotor at Specific Rating = 0.31 (Page 2 of 2)

25% Station Mx	
Range (kN-m)	Counts
15.0	226,085,688
45.0	85,074,972
75.0	46,952,124
105.0	26,240,253
135.0	15,777,162
165.0	8,671,375
195.0	5,506,000
225.0	2,473,136
255.0	1,812,005
285.0	917,739
315.0	507,062
345.0	196,475
375.0	192,262
405.0	131,567
435.0	58,470
465.0	43,980
495.0	156,336
525.0	289,756
555.0	608,260
585.0	2,088,937
615.0	3,512,623
645.0	8,476,584
675.0	18,157,631
705.0	33,524,079
735.0	26,723,238
765.0	19,808,642
795.0	11,659,176
825.0	6,847,209
855.0	4,401,241
885.0	3,255,868
915.0	2,194,321
945.0	1,856,771
975.0	1,035,405
1,005.0	659,180
1,035.0	673,164
1,065.0	66,895
1,095.0	152,124
1,125.0	220,872
1,155.0	110,504
1,185.0	64,536
1,215.0	87,588
1,245.0	22,916
1,275.0	8,425
1,305.0	18,703
1,335.0	0
1,365.0	0
1,395.0	4,213
1,425.0	0
1,455.0	4,213
1,485.0	0
1,515.0	0
1,545.0	0

25% Station My	
Range (kN-m)	Counts
20.0	276,049,242
60.0	105,539,495
100.0	62,139,807
140.0	39,466,426
180.0	28,058,308
220.0	18,565,843
260.0	15,458,589
300.0	15,158,845
340.0	13,031,585
380.0	12,616,345
420.0	10,941,037
460.0	10,199,172
500.0	8,572,184
540.0	7,768,608
580.0	7,328,606
620.0	8,305,163
660.0	6,292,533
700.0	5,584,540
740.0	4,215,064
780.0	2,867,872
820.0	2,735,198
860.0	2,480,492
900.0	2,812,411
940.0	1,867,035
980.0	1,855,558
1,020.0	1,512,063
1,060.0	1,243,694
1,100.0	1,546,099
1,140.0	707,468
1,180.0	618,668
1,220.0	910,743
1,260.0	977,167
1,300.0	574,282
1,340.0	254,341
1,380.0	390,444
1,420.0	398,270
1,460.0	471,598
1,500.0	72,961
1,540.0	170,963
1,580.0	363,316
1,620.0	27,129
1,660.0	221,239
1,700.0	129,438
1,740.0	4,213
1,780.0	152,354
1,820.0	125,131
1,860.0	60,459
1,900.0	8,425
1,940.0	18,703
1,980.0	0
2,020.0	22,916
2,060.0	56,246

Root Station Mx	
Range (kN-m)	Counts
27.5	204,559,377
82.5	58,642,825
137.5	26,872,784
192.5	15,017,986
247.5	8,416,986
302.5	4,623,122
357.5	2,284,072
412.5	1,557,709
467.5	513,360
522.5	267,584
577.5	52,405
632.5	146,430
687.5	72,961
742.5	4,213
797.5	4,213
852.5	0
907.5	0
962.5	60,459
1,017.5	4,213
1,072.5	0
1,127.5	62,683
1,182.5	183,465
1,237.5	310,684
1,292.5	756,311
1,347.5	1,654,050
1,402.5	3,788,351
1,457.5	7,296,166
1,512.5	12,646,989
1,567.5	27,789,371
1,622.5	32,140,393
1,677.5	24,294,958
1,732.5	13,472,299
1,787.5	7,756,761
1,842.5	5,090,037
1,897.5	2,909,163
1,952.5	1,926,937
2,007.5	1,884,668
2,062.5	1,000,084
2,117.5	719,362
2,172.5	343,917
2,227.5	243,924
2,282.5	110,368
2,337.5	147,911
2,392.5	22,916
2,447.5	102,078
2,502.5	8,425
2,557.5	22,916
2,612.5	0
2,667.5	0
2,722.5	4,213
2,777.5	4,213
2,832.5	0

Root Station My	
Range (kN-m)	Counts
37.5	427,080,313
112.5	110,563,204
187.5	58,518,831
262.5	34,564,123
337.5	20,970,811
412.5	13,472,074
487.5	12,523,722
562.5	12,714,147
637.5	12,956,385
712.5	11,687,127
787.5	10,952,322
862.5	9,514,385
937.5	9,078,377
1,012.5	9,637,080
1,087.5	6,277,001
1,162.5	8,908,851
1,237.5	6,637,131
1,312.5	4,731,660
1,387.5	5,131,269
1,462.5	2,980,841
1,537.5	2,920,805
1,612.5	2,835,434
1,687.5	2,806,282
1,762.5	2,465,615
1,837.5	1,238,555
1,912.5	1,862,226
1,987.5	1,393,672
2,062.5	792,320
2,137.5	777,128
2,212.5	1,151,295
2,287.5	618,668
2,362.5	590,296
2,437.5	369,289
2,512.5	600,805
2,587.5	147,911
2,662.5	321,560
2,737.5	21,064
2,812.5	448,543
2,887.5	62,683
2,962.5	212,813
3,037.5	4,213
3,112.5	135,408
3,187.5	31,341
3,262.5	8,425
3,337.5	56,246
3,412.5	0
3,487.5	18,703
3,562.5	0
3,637.5	4,213
3,712.5	4,213
3,787.5	0
3,862.5	0

Table A-2. Blade Fatigue Loads, 1.5 MW Rotor at Specific Rating = 0.39 (Page 1 of 4)

75% Station Mx	
Range (kN-m)	Counts
0.5	344,340,587
1.5	148,126,269
2.5	98,538,486
3.5	75,224,651
4.5	53,297,550
5.5	43,618,136
6.5	35,007,940
7.5	26,464,677
8.5	20,139,804
9.5	19,113,914
10.5	11,916,677
11.5	10,359,523
12.5	7,391,343
13.5	6,067,884
14.5	3,480,164
15.5	2,668,735
16.5	2,009,351
17.5	1,662,575
18.5	1,921,985
19.5	3,573,681
20.5	7,348,592
21.5	13,442,244
22.5	19,130,079
23.5	18,247,723
24.5	18,095,484
25.5	14,995,983
26.5	13,184,549
27.5	10,599,361
28.5	8,177,728
29.5	6,738,746
30.5	5,604,616
31.5	5,240,582
32.5	3,256,418
33.5	2,762,592
34.5	1,984,126
35.5	2,375,813
36.5	1,004,909
37.5	861,952
38.5	878,667
39.5	550,485
40.5	358,643
41.5	206,518
42.5	95,877
43.5	296,189
44.5	202,535
45.5	45,832
46.5	114,716
47.5	16,851
48.5	27,129
49.5	18,703
50.5	8,425
51.5	12,638
52.5	4,213
53.5	4,213

75% Station My	
Range (kN-m)	Counts
1.5	733,265,974
4.5	158,058,872
7.5	85,705,538
10.5	57,113,329
13.5	44,444,316
16.5	32,283,719
19.5	24,828,230
22.5	20,606,124
25.5	15,853,251
28.5	12,299,882
31.5	10,145,576
34.5	7,362,744
37.5	8,128,734
40.5	6,112,846
43.5	4,560,868
46.5	3,763,513
49.5	3,459,027
52.5	3,419,474
55.5	2,350,213
58.5	2,234,625
61.5	1,584,791
64.5	1,080,739
67.5	1,643,053
70.5	1,232,189
73.5	812,136
76.5	781,815
79.5	580,113
82.5	887,827
85.5	792,657
88.5	610,979
91.5	536,874
94.5	643,572
97.5	542,804
100.5	409,283
103.5	650,474
106.5	427,523
109.5	118,929
112.5	202,400
115.5	147,911
118.5	356,743
121.5	365,304
124.5	188,045
127.5	148,141
130.5	39,767
133.5	413,127
136.5	170,963
139.5	27,129
142.5	18,703
145.5	27,129
148.5	64,672
151.5	114,948
154.5	68,885
157.5	93,653
160.5	64,672

50% Station Mx	
Range (kN-m)	Counts
2.5	222,450,755
7.5	106,999,095
12.5	74,742,834
17.5	53,373,404
22.5	40,747,564
27.5	30,699,695
32.5	23,271,445
37.5	18,306,156
42.5	15,004,622
47.5	11,486,599
52.5	8,001,023
57.5	5,542,116
62.5	5,473,089
67.5	2,732,188
72.5	2,449,986
77.5	1,452,341
82.5	1,417,715
87.5	836,580
92.5	514,844
97.5	312,673
102.5	190,038
107.5	196,239
112.5	239,943
117.5	219,019
122.5	298,413
127.5	1,383,210
132.5	2,942,441
137.5	6,086,671
142.5	14,495,038
147.5	19,456,138
152.5	20,662,522
157.5	18,150,162
162.5	14,568,781
167.5	12,972,011
172.5	10,291,816
177.5	8,424,905
182.5	5,346,092
187.5	5,417,106
192.5	4,441,995
197.5	2,502,854
202.5	3,056,923
207.5	1,894,449
212.5	1,384,940
217.5	919,406
222.5	1,530,384
227.5	431,833
232.5	574,048
237.5	408,317
242.5	177,028
247.5	304,478
252.5	196,470
257.5	50,045
262.5	181,241
267.5	25,276

50% Station My	
Range (kN-m)	Counts
5.0	277,461,464
15.0	93,460,125
25.0	73,198,665
35.0	51,499,221
45.0	38,578,776
55.0	30,353,617
65.0	26,267,330
75.0	20,989,628
85.0	18,488,665
95.0	14,891,937
105.0	12,118,880
115.0	12,797,793
125.0	9,479,172
135.0	8,200,035
145.0	7,060,666
155.0	5,599,421
165.0	5,075,390
175.0	5,882,862
185.0	4,156,370
195.0	4,365,975
205.0	3,078,174
215.0	3,098,869
225.0	3,119,146
235.0	2,495,119
245.0	1,760,154
255.0	1,689,323
265.0	2,272,939
275.0	865,149
285.0	1,165,217
295.0	1,203,167
305.0	994,536
315.0	464,563
325.0	969,114
335.0	586,179
345.0	746,963
355.0	557,430
365.0	685,656
375.0	546,548
385.0	270,579
395.0	455,216
405.0	340,169
415.0	516,726
425.0	302,761
435.0	268,219
445.0	258,646
455.0	146,289
465.0	212,813
475.0	300,496
485.0	262,859
495.0	400,258
505.0	146,289
515.0	87,588
525.0	137,864
535.0	60,459

Table A-2. Blade Fatigue Loads, 1.5 MW Rotor at Specific Rating = 0.39 (Page 2 of 4)

75% Station Mx	
Range (kN-m)	Counts
54.5	8,425
55.5	18,703
56.5	0
57.5	4,213
58.5	0
59.5	0
60.5	0
61.5	0
62.5	0
63.5	0
64.5	0
65.5	0
66.5	0
67.5	0
68.5	0
69.5	0
70.5	0
71.5	0
72.5	0
73.5	0
74.5	0
75.5	0
76.5	0

75% Station My	
Range (kN-m)	Counts
163.5	37,406
166.5	0
169.5	56,246
172.5	0
175.5	18,703
178.5	0
181.5	60,459
184.5	4,213
187.5	0
190.5	18,703
193.5	0
196.5	0
199.5	4,213
202.5	0
205.5	0
208.5	0
211.5	0
214.5	0
217.5	0
220.5	0
223.5	0
226.5	0
229.5	0

50% Station Mx	
Range (kN-m)	Counts
272.5	58,470
277.5	8,425
282.5	22,916
287.5	8,425
292.5	8,425
297.5	8,425
302.5	18,703
307.5	0
312.5	4,213
317.5	18,703
322.5	4,213
327.5	4,213
332.5	0
337.5	0
342.5	0
347.5	0
352.5	4,213
357.5	0
362.5	0
367.5	0
372.5	0
377.5	0
382.5	0

50% Station My	
Range (kN-m)	Counts
545.0	119,160
555.0	60,459
565.0	27,129
575.0	60,459
585.0	68,885
595.0	110,735
605.0	37,406
615.0	74,949
625.0	79,162
635.0	0
645.0	83,375
655.0	0
665.0	18,703
675.0	0
685.0	0
695.0	56,246
705.0	0
715.0	4,213
725.0	22,916
735.0	0
745.0	0
755.0	0
765.0	4,213

Table A-2. Blade Fatigue Loads, 1.5 MW Rotor at Specific Rating = 0.39 (Page 3 of 4)

25% Station Mx	
Range (kN-m)	Counts
7.5	206,112,239
22.5	87,366,055
37.5	54,438,539
52.5	35,049,163
67.5	24,753,830
82.5	16,069,145
97.5	12,441,174
112.5	6,677,865
127.5	5,038,442
142.5	3,278,017
157.5	2,274,738
172.5	2,053,557
187.5	690,156
202.5	459,006
217.5	418,828
232.5	248,137
247.5	108,516
262.5	127,355
277.5	43,980
292.5	45,832
307.5	52,405
322.5	204,021
337.5	204,157
352.5	383,504
367.5	1,267,265
382.5	1,261,236
397.5	2,490,112
412.5	5,048,785
427.5	8,191,347
442.5	16,661,718
457.5	24,298,123
472.5	25,809,494
487.5	18,893,839
502.5	15,433,626
517.5	10,566,393
532.5	7,895,172
547.5	5,101,999
562.5	3,308,301
577.5	4,004,329
592.5	2,025,376
607.5	1,664,047
622.5	1,074,258
637.5	701,403
652.5	777,087
667.5	254,202
682.5	379,427
697.5	254,066
712.5	179,388
727.5	154,112
742.5	106,291
757.5	48,192
772.5	87,588
787.5	12,638
802.5	22,916

25% Station My	
Range (kN-m)	Counts
12.5	264,656,777
37.5	110,720,645
62.5	70,242,894
87.5	48,124,427
112.5	31,690,771
137.5	22,452,976
162.5	20,617,173
187.5	15,208,880
212.5	16,123,528
237.5	16,081,196
262.5	12,585,814
287.5	10,815,176
312.5	11,204,954
337.5	8,379,416
362.5	9,245,514
387.5	5,384,928
412.5	5,871,466
437.5	6,062,247
462.5	4,481,063
487.5	4,066,845
512.5	4,104,797
537.5	3,435,423
562.5	3,249,691
587.5	2,339,570
612.5	2,791,962
637.5	2,253,691
662.5	1,705,574
687.5	1,411,133
712.5	949,947
737.5	844,129
762.5	722,640
787.5	1,044,531
812.5	952,091
837.5	802,597
862.5	822,050
887.5	360,250
912.5	628,262
937.5	271,192
962.5	391,592
987.5	129,208
1,012.5	323,456
1,037.5	292,578
1,062.5	397,521
1,087.5	429,840
1,112.5	315,031
1,137.5	27,129
1,162.5	179,619
1,187.5	129,438
1,212.5	83,375
1,237.5	22,916
1,262.5	60,459
1,287.5	97,865
1,312.5	189,897
1,337.5	4,213

Root Station Mx	
Range (kN-m)	Counts
12.5	179,288,344
37.5	66,480,995
62.5	37,328,024
87.5	24,980,420
112.5	14,490,333
137.5	10,027,315
162.5	5,806,053
187.5	4,842,798
212.5	3,201,291
237.5	2,123,413
262.5	1,355,596
287.5	1,025,647
312.5	260,639
337.5	285,543
362.5	246,148
387.5	187,678
412.5	151,650
437.5	45,832
462.5	16,851
487.5	18,703
512.5	112,493
537.5	27,129
562.5	4,213
587.5	27,129
612.5	4,213
637.5	0
662.5	12,638
687.5	21,064
712.5	0
737.5	50,045
762.5	83,239
787.5	204,157
812.5	325,311
837.5	825,753
862.5	1,142,170
887.5	1,579,976
912.5	2,967,135
937.5	4,301,048
962.5	7,520,225
987.5	11,895,199
1,012.5	21,613,991
1,037.5	25,481,599
1,062.5	20,050,156
1,087.5	16,187,036
1,112.5	11,252,820
1,137.5	9,011,564
1,162.5	6,704,559
1,187.5	4,741,183
1,212.5	3,432,508
1,237.5	2,538,893
1,262.5	2,055,325
1,287.5	1,257,490
1,312.5	1,025,047
1,337.5	594,137

Root Station My	
Range (kN-m)	Counts
25.0	417,517,492
75.0	124,825,614
125.0	64,902,594
175.0	43,308,942
225.0	21,394,403
275.0	17,312,714
325.0	16,780,091
375.0	16,254,767
425.0	17,880,326
475.0	12,559,441
525.0	11,641,545
575.0	9,665,847
625.0	11,724,796
675.0	8,714,028
725.0	6,595,445
775.0	6,493,126
825.0	6,511,454
875.0	4,592,033
925.0	4,127,671
975.0	4,679,713
1,025.0	3,993,235
1,075.0	2,520,126
1,125.0	2,739,316
1,175.0	2,754,313
1,225.0	2,181,561
1,275.0	1,199,060
1,325.0	980,840
1,375.0	1,396,737
1,425.0	1,030,412
1,475.0	1,064,992
1,525.0	907,277
1,575.0	619,268
1,625.0	354,797
1,675.0	434,052
1,725.0	466,542
1,775.0	400,722
1,825.0	508,392
1,875.0	360,632
1,925.0	252,581
1,975.0	146,289
2,025.0	41,619
2,075.0	110,504
2,125.0	60,459
2,175.0	200,083
2,225.0	114,948
2,275.0	22,916
2,325.0	60,459
2,375.0	97,865
2,425.0	0
2,475.0	4,213
2,525.0	18,703
2,575.0	0
2,625.0	0
2,675.0	4,213

Table A-2. Blade Fatigue Loads, 1.5 MW Rotor at Specific Rating = 0.39 (Page 4 of 4)

25% Station Mx	
Range (kN-m)	Counts
817.5	8,425
832.5	18,703
847.5	8,425
862.5	4,213
877.5	22,916
892.5	0
907.5	0
922.5	4,213
937.5	0
952.5	0
967.5	0
982.5	4,213
997.5	0
1,012.5	0
1,027.5	0
1,042.5	0
1,057.5	0
1,072.5	0
1,087.5	0
1,102.5	0
1,117.5	0
1,132.5	0
1,147.5	0

25% Station My	
Range (kN-m)	Counts
1,362.5	56,246
1,387.5	79,162
1,412.5	4,213
1,437.5	74,949
1,462.5	0
1,487.5	4,213
1,512.5	18,703
1,537.5	0
1,562.5	0
1,587.5	4,213
1,612.5	0
1,637.5	0
1,662.5	0
1,687.5	0
1,712.5	0
1,737.5	0
1,762.5	0
1,787.5	0
1,812.5	0
1,837.5	0
1,862.5	0
1,887.5	0
1,912.5	0

Root Station Mx	
Range (kN-m)	Counts
1,362.5	414,982
1,387.5	401,870
1,412.5	260,131
1,437.5	310,818
1,462.5	156,336
1,487.5	97,865
1,512.5	129,208
1,537.5	73,097
1,562.5	31,341
1,587.5	8,425
1,612.5	4,213
1,637.5	22,916
1,662.5	0
1,687.5	8,425
1,712.5	0
1,737.5	22,916
1,762.5	0
1,787.5	0
1,812.5	4,213
1,837.5	0
1,862.5	0
1,887.5	4,213
1,912.5	0

Root Station My	
Range (kN-m)	Counts
2,725.0	0
2,775.0	0
2,825.0	0
2,875.0	0
2,925.0	0
2,975.0	0
3,025.0	0
3,075.0	0
3,125.0	0
3,175.0	0
3,225.0	0
3,275.0	0
3,325.0	0
3,375.0	0
3,425.0	0
3,475.0	0
3,525.0	0
3,575.0	0
3,625.0	0
3,675.0	0
3,725.0	0
3,775.0	0
3,825.0	0

Table A-3. Blade Fatigue Loads, 3.0 MW Rotor at Specific Rating = 0.39 (Page 1 of 4)

75% Station Mx	
Range (kN-m)	Counts
1.5	404,971,442
4.5	130,163,872
7.5	83,905,311
10.5	55,715,571
13.5	45,487,761
16.5	32,717,596
19.5	28,244,647
22.5	19,443,842
25.5	14,060,069
28.5	10,922,860
31.5	7,914,343
34.5	5,864,034
37.5	4,814,156
40.5	3,237,248
43.5	2,242,331
46.5	2,046,769
49.5	1,193,205
52.5	770,131
55.5	638,044
58.5	369,696
61.5	188,066
64.5	342,288
67.5	934,008
70.5	3,517,166
73.5	6,787,773
76.5	12,918,156
79.5	14,119,498
82.5	14,426,580
85.5	12,772,830
88.5	10,013,501
91.5	6,991,900
94.5	7,647,681
97.5	3,788,800
100.5	4,250,590
103.5	3,583,537
106.5	3,042,691
109.5	2,286,175
112.5	1,061,248
115.5	759,299
118.5	964,078
121.5	921,752
124.5	404,741
127.5	753,233
130.5	227,833
133.5	77,181
136.5	212,602
139.5	165,007
142.5	22,918
145.5	81,530
148.5	60,329
151.5	12,639
154.5	12,639
157.5	12,639
160.5	18,705

75% Station My	
Range (kN-m)	Counts
3.5	648,824,470
10.5	146,234,994
17.5	70,658,208
24.5	45,288,762
31.5	33,259,189
38.5	26,191,600
45.5	20,879,158
52.5	16,117,318
59.5	15,211,081
66.5	11,153,488
73.5	9,559,930
80.5	7,473,524
87.5	6,024,643
94.5	6,189,597
101.5	4,318,504
108.5	4,123,070
115.5	3,331,844
122.5	3,815,780
129.5	2,879,970
136.5	2,521,590
143.5	2,183,419
150.5	1,151,673
157.5	1,700,957
164.5	1,743,313
171.5	1,245,605
178.5	759,571
185.5	1,354,503
192.5	858,927
199.5	642,388
206.5	584,516
213.5	986,522
220.5	557,888
227.5	577,942
234.5	730,079
241.5	339,463
248.5	515,350
255.5	904,525
262.5	423,203
269.5	260,894
276.5	411,174
283.5	555,260
290.5	320,282
297.5	336,217
304.5	369,550
311.5	83,383
318.5	229,685
325.5	129,355
332.5	93,661
339.5	217,046
346.5	246,030
353.5	96,022
360.5	239,965
367.5	119,171
374.5	60,465

50% Station Mx	
Range (kN-m)	Counts
8.5	231,062,996
25.5	84,888,231
42.5	53,414,053
59.5	39,691,653
76.5	27,809,427
93.5	20,569,970
110.5	14,229,892
127.5	10,951,997
144.5	7,343,443
161.5	4,666,837
178.5	3,670,317
195.5	2,465,298
212.5	1,929,682
229.5	1,347,329
246.5	766,755
263.5	461,136
280.5	477,004
297.5	248,395
314.5	183,482
331.5	181,493
348.5	43,984
365.5	91,673
382.5	21,066
399.5	45,836
416.5	16,853
433.5	35,557
450.5	135,792
467.5	726,102
484.5	773,227
501.5	4,479,061
518.5	10,102,218
535.5	15,661,486
552.5	15,779,374
569.5	16,042,324
586.5	11,920,127
603.5	8,562,382
620.5	6,354,272
637.5	5,683,317
654.5	4,149,732
671.5	3,140,379
688.5	1,979,581
705.5	1,973,833
722.5	1,463,078
739.5	624,248
756.5	907,260
773.5	638,134
790.5	377,610
807.5	287,697
824.5	141,859
841.5	91,809
858.5	156,581
875.5	50,049
892.5	102,087
909.5	4,213

50% Station My	
Range (kN-m)	Counts
15.5	319,407,403
46.5	80,823,832
77.5	49,141,913
108.5	36,747,249
139.5	27,615,298
170.5	22,584,729
201.5	17,634,432
232.5	15,662,231
263.5	14,271,376
294.5	10,933,686
325.5	7,185,409
356.5	7,922,568
387.5	7,012,945
418.5	6,498,239
449.5	4,188,582
480.5	4,851,745
511.5	3,534,807
542.5	3,494,769
573.5	3,812,730
604.5	2,523,456
635.5	1,675,762
666.5	2,568,070
697.5	1,730,950
728.5	1,681,555
759.5	1,182,881
790.5	1,624,471
821.5	577,711
852.5	1,132,589
883.5	792,768
914.5	543,165
945.5	1,023,697
976.5	817,638
1,007.5	350,478
1,038.5	765,265
1,069.5	909,951
1,100.5	860,301
1,131.5	582,252
1,162.5	285,936
1,193.5	110,514
1,224.5	468,437
1,255.5	146,072
1,286.5	135,421
1,317.5	206,767
1,348.5	35,557
1,379.5	135,792
1,410.5	332,004
1,441.5	281,819
1,472.5	260,658
1,503.5	120,793
1,534.5	198,341
1,565.5	287,928
1,596.5	8,426
1,627.5	210,380
1,658.5	4,213

Table A-3. Blade Fatigue Loads, 3.0 MW Rotor at Specific Rating = 0.39 (Page 2 of 4)

75% Station Mx	
Range (kN-m)	Counts
163.5	4,213
166.5	18,705
169.5	12,639
172.5	0
175.5	4,213
178.5	0
181.5	0
184.5	4,213
187.5	0
190.5	0
193.5	0
196.5	0
199.5	4,213
202.5	0
205.5	0
208.5	0
211.5	0
214.5	0
217.5	0
220.5	0
223.5	0
226.5	0
229.5	0
232.5	0
235.5	0
238.5	0
241.5	0

75% Station My	
Range (kN-m)	Counts
381.5	79,034
388.5	137,876
395.5	195,888
402.5	123,385
409.5	56,251
416.5	60,465
423.5	194,128
430.5	79,169
437.5	18,705
444.5	31,344
451.5	56,251
458.5	0
465.5	18,705
472.5	4,213
479.5	0
486.5	8,426
493.5	18,705
500.5	0
507.5	56,251
514.5	0
521.5	18,705
528.5	0
535.5	0
542.5	0
549.5	22,918
556.5	0
563.5	56,251

50% Station Mx	
Range (kN-m)	Counts
926.5	8,426
943.5	35,557
960.5	18,705
977.5	8,426
994.5	37,410
1,011.5	4,213
1,028.5	4,213
1,045.5	4,213
1,062.5	0
1,079.5	4,213
1,096.5	0
1,113.5	0
1,130.5	0
1,147.5	0
1,164.5	4,213
1,181.5	0
1,198.5	0
1,215.5	0
1,232.5	0
1,249.5	0
1,266.5	0
1,283.5	0
1,300.5	0
1,317.5	0
1,334.5	0
1,351.5	0
1,368.5	0

50% Station My	
Range (kN-m)	Counts
1,689.5	45,836
1,720.5	129,450
1,751.5	12,639
1,782.5	56,251
1,813.5	4,213
1,844.5	18,705
1,875.5	0
1,906.5	74,956
1,937.5	0
1,968.5	0
1,999.5	0
2,030.5	0
2,061.5	0
2,092.5	22,918
2,123.5	0
2,154.5	0
2,185.5	56,251
2,216.5	22,918
2,247.5	0
2,278.5	0
2,309.5	0
2,340.5	0
2,372	0
2,402.5	0
2,433.5	0
2,464.5	0
2,495.5	0

Table A-3. Blade Fatigue Loads, 3.0 MW Rotor at Specific Rating = 0.39 (Page 3 of 4)

25% Station Mx	
Range (kN-m)	Counts
24.0	155,567,444
72.0	62,968,915
120.0	36,224,359
168.0	23,030,163
216.0	15,478,953
264.0	10,704,618
312.0	5,421,125
360.0	4,905,787
408.0	2,459,570
456.0	1,144,365
504.0	915,691
552.0	741,984
600.0	444,419
648.0	159,083
696.0	158,575
744.0	304,506
792.0	62,689
840.0	189,074
888.0	12,639
936.0	8,426
984.0	18,705
1,032.0	8,426
1,080.0	16,853
1,128.0	50,049
1,176.0	54,262
1,224.0	74,956
1,272.0	89,956
1,320.0	285,569
1,368.0	429,419
1,416.0	892,632
1,464.0	1,404,690
1,512.0	3,361,864
1,560.0	4,002,491
1,608.0	5,776,568
1,656.0	12,548,701
1,704.0	19,134,073
1,752.0	17,403,747
1,800.0	14,092,767
1,848.0	9,168,600
1,896.0	7,335,948
1,944.0	3,895,976
1,992.0	4,197,765
2,040.0	3,060,264
2,088.0	1,426,782
2,136.0	938,094
2,184.0	765,309
2,232.0	639,282
2,280.0	267,096
2,328.0	252,004
2,376.0	304,642
2,424.0	181,258
2,472.0	120,793
2,520.0	68,891
2,568.0	31,344

25% Station My	
Range (kN-m)	Counts
35.0	222,521,776
105.0	85,046,881
175.0	52,735,388
245.0	34,877,725
315.0	26,044,878
385.0	16,424,732
455.0	11,238,245
525.0	10,736,511
595.0	8,562,794
665.0	9,483,124
735.0	8,927,367
805.0	10,404,972
875.0	5,847,900
945.0	6,305,456
1,015.0	6,429,980
1,085.0	5,154,895
1,155.0	4,956,767
1,225.0	6,049,918
1,295.0	3,925,714
1,365.0	3,171,700
1,435.0	2,701,974
1,505.0	3,150,588
1,575.0	2,848,228
1,645.0	2,417,866
1,715.0	1,934,489
1,785.0	1,860,675
1,855.0	2,281,193
1,925.0	996,808
1,995.0	1,382,108
2,065.0	820,918
2,135.0	913,326
2,205.0	797,852
2,275.0	1,497,897
2,345.0	930,674
2,415.0	889,488
2,485.0	204,176
2,555.0	745,079
2,625.0	700,019
2,695.0	514,412
2,765.0	367,562
2,835.0	444,004
2,905.0	295,375
2,975.0	48,197
3,045.0	35,557
3,115.0	373,764
3,185.0	106,301
3,255.0	235,752
3,325.0	273,297
3,395.0	198,341
3,465.0	154,126
3,535.0	18,705
3,605.0	244,408
3,675.0	260,658
3,745.0	60,465

Root Station Mx	
Range (kN-m)	Counts
50.0	161,720,132
150.0	42,260,546
250.0	25,506,786
350.0	11,931,338
450.0	6,687,346
550.0	4,055,429
650.0	1,778,463
750.0	1,148,993
850.0	732,072
950.0	283,581
1,050.0	269,089
1,150.0	150,285
1,250.0	135,657
1,350.0	8,426
1,450.0	12,639
1,550.0	12,639
1,650.0	4,213
1,750.0	4,213
1,850.0	110,745
1,950.0	149,303
2,050.0	0
2,150.0	0
2,250.0	18,705
2,350.0	0
2,450.0	0
2,550.0	12,639
2,650.0	12,639
2,750.0	64,542
2,850.0	96,022
2,950.0	85,743
3,050.0	408,587
3,150.0	423,354
3,250.0	1,232,094
3,350.0	1,533,637
3,450.0	3,641,272
3,550.0	4,400,885
3,650.0	7,660,782
3,750.0	17,493,564
3,850.0	20,297,617
3,950.0	19,595,641
4,050.0	11,817,368
4,150.0	8,426,322
4,250.0	5,146,906
4,350.0	4,061,667
4,450.0	2,467,835
4,550.0	982,452
4,650.0	977,629
4,750.0	547,609
4,850.0	199,826
4,950.0	292,141
5,050.0	204,176
5,150.0	148,060
5,250.0	18,705
5,350.0	97,874

Root Station My	
Range (kN-m)	Counts
60.0	418,723,838
180.0	95,253,172
300.0	54,072,431
420.0	32,433,459
540.0	21,258,497
660.0	14,667,714
780.0	8,787,119
900.0	6,884,967
1,020.0	6,964,109
1,140.0	6,934,477
1,260.0	7,151,540
1,380.0	8,040,329
1,500.0	7,825,130
1,620.0	7,207,773
1,740.0	5,652,907
1,860.0	5,143,092
1,980.0	5,635,025
2,100.0	5,345,741
2,220.0	3,618,380
2,340.0	5,028,549
2,460.0	5,117,536
2,580.0	2,404,314
2,700.0	3,005,230
2,820.0	3,014,377
2,940.0	2,718,873
3,060.0	2,348,663
3,180.0	2,101,933
3,300.0	2,035,577
3,420.0	1,992,961
3,540.0	1,563,776
3,660.0	1,138,159
3,780.0	1,241,080
3,900.0	863,103
4,020.0	1,075,406
4,140.0	1,311,431
4,260.0	1,157,466
4,380.0	553,307
4,500.0	694,048
4,620.0	846,286
4,740.0	596,416
4,860.0	245,938
4,980.0	308,855
5,100.0	240,976
5,220.0	254,964
5,340.0	298,440
5,460.0	163,155
5,580.0	195,750
5,700.0	129,220
5,820.0	436,083
5,940.0	120,793
6,060.0	21,066
6,180.0	286,032
6,300.0	129,450
6,420.0	116,716

Table A-3. Blade Fatigue Loads, 3.0 MW Rotor at Specific Rating = 0.39 (Page 4 of 4)

25% Station Mx	
Range (kN-m)	Counts
2,616.0	22,918
2,664.0	60,465
2,712.0	37,410
2,760.0	12,639
2,808.0	0
2,856.0	27,131
2,904.0	18,705
2,952.0	0
3,000.0	4,213
3,048.0	0
3,096.0	0
3,144.0	0
3,192.0	4,213
3,240.0	0
3,288.0	0
3,336.0	0
3,384.0	0
3,432.0	0
3,480.0	0
3,528.0	0

25% Station My	
Range (kN-m)	Counts
3,815.0	16,853
3,885.0	133,663
3,955.0	60,465
4,025.0	18,705
4,095.0	0
4,165.0	18,705
4,235.0	56,251
4,305.0	22,918
4,375.0	0
4,445.0	0
4,515.0	0
4,585.0	56,251
4,655.0	0
4,725.0	0
4,795.0	22,918
4,865.0	0
4,935.0	0
5,005.0	0
5,075.0	0
5,145.0	0

Root Station Mx	
Range (kN-m)	Counts
5,450.0	18,705
5,550.0	21,066
5,650.0	18,705
5,750.0	0
5,850.0	22,918
5,950.0	0
6,050.0	0
6,150.0	4,213
6,250.0	0
6,350.0	0
6,450.0	0
6,550.0	0
6,650.0	0
6,750.0	0
6,850.0	0
6,950.0	0
7,050.0	0
7,150.0	0
7,250.0	0
7,350.0	0

Root Station My	
Range (kN-m)	Counts
6,540.0	143,847
6,660.0	119,171
6,780.0	18,705
6,900.0	22,918
7,020.0	0
7,140.0	74,956
7,260.0	0
7,380.0	4,213
7,500.0	18,705
7,620.0	0
7,740.0	0
7,860.0	56,251
7,980.0	0
8,100.0	0
8,220.0	18,705
8,340.0	0
8,460.0	0
8,580.0	0
8,700.0	0
8,820.0	4,213

Table A-4. Blade Fatigue Loads, 5.0 MW Rotor at Specific Rating = 0.39 (Page 1 of 2)

75% Station Mx	
Range (kN-m)	Counts
4.3	511,325,260
12.8	116,461,324
21.3	68,569,872
29.8	46,167,160
38.3	31,315,227
46.8	21,449,076
55.3	17,047,311
63.8	11,006,143
72.3	7,403,972
80.8	6,138,756
89.3	3,127,931
97.8	2,652,159
106.3	1,797,339
114.8	1,142,959
123.3	826,633
131.8	453,176
140.3	342,808
148.8	510,386
157.3	60,831
165.8	549,538
174.3	797,539
182.8	2,769,186
191.3	7,761,210
199.8	12,039,801
208.3	14,562,662
216.8	12,062,652
225.3	9,525,705
233.8	7,370,951
242.3	4,804,697
250.8	4,514,723
259.3	2,690,685
267.8	2,362,436
276.3	1,284,251
284.8	887,970
293.3	976,669
301.8	930,931
310.3	296,561
318.8	415,349
327.3	123,142
335.8	296,561
344.3	102,078
352.8	58,470
361.3	31,341
369.8	16,851
378.3	8,425
386.8	18,703
395.3	0
403.8	0
412.3	0
420.8	8,425
429.3	0
437.8	4,213

75% Station My	
Range (kN-m)	Counts
12.5	810,916,853
37.5	107,802,703
62.5	56,573,431
87.5	31,999,040
112.5	22,800,315
137.5	18,958,908
162.5	13,290,346
187.5	8,781,145
212.5	6,785,751
237.5	5,325,866
262.5	4,723,255
287.5	2,764,811
312.5	3,378,669
337.5	2,373,764
362.5	2,529,913
387.5	1,606,222
412.5	1,620,276
437.5	1,440,712
462.5	927,505
487.5	1,100,505
512.5	559,049
537.5	706,623
562.5	570,069
587.5	300,173
612.5	1,073,267
637.5	429,840
662.5	456,968
687.5	644,650
712.5	354,195
737.5	337,808
762.5	222,999
787.5	246,008
812.5	285,910
837.5	39,767
862.5	171,058
887.5	133,651
912.5	81,523
937.5	166,981
962.5	68,885
987.5	18,703
1,012.5	22,916
1,037.5	0
1,062.5	27,129
1,087.5	0
1,112.5	135,408
1,137.5	0
1,162.5	0
1,187.5	0
1,212.5	0
1,237.5	0
1,262.5	56,246
1,287.5	0

50% Station Mx	
Range (kN-m)	Counts
27.5	272,924,998
82.5	69,090,907
137.5	42,955,382
192.5	23,026,332
247.5	16,764,221
302.5	10,001,766
357.5	5,750,384
412.5	4,098,339
467.5	1,844,691
522.5	1,331,335
577.5	765,335
632.5	488,589
687.5	375,494
742.5	129,579
797.5	62,683
852.5	72,961
907.5	4,213
962.5	12,638
1,017.5	8,425
1,072.5	74,949
1,127.5	157,715
1,182.5	110,504
1,237.5	521,740
1,292.5	1,239,934
1,347.5	4,101,584
1,402.5	12,007,025
1,457.5	17,602,871
1,512.5	15,730,742
1,567.5	11,570,574
1,622.5	9,031,601
1,677.5	4,759,794
1,732.5	3,417,183
1,787.5	2,089,063
1,842.5	1,804,969
1,897.5	1,234,810
1,952.5	294,108
2,007.5	703,256
2,062.5	334,104
2,117.5	267,207
2,172.5	114,581
2,227.5	110,504
2,282.5	41,619
2,337.5	45,832
2,392.5	0
2,447.5	8,425
2,502.5	27,129
2,557.5	0
2,612.5	0
2,667.5	0
2,722.5	0
2,777.5	4,213
2,832.5	0

50% Station My	
Range (kN-m)	Counts
55.0	401,365,010
165.0	76,999,985
275.0	45,184,361
385.0	27,963,191
495.0	19,667,450
605.0	16,615,813
715.0	12,916,782
825.0	8,812,478
935.0	6,928,090
1,045.0	6,547,951
1,155.0	4,516,971
1,265.0	3,200,289
1,375.0	3,268,998
1,485.0	3,435,615
1,595.0	2,445,755
1,705.0	1,694,304
1,815.0	1,963,062
1,925.0	1,328,594
2,035.0	1,486,314
2,145.0	440,626
2,255.0	986,578
2,365.0	996,846
2,475.0	470,755
2,585.0	853,155
2,695.0	671,069
2,805.0	542,104
2,915.0	690,346
3,025.0	225,451
3,135.0	87,452
3,245.0	338,039
3,355.0	195,870
3,465.0	248,368
3,575.0	22,916
3,685.0	142,076
3,795.0	183,696
3,905.0	4,213
4,015.0	8,425
4,125.0	74,949
4,235.0	0
4,345.0	60,459
4,455.0	27,129
4,565.0	0
4,675.0	0
4,785.0	60,459
4,895.0	0
5,005.0	0
5,115.0	0
5,225.0	0
5,335.0	0
5,445.0	0
5,555.0	0
5,665.0	0

Table A-4. Blade Fatigue Loads, 5.0 MW Rotor at Specific Rating = 0.39 (Page 2 of 2)

25% Station Mx	
Range (kN-m)	Counts
75.0	145,645,753
225.0	48,114,948
375.0	22,011,614
525.0	12,127,563
675.0	7,064,538
825.0	3,592,519
975.0	1,350,916
1,125.0	1,454,237
1,275.0	680,203
1,425.0	402,759
1,575.0	169,346
1,725.0	106,155
1,875.0	21,064
2,025.0	8,425
2,175.0	27,129
2,325.0	8,425
2,475.0	0
2,625.0	4,213
2,775.0	0
2,925.0	0
3,075.0	4,213
3,225.0	45,832
3,375.0	129,208
3,525.0	123,142
3,675.0	451,176
3,825.0	879,409
3,975.0	925,883
4,125.0	2,163,423
4,275.0	3,278,920
4,425.0	6,200,941
4,575.0	12,306,418
4,725.0	20,516,539
4,875.0	14,444,249
5,025.0	10,166,945
5,175.0	5,634,601
5,325.0	3,608,801
5,475.0	2,238,024
5,625.0	1,399,324
5,775.0	1,310,262
5,925.0	582,102
6,075.0	444,238
6,225.0	189,667
6,375.0	77,174
6,525.0	83,375
6,675.0	56,110
6,825.0	87,588
6,975.0	27,129
7,125.0	0
7,275.0	18,703
7,425.0	0
7,575.0	4,213
7,725.0	0

25% Station My	
Range (kN-m)	Counts
125.0	288,890,151
375.0	71,244,471
625.0	37,871,115
875.0	20,050,561
1,125.0	12,062,804
1,375.0	9,719,526
1,625.0	10,538,599
1,875.0	8,872,731
2,125.0	9,637,550
2,375.0	8,371,602
2,625.0	5,311,447
2,875.0	5,644,674
3,125.0	5,459,927
3,375.0	3,537,596
3,625.0	3,632,139
3,875.0	3,133,830
4,125.0	2,973,040
4,375.0	1,385,857
4,625.0	1,731,245
4,875.0	1,930,044
5,125.0	1,437,345
5,375.0	1,132,728
5,625.0	1,017,035
5,875.0	830,005
6,125.0	685,328
6,375.0	425,398
6,625.0	892,544
6,875.0	295,822
7,125.0	477,663
7,375.0	204,157
7,625.0	488,410
7,875.0	231,424
8,125.0	27,129
8,375.0	127,586
8,625.0	83,375
8,875.0	137,864
9,125.0	133,651
9,375.0	22,916
9,625.0	60,459
9,875.0	0
10,125.0	27,129
10,375.0	56,246
10,625.0	4,213
10,875.0	0
11,125.0	0
11,375.0	0
11,625.0	0
11,875.0	0
12,125.0	0
12,375.0	0
12,625.0	0
12,875.0	0

Root Station Mx	
Range (kN-m)	Counts
150.0	162,046,070
450.0	27,285,805
750.0	12,638,535
1,050.0	5,233,885
1,350.0	2,095,460
1,650.0	1,562,984
1,950.0	684,829
2,250.0	204,529
2,550.0	187,542
2,850.0	12,638
3,150.0	25,276
3,450.0	0
3,750.0	0
4,050.0	4,213
4,350.0	0
4,650.0	0
4,950.0	18,703
5,250.0	0
5,550.0	0
5,850.0	0
6,150.0	0
6,450.0	0
6,750.0	0
7,050.0	4,213
7,350.0	60,459
7,650.0	31,341
7,950.0	31,341
8,250.0	127,219
8,550.0	370,298
8,850.0	358,369
9,150.0	1,052,962
9,450.0	1,662,843
9,750.0	2,914,168
10,050.0	4,686,771
10,350.0	6,895,611
10,650.0	17,505,962
10,950.0	21,411,775
11,250.0	12,466,904
11,550.0	7,960,963
11,850.0	3,814,524
12,150.0	2,583,799
12,450.0	1,635,095
12,750.0	721,959
13,050.0	536,270
13,350.0	250,220
13,650.0	87,452
13,950.0	79,162
14,250.0	124,995
14,550.0	0
14,850.0	18,703
15,150.0	4,213
15,450.0	0

Root Station My	
Range (kN-m)	Counts
220.0	569,750,041
660.0	71,567,826
1,100.0	33,599,732
1,540.0	17,084,336
1,980.0	7,330,275
2,420.0	5,309,195
2,860.0	6,363,457
3,300.0	9,898,616
3,740.0	8,805,158
4,180.0	7,957,604
4,620.0	6,923,517
5,060.0	5,953,561
5,500.0	5,367,511
5,940.0	4,164,037
6,380.0	4,229,879
6,820.0	3,749,770
7,260.0	4,123,082
7,700.0	2,672,932
8,140.0	1,776,378
8,580.0	1,982,772
9,020.0	1,912,961
9,460.0	1,622,426
9,900.0	1,585,115
10,340.0	824,446
10,780.0	1,085,919
11,220.0	658,809
11,660.0	850,321
12,100.0	448,451
12,540.0	477,432
12,980.0	592,244
13,420.0	358,966
13,860.0	204,157
14,300.0	198,092
14,740.0	160,780
15,180.0	131,799
15,620.0	114,948
16,060.0	54,257
16,500.0	79,162
16,940.0	4,213
17,380.0	64,672
17,820.0	22,916
18,260.0	0
18,700.0	4,213
19,140.0	0
19,580.0	0
20,020.0	0
20,460.0	0
20,900.0	0
21,340.0	0
21,780.0	0
22,220.0	0
22,660.0	0

DISTRIBUTION

J. Ahlgrimm
Office of Wind and Hydro Technology
EE-12
U.S. Department of Energy
1000 Independence Avenue SW
Washington, DC 20585

C. Arendt
HITCO Carbon Composites, Inc.
1600 West 135th St.
Gardena, CA 90249

H. Ashley
Dept. of Aeronautics and
Astronautics Mechanical Engr.
Stanford University
Stanford, CA 94305

K. Bennett
U.S. Department of Energy
GFO/Office of Project Management
1617 Cole Blvd.
Golden, CO 80401

K. Bergey
University of Oklahoma
Aero Engineering Department
Norman, OK 73069

D. Berry
TPI Composites Inc.
373 Market Street
Warren, RI 02885

R. Blakemore
GE Wind
13681 Chantico Road
Tehachapi, CA 93561

C. P. Butterfield
NREL
1617 Cole Boulevard
Golden, CO 80401

G. Bywaters
Northern Power Systems
Box 999
Waitsfield,VT 05673

J. Cadogan
Office of Wind and Hydro Technology
EE-12
U.S. Department of Energy
1000 Independence Avenue SW
Washington, DC 20585

D. Cairns
Montana State University
Mechanical & Industrial Engineering Dept.
220 Roberts Hall
Bozeman, MT 59717

S. Calvert
Office of Wind and Hydro Technology
EE-12
U.S. Department of Energy
1000 Independence Avenue SW
Washington, DC 20585

J. Chapman
OEM Development Corp.
840 Summer St.
Boston, MA 02127-1533

Kip Cheney
PO Box 456
Middlebury, CT 06762

C. Christensen, Vice President
GE Wind
13681 Chantico Road
Tehachapi, CA 93561

R. N. Clark
USDA
Agricultural Research Service
P.O. Drawer 10
Bushland, TX 79012

C. Cohee
Foam Matrix, Inc.
1123 East Redondo Blvd.
Inglewood, CA 90302

J. Cohen
Princeton Economic Research, Inc.
1700 Rockville Pike
Suite 550
Rockville, MD 20852

C. Coleman
Northern Power Systems
Box 999
Waitsfield, VT 05673

K. J. Deering
The Wind Turbine Company
1261 120th Ave. NE
Bellevue, WA 98005

A. J. Eggers, Jr.
RANN, Inc.
744 San Antonio Road, Ste. 26
Palo Alto, CA 94303

S. Finn
GE Global Research
One Research Circle
Niskayuna, NY 12309

P. Finnegan
GE Global Research
One Research Circle
Niskayuna, NY 12309

P. R. Goldman
Director
Office of Wind and Hydro Technology
EE-12
U.S. Department of Energy
1000 Independence Avenue SW
Washington, DC 20585

R. Gopalakrishnan
GE Wind Energy
GTTC, 300 Garlington Road
Greenville, SC 29602

D. Griffin (5)
GEC
5729 Lakeview Drive NE, Ste. 100
Kirkland, WA 98033

C. Hansen
Windward Engineering
4661 Holly Lane
Salt Lake City, UT 84117

T. Hermann
Wetzel Engineering, Inc.
P.O. Box 4153
Lawrence, KS 66046-1153

D. Hodges
Georgia Institute of Technology
270 Ferst Drive
Atlanta, GA 30332

W. Holley
GE Wind Energy
GTTC, 300 Garlington Road
Greenville, SC 29602

S. Hughes
NREL
1617 Cole Boulevard
Golden, CO 80401

K. Jackson
Dynamic Design
123 C Street
Davis, CA 95616

E. Jacobsen
GE Wind Energy
GTTC, 300 Garlington Road
Greenville, SC 29602

G. James
Structures & Dynamics Branch, Mail Code ES2
NASA Johnson Space Center
2101 NASA Rd 1
Houston, TX 77058

G. Kanaby
Knight & Carver Yacht Center
1313 Bay Marina Drive
National City, CA 91950

D. Kasperski
GE Wind Energy
GTTC, 300 Garlington Road
Greenville, SC 29602

M. Kramer
Foam Matrix, Inc.
PO Box 6394
Malibu CA 90264

A. Laxson
NREL
1617 Cole Boulevard
Golden, CO 80401

Bill Leighty
Alaska Applied Sciences, Inc.
P.O. Box 020993
Juneau, AK 99802

Wendy Lin
GE Global Research
One Research Circle
Niskayuna, NY 12309

S. Lockard
TPI Composites Inc.
373 Market Street
Warren, RI 02885

J. Locke, Associate Professor
Wichita State University
207 Wallace Hall, Box 44
Wichita, KS 67620-0044

D. Malcolm
GEC
5729 Lakeview Drive NE, Ste. 100
Kirkland, WA 98033

J. F. Mandell
Montana State University
302 Cableigh Hall
Bozeman, MT 59717

T. McCoy
GEC
5729 Lakeview Drive NE, Ste. 100
Kirkland, WA 98033

L. McKittrick
Montana State University
Mechanical & Industrial Engineering Dept.
220 Roberts Hall
Bozeman, MT 59717

P. Migliore
NREL
1617 Cole Boulevard
Golden, CO 80401

A. Mikhail
Clipper Windpower Technology, Inc.
7985 Armas Canyon Road
Goleta, CA 93117

W. Musial
NREL
1617 Cole Boulevard
Golden, CO 80401

NWTC Library (5)
NREL
1617 Cole Boulevard
Golden, CO 80401

B. Neal
USDA
Agricultural Research Service
P.O. Drawer 10
Bushland, TX 79012

T. Olsen
Tim Olsen Consulting
1428 S. Humboldt St.
Denver, CO 80210

R. Z. Poore
Global Energy Concepts, Inc.
5729 Lakeview Drive NE
Suite 100
Kirkland, WA 98033

J. Richmond
MDEC
3368 Mountain Trail Ave.
Newbury Park, CA 91320

Michael Robinson
NREL
1617 Cole Boulevard
Golden, CO 80401

D. Sanchez
U.S. Dept. of Energy
Albuquerque Operations Office
P.O. Box 5400
Albuquerque, NM 87185

R. Santos
NREL
1617 Cole Boulevard
Golden, CO 80401

S. Schreck
NREL
1617 Cole Boulevard
Golden, CO 80401

Brian Smith
NREL
1617 Cole Boulevard
Golden, CO 80401

J. Sommer
Molded Fiber Glass Companies/West
9400 Holly Road
Adelanto, CA 93201

K. Starcher
AEI
West Texas State University
P.O. Box 248
Canyon, TX 79016

A. Swift
University of Texas at El Paso
320 Kent Ave.
El Paso, TX 79922

J. Thompson
ATK Composite Structures
PO Box 160433
MS YC14
Clearfield, UT 84016-0433

R. W. Thresher
NREL
1617 Cole Boulevard
Golden, CO 80401

S. Tsai
Stanford University
Aeronautics & Astronautics
Durand Bldg. Room 381
Stanford, CA 94305-4035

W. A. Vachon
W. A. Vachon & Associates
P.O. Box 149
Manchester, MA 01944

C. P. van Dam
Dept of Mech and Aero Eng.
University of California, Davis
One Shields Avenue
Davis, CA 95616-5294

B. Vick
USDA, Agricultural Research Service
P.O. Drawer 10
Bushland, TX 79012

K. Wetzel
Wetzel Engineering, Inc.
PO Box 4153
4108 Spring Hill Drive
Lawrence, KS 66046-1153

R. E. Wilson
Mechanical Engineering Dept.
Oregon State University
Corvallis, OR 97331

M. Zuteck
MDZ Consulting
601 Clear Lake Road
Clear Lake Shores, TX 77565

M.S. 0557	T. J. Baca, 9125	
M.S. 0557	T. G. Carne, 9124	
M.S. 0708	P. S. Veers, 6214	(20)
M.S. 0708	T. D. Ashwill, 6214	(10)
M.S. 0708	S. Begay-Campbell, 6214	
M.S. 0708	D. E. Berg, 6214	
M.S. 0708	P. L. Jones 6214	
M.S. 0708	D. L. Laird, 6214	
M.S. 0708	D. W. Lobitz, 6214	
M.S. 0708	M. A. Rumsey, 6214	
M.S. 0708	H. J. Sutherland, 6214	
M.S. 0708	J. Zayas, 6214	
M.S. 0847	K. E. Metzinger, 9126	
M.S. 0958	M. Donnelly, 14172	
M.S. 1490	A. M. Lucero, 12660	
M.S. 0899	Technical Library, 9616	(2)
M.S. 9018	Central Technical Files, 8945-1	